Available online at www.sciencedirect.com
SCIENCE DIRECT®
International Journal of Mass Spectrometry 232 (2004) 277–317
International Journal of Mass Spectrometry
www.elsevier.com/locate/ijms

Review

Enantioselectivity in gas-phase ion–molecule reactions

Maurizio Speranza*

Dipartimento degli Studi di Chimica e Tecnologia delle Sostanze Biologicamente Attive, Università di Ronia "La Sapienza", 00185 Roma, Italy

Received 18 December 2003; accepted 12 February 2004

Dedicated to the memory of Fulvio Cacace, a truly exceptional scientist, mentor, and friend

Abstract

Comprehensive understanding of information transfer between chiral molecules in living systems and in supramolecular assemblies requires the quantitative determination of the intrinsic short-range forces controlling enantioselectivity in simplified models, such as diastereomeric ion–molecule complexes in the isolated state. This review article describes the state-of-art in this field. Emphasis is put on the generation of diastereomeric ion–molecule aggregates in the gas phase and the determination of their relative stability and reactivity by mass spectrometric and radiolytic techniques.

Keywords: Gas-phase enantioselectivity; Noncovalent interactions; Mass spectrometry; Radiolysis

1. Introduction

Ion–neutral complexes (INC) are transient, noncovalent species often involved in chemical and biochemical transformations. In solution, they evolve to products while in continuous contact with the liquid medium. Since the forces between the ion and a polar or polarizable solvent molecule can be as strong as those involved in covalent bonding, solvation may profoundly influence the INC evolution. A solvent that only weakly perturbs INC may interrupt and redirect motion on its potential energy surface (PES) by blocking the path of a departing group or by removing any excess energy. A solvent that strongly perturbs INC may even change the topography of its PES. This is not new to chemists, who have long appreciated that a solvent will affect the mechanism and the kinetics of ionic reactions by modifying the transition state relative to reactants or products.

Understanding the full impact of solvation on INC dynamics and reactivity requires the use of experimental methodologies, capable of characterizing INC in the gas phase and probing their chemical evolution on an extremely short time scale. Their application is intended to answer a fundamental query, which trespasses the purely chemical threshold by interlocking the physical and life sciences: what is the nature of noncovalent specific interactions in ionic aggregates and how do they affect their structure, stability, and reactivity?

These aspects are extremely important in life sciences. From the beginning of evolutionary processes right up to the present biodiversity, life relies on biological specificity, which arises from the fact that individual biomolecules "communicate" through noncovalent interactions [1,2]. Molecular and chiral recognition rely on these weak bonds [3]. Natural and synthetic enzymes are characterized by asymmetric structures with a cavity of appropriate shape and size holding suitable functionalities in specific positions. Their exceptional enantioselectivity towards chiral molecules is due to shape-specific intermolecular forces acting on their complementary surfaces. However, the precise positioning of reactants functionalities in a chiral molecule/enzyme complex is only one of the factors determining the efficiency of the enzyme catalysis in stabilizing diastereomeric transition states for a particular reaction. Most of the remarkable catalytic proficiency of natural and synthetic enzymes may in fact result from the exceptional activity of its functionalities in the apolar environment of the active site determined by extensive desolvation of reactants in the host cavity [4]. Thus, solvation/desolvation phenomena may strongly affect chiral recognition and rate acceleration of enzymes and complicate the understanding of the underlying principles.

This review is intended to report on the generation and characterization of chiral INC in the gas phase and on the

* Tel.: +39-064-991-3497; fax: +39-064-991-3602.
E-mail address: maurizio.speranza@uniromal.it (M. Speranza).

1387-3806/$ – see front matter © 2004 Elsevier B.V. All rights reserved.
doi:10.1016/j.ijms.2004.02.008

enantioselectivity of their evolution to products. The first part of the review will cover aspects related to the stability and reactivity of diastereomeric INC in the isolated state. The last part of the review will focus on enantioselectivity of chiral ion–molecule reactions both in rarefied and dense gaseous media and its comparison with solution data.

2. Stability and reactivity of diastereomerie INC

Enantiomers cannot be directly discriminated by mass spectrometry. However, mass spectrometry is able to distinguish enantiomers by complexation with a charged selector (diastereomeric INC). In the field of diastereomeric INC chemistry, mass spectrometry, sometimes in combination with chiral chromatography, has been extensively applied to studies of proton- and metal-bound clusters, self-recognition processes, cyclodextrin and crown ethers inclusion complexes, carbohydrate complexes, and others. Several excellent reviews on this topic are nowadays available [5–10]. A survey of the most relevant examples will be given in this section. Most of the studies were based on ion abundance analysis, often coupled with MIKE and CD ion fragmentation on MS^n and FT-ICR mass spectrometric instruments, using CI, MALDI, FAB, and ESI, and Atmospheric Pressure Ionization (API) methods.

2.1. Proton-bound complexes

The first example of chiral recognition by mass spectrometry was reported by Fales and Wright [11]. Their study demonstrated that the configuration of dialkytartrates (**1**; Plate 1) strongly influences the stability of their diastereomeric proton-bound dimers, generated by isobutane chemical ionization (CIMS) of their racemic mixtures [12,13].

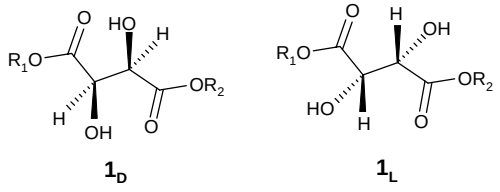

Plate 1.

Thus, CIMS of an equimolar mixture of one dialkyltartrate enantiomer, deuterium labeled at the estereal function ($\mathbf{1}_D^d$), with the other unlabeled enantiomer ($\mathbf{1}_L$) leads to the formation of three proton-bound dimers ($[\mathbf{1}_D^d \cdot \mathbf{1}_D^d \cdot H]^+$, $[\mathbf{1}_D^d \cdot \mathbf{1}_L \cdot H]^+$, and $[\mathbf{1}_L \cdot \mathbf{1}_L \cdot H]^+$), whose relative abundance appreciably diverges from the expected 1:2:1 one and, therefore, indicates a chiral recognition pattern.

The internal chirality effect, defined as the chirospecific ratio of the virtual equilibrium constants and regarded as a measure of the relative stability of the homochiral versus the heterochiral dimers, is defined as:

$$\frac{K_{homo}}{K_{hetero}} = \frac{2\sqrt{[\mathbf{1}_D^d \cdot \mathbf{1}_D^d \cdot H]^+ \times [\mathbf{1}_L \cdot \mathbf{1}_L \cdot H]^+}}{[\mathbf{1}_D^d \cdot \mathbf{1}_L \cdot H]^+} \quad (1)$$

If a third chiral component is added as the reference substrate (**ref**) to the above racemate, the CIMS of the mixture typically gives five ions in the dimer region, i.e., ($[\mathbf{ref} \cdot \mathbf{1}_D^d \cdot H]^+$, $[\mathbf{ref} \cdot \mathbf{1}_L \cdot H]^+$, $[\mathbf{1}_D^d \cdot \mathbf{1}_D^d \cdot H]^+$, $[\mathbf{1}_D^d \cdot \mathbf{1}_L \cdot H]^+$, and $[\mathbf{1}_L \cdot \mathbf{1}_L \cdot H]^+$) and a new chirality effect (external chirality effect $= K_{homo}^{ref}/K_{hetero}^{ref}$) can be defined as in Eq. (2) (if **ref** has the D configuration) [12].

$$\frac{K_{homo}^{ref}}{K_{hetero}^{ref}} = \frac{[\mathbf{ref} \cdot \mathbf{1}_D^d \cdot H]^+/[\mathbf{ref} \cdot \mathbf{1}_L \cdot H]^+}{\sqrt{[\mathbf{1}_D^d \cdot \mathbf{1}_D^d \cdot H]^+/[\mathbf{1}_L \cdot \mathbf{1}_L \cdot H]^+}} \quad (2)$$

Since the monochiral experiment reported on the last row of Table 1 excludes any significant deuterium isotope effect in the formation of the proton-bound dimers, the other figures demonstrate that the homochiral dimer is relatively more stable than the heterochiral one. The lower stability of the heterochiral dimer is ascribed to steric repulsion between the estereal functions of the two monomers in the hydrogen bonded basket-type structure of the complex. Similar chirality effects have been measured for the same systems using FAB as the ionization mode [14]. A linear correlation is observed between the optical purity of a **ref** = diethyltartrate specimen and the $K_{homo}^{ref}/K_{hetero}^{ref}$ value. These findings suggest the possibility of using the FAB-MS method for chirally titrating **ref**.

A chiral recognition pattern can be also estimated by B/E linked scanning in FAB-MS experiments [13,14]. It can be expressed as in Eq. (3), where $[\mathbf{1}_D^d \cdot H]^+$ and $[\mathbf{1}_L \cdot H]^+$ correspond to the peak intensities of monomer ions produced

Table 1
Chirality effects in the dimerization of homologous taitrate esters (Plate 1)

Unlabeled tartrate	Labeled tartrate	**Ref**	K_{homo}/K_{hetero}	$K_{homo}^{ref}/K_{hetero}^{ref}$	Ext/int
$\mathbf{1}_D$ ($R_1 = R_2 = i\text{-}C_3H_7$)	$\mathbf{1}_L^d$ ($R_1 = R_2 = i\text{-}C_3D_7$)	$\mathbf{1}_D$ ($R_1 = R_2 = CH_3$)	1.57 ± 0.16	1.54 ± 0.17	0.99 ± 0.12
$\mathbf{1}_D$ ($R_1 = R_2 = i\text{-}C_3H_7$)	$\mathbf{1}_L^d$ ($R_1 = R_2 = i\text{-}C_3D_7$)	$\mathbf{1}_D$ ($R_1 = R_2 = C_2H_5$)	1.47 ± 0.04	1.55 ± 0.10	1.05 ± 0.08
$\mathbf{1}_D$ ($R_1 = R_2 = i\text{-}C_3H_7$)	$\mathbf{1}_L^d$ ($R_1 = R_2 = i\text{-}C_3D_7$)	$\mathbf{1}_D$ ($R_1 = R_2 =$ Py[a])	1.43 ± 0.05	1.23 ± 0.14	0.86 ± 0.10
$\mathbf{1}_D$ ($R_1 = R_2 = i\text{-}C_3H_7$)	$\mathbf{1}_L^d$ ($R_1 = R_2 = i\text{-}C_3D_7$)	$\mathbf{1}_L$ ($R_1 = R_2 = CH_3$)	1.51 ± 0.16	1.35 ± 0.14	0.88 ± 0.11
$\mathbf{1}_D$ ($R_1 = R_2 = i\text{-}C_3H_7$)	$\mathbf{1}_L^d$ ($R_1 = R_2 = i\text{-}C_3D_7$)	$\mathbf{1}_L$ ($R_1 = R_2 = C_2H_5$)	1.49 ± 0.05	1.46 ± 0.10	0.98 ± 0.08
$\mathbf{1}_D$ ($R_1 = R_2 = i\text{-}C_3H_7$)	$\mathbf{1}_L^d$ ($R_1 = R_2 = i\text{-}C_3D_7$)	None	1.71 ± 0.04		
$\mathbf{1}_L$ ($R_1 = R_2 = i\text{-}C_3H_7$)	$\mathbf{1}_L^d$ ($R_1 = R_2 = i\text{-}C_3D_7$)	None	1.01 ± 0.05		

[a] Pyrrolidyl.

by unimolecular decomposition of the relevant protonated dimer species.

$$\frac{k^{\text{fragm}}_{\text{homo}}}{k^{\text{fragm}}_{\text{hetero}}} = \frac{[\mathbf{1}^{\text{d}}_{\text{D}} \cdot \text{H}]^+/[\mathbf{1}_{\text{L}} \cdot \mathbf{1}^{\text{d}}_{\text{D}} \cdot \text{H}]^+}{([\mathbf{1}^{\text{d}}_{\text{D}} \cdot \text{H}]^+[\mathbf{1}_{\text{L}} \cdot \text{H}]^+)/[\mathbf{1}^{\text{d}}_{\text{D}} \cdot \mathbf{1}_{\text{L}} \cdot \text{H}]^+} \quad (3)$$

The experimental results ($k^{\text{fragm}}_{\text{homo}}/k^{\text{fragm}}_{\text{hetero}} = 0.67(\mathbf{1}\,(R_1 = R_2 = i\text{-}C_3H_7) + \mathbf{1}^{\text{d}}(R_1 = R_2 = i\text{-}C_3D_7))$; $0.77(\mathbf{1}\,(R_1 = R_2 = C_2H_5) + \mathbf{1}^{\text{d}}(R_1 = R_2 = C_2D_5)))$ confirm the higher stability of the homochiral dimer relative to the heterochiral one by indicating that the latter has a higher tendency toward unimolecular fragmentation.

More comprehensive CIMS investigations on tartrate systems indicate that the dimer chirality effects disappear when the ester functions of tartrates is replaced by H or an alkyl function, e.g., methyl or cyclohexyl [13]. A similar effect is observed when the proton in the proton-bound dimers is replaced by lithium or ammonium ion [12–14]. These observations are attributed to a dramatic change in the basket-type structure of tartrate dimer ions.

The same CIMS approach has been used for investigating the self-recognition processes in proton-bound tartrate trimers [13–17]. The trimer chirality effect is consistent with the heterochiral trimers as more stable than the homochiral ones. The reverse is true when the proton in the proton-bound trimers is replaced by hydronium, ammonium ion, or primary aminium ions [18,19]. This changeover is ascribed to the formation of an especially stable supramolecular propeller structure accessible only to the homochiral aggregation.

The relative stability of the homochiral and the heterochiral dimers arising from self-CI of an equimolar mixture of the L and the D enantiomers of dimethyl- and di-isopropyltartrate has been evaluated by Nikolaev and coworkers using the FT-ICR technique [20–23]. The dimer chirality effect, $K_{\text{homo}}/K_{\text{hetero}} = 0.33$ corresponds to a $\Delta\Delta G^{\circ}_{298} = -RT\ln(K_{\text{homo}}/K_{\text{hetero}}) = 0.65\,\text{kcal mol}^{-1}$ value at 20 °C, a value which is slightly larger than those measured in the CIMS experiments (0.25–0.50 kcal mol^{-1}) [12,13]. The lack of chirality effects, observed when the used tartrates are replaced by the L and the D enantiomers of methyl lactate, alaninamide, and *N*-acetyl-α-methyl-benzylamine, is attributed to their extensive racemization after protonation.

Proton-induced association of a number of chiral compounds, including carboxylic acids, amino acids, and amines has been investigated using CIMS and FAB-MS techniques. The first controversial [14] evidence of chiral discrimination in these systems was based upon the relative intensities of proton-bound complexes generated by CIMS of mixtures containing a chiral selector S_S (i.e., (*S*)-2-methyl-1-butanol) and the enantiomers of a target molecule M (i.e., mandelic acid **8** or phenylalanine **3**) (Plate 2) [24]. The resulting chiral discrimination term, defined as $[S_S{\cdot}M_R{\cdot}H]^+/[S_S{\cdot}M_S{\cdot}H]^+$, ranged from >9 (M = **8**) to 2.3 (M = **3**). The same approach has been applied to a number of systems [25–30], whose results are summarized in Table 2.

Analysis of Table 2 reveals that the stability of the homochiral complexes is higher than that of the heterochiral ones, except in the cases with the chiral succinic anhydrides **13**. Similar results have been obtained by using (*R*)- and (*S*)-1-naphthylethylamine as optically resolving reagents S [31].

2.2. The kinetic method

The relative stability of diastereomeric INC can be conveniently measured using the so-called "kinetic method," first introduced by Cooks and coworkers about 20 years ago for the determination of proton affinities [32,33]:

$$(k')\quad [\text{M} \cdot \text{I}]^+ + \text{S} \leftarrow [\text{M} \cdot \text{I} \cdot \text{S}]^+ \rightarrow \text{M} + [\text{I} \cdot \text{S}]^+ \quad (k'') \quad (4)$$

Table 2
Relative abundances of diastereomeric proton-bound complexes from CI, FAB, and API mass spectrometry

MS procedure	S	M	$[S{\cdot}M{\cdot}H]^+/[S{\cdot}H]^+$	Reference	MS techniques	S	M	$[S{\cdot}M{\cdot}H]^+$ $[S{\cdot}H]^+$	Reference
CIMS	$\mathbf{2}_S$	$\mathbf{10}_S$	0.05[a]	[25]	FAB	$\mathbf{6}_S$	$\mathbf{13}_{RR}$	0.16	[27]
CIMS	$\mathbf{2}_S$	$\mathbf{10}_R$	0.01[a]	[25]	FAB	$\mathbf{7}_R$	$\mathbf{13}_{SS}$	0.30	[27]
CIMS	$\mathbf{2}_R$	$\mathbf{10}_S$	0.08[a]	[25]	FAB	$\mathbf{7}_R$	$\mathbf{13}_{RR}$	0.05	[27]
CIMS	$\mathbf{2}_R$	$\mathbf{10}_R$	0.17[a]	[25]	LC/API	$\mathbf{8}_S$	$\mathbf{14}_S$	7.11	[28]
CIMS	$\mathbf{3}_S$	$\mathbf{11}_S$	0.09	[25]	LC/API	$\mathbf{8}_S$	$\mathbf{14}_R$	5.31	[28]
CIMS	$\mathbf{3}_S$	$\mathbf{11}_R$	0.04	[25]	LC/API	$\mathbf{8}_R$	$\mathbf{14}_S$	3.70	[28]
CIMS	$\mathbf{3}_R$	$\mathbf{11}_S$	0.07	[25]	LC/API	$\mathbf{8}_R$	$\mathbf{14}_R$	8.50	[28]
CIMS	$\mathbf{3}_R$	$\mathbf{11}_R$	0.11	[25]	GC/CIMS	$\mathbf{9}_S$	$\mathbf{15}_R$	0.12	[29]
CIMS	$\mathbf{4}_S$	$\mathbf{10}_S$	1.39	[26]	GC/CIMS	$\mathbf{9}_S$	$\mathbf{15}_S$	0.01	[29]
CIMS	$\mathbf{4}_S$	$\mathbf{10}_R$	0.09	[26]	GC/CIMS	$\mathbf{9}_R$	$\mathbf{15}_R$	0.02	[29]
CIMS	$\mathbf{4}_R$	$\mathbf{10}_S$	0.04	[26]	GC/CIMS	$\mathbf{9}_R$	$\mathbf{15}_S$	0.09	[29]
CIMS	$\mathbf{4}_R$	$\mathbf{10}_R$	0.82	[26]	HPLC/API	$\mathbf{3}_S$	$\mathbf{10}_S$	0.84	[30]
CIMS	$\mathbf{5}_{SSS}$	$\mathbf{12}_S$	5.00	[26]	HPLC/API	$\mathbf{3}_S$	$\mathbf{10}_R$	0.46	[30]
CIMS	$\mathbf{5}_{SSS}$	$\mathbf{12}_R$	1.27	[26]	HPLC/API	$\mathbf{3}_R$	$\mathbf{10}_S$	0.53	[30]
CIMS	$\mathbf{5}_{RRR}$	$\mathbf{12}_S$	1.52	[26]	HPLC/API	$\mathbf{3}_R$	$\mathbf{10}_R$	0.75	[30]
CIMS	$\mathbf{5}_{RRR}$	$\mathbf{12}_R$	5.56	[26]	HPLC/API	$\mathbf{3}_S$	$\mathbf{8}_S$	0.85	[30]
FAB	$\mathbf{6}_S$	$\mathbf{13}_{SS}$	0.02	[27]	HPLC/API	$\mathbf{3}_R$	$\mathbf{8}_S$	0.53	[30]

[a] $[S{\cdot}M{\cdot}H\text{-}H_2O]^+/[S{\cdot}H]^+$ value.

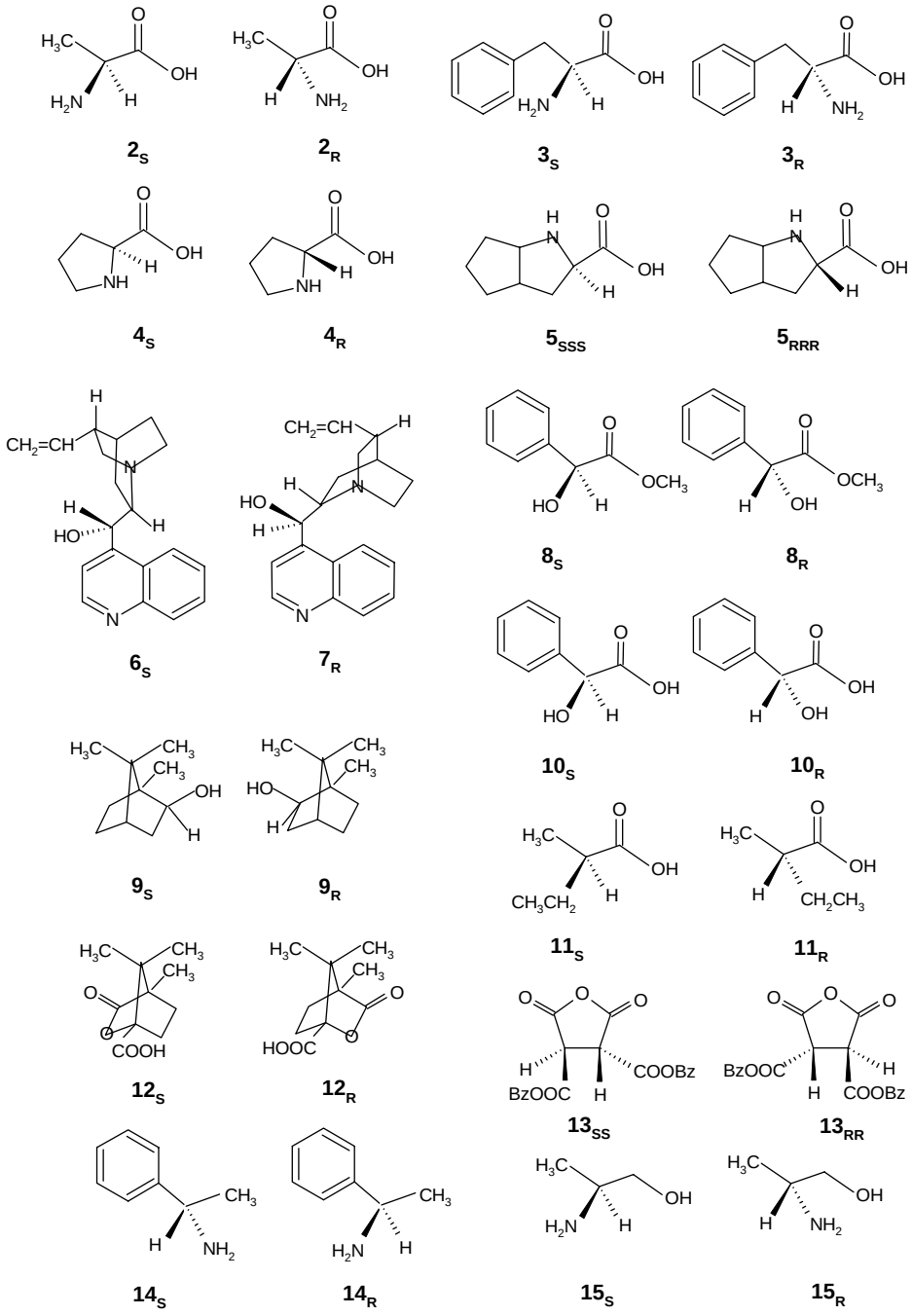

Plate 2.

(k_1) (doubly degenerate)

$$[M \cdot I \cdot S]^+ + S \leftarrow [M \cdot I \cdot S_2]^+ \rightarrow M + [I \cdot S_2]^+ \quad (k_2) \tag{5}$$

The kinetic method is based on the rates of competitive dissociations of a mass selected cluster ion (Eq. (4), where I^+ is a metal ion, a proton, or another cationic species binding a molecule M of unknown affinity for I^+ and another molecule S, whose affinity for I^+ is known): under appropriate conditions, the kinetics of the dissociation of a cluster ion can yield relative, but nevertheless quantitative, thermochemical information on the constituent species. In particular, the relative abundance of the fragment ions deriving from the fragmentation of a mass selected cluster ion is representative of the relative stability of the fragment ions themselves. A number of assumptions have to be made to correctly apply the kinetic method: (i) the method applies to weakly bound complexes; (ii) comparisons should be made for competitive dissociation of clusters having no other decomposition channels; (iii) there must be no reverse activation barriers to the dissociations process; (iv) the fraction of cluster ions

that undergo dissociations is characterized by an "effective temperature" T_{eff} defined as the temperature of the canonical ensemble for which fragmentation would yield the same branching ratios as observed experimentally [34,35].

Being valid these assumptions, the difference in the affinity of M and S for I^+ will be reflected in the experimentally measured branching ratio $[M{\cdot}I]^+/[I{\cdot}S]^+$. From the absolute reaction rate theory, the branching ratio can be expressed as:

$$\ln\frac{[M\cdot I]^+}{[I\cdot S]^+} = \ln\frac{k'}{k''} = -\frac{(\Delta H' - \Delta H'')}{RT_{\text{eff}}} + \ln\frac{Q'^*}{Q''^*} \quad (6)$$

where Q'^*, $\Delta H'$ and Q''^*, $\Delta H''$ are the partition function of the transition state and the dissociation enthalpy for the competing network 4. Eq. (6) is valid for systems in thermal equilibrium. If the competing dissociations involve species that are chemically similar, entropic effects can be ignored, and thus $Q'^* = Q''^*$. As a consequence, the term $\ln(Q'^*/Q''^*)$ is neglected in Eq. (6), giving:

$$\ln\frac{k'}{k''} = -\frac{(\Delta H' - \Delta H'')}{RT_{\text{eff}}} \quad (7)$$

The plot of $\ln(k'/k'')$ versus $\Delta H''$, named the "kinetic plot," is a straight line with a slope $m = 1/RT_{\text{eff}}$ and an intercept $q = (-\Delta H'/RT_{\text{eff}})$. Hence the unknown value of the affinity of M for I^+ can be determined. However, the assumption of negligible entropy effects cannot be applied in a large number of cases, and thus, in 1993, Fenselau and coworkers [36,37] suggested a means to overcome this limitation, which was later refined by Wesdemiotis and coworkers [38–41]. Assuming that $\ln(Q'^*/Q''^*)$ is constant over the range of effective temperatures sampled experimentally, Eq. (6) becomes:

$$\ln\frac{k'}{k''} = -\frac{(\Delta H' - \Delta H'')}{RT_{\text{eff}}} - \frac{\Delta(\Delta S)}{R} \quad (8)$$

where $\Delta(\Delta S)$ is the difference between the complexation entropies of the molecules M and S with ion I^+. The kinetic plot is a straight line with a slope $m_1 = 1/RT_{\text{eff}}$ and an intercept $q_1 = (-\Delta H'/RT_{\text{eff}}) - \Delta(\Delta S)/R$. The differences in the entropies of dissociation can be estimated by examining the dependence of the competition on the effective temperature of the dissociating cluster ion. The branching ratios are measured at different collision energies, corresponding to different T_{eff} values, in order to independently determine $\Delta H'$ and $\Delta(\Delta S)$. The plot of the intercepts q_1 obtained from the first kinetic plot (i.e., $\ln(k'/k'')$ versus $\Delta H''$) versus the corresponding slopes m_1 will give a straight line, with slope $m_2 = -\Delta H'$ and intercept $q_2 = \Delta(\Delta S)/R$ [42].

The kinetic method can be conveniently applied to characterize chiral ions. If M is a chiral target molecule and S is a chiral selector of defined configuration, the stability difference between their homochiral and heterochiral complexes with I^+, $[M_R{\cdot}I{\cdot}S]^+$ and $[M_S{\cdot}I{\cdot}S]^+$, can be determined by the dissociation of the corresponding $[M_R{\cdot}I{\cdot}S_2]^+$ and $[M_S{\cdot}I{\cdot}S_2]^+$ clusters (competing network (5)). The dissociation of $[M_R{\cdot}I{\cdot}S_2]^+$ is achieved in a MS^2 experiment

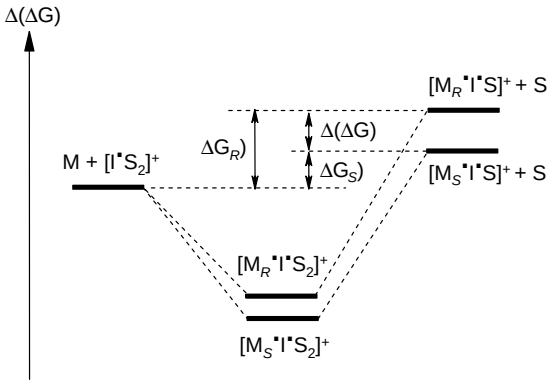

Fig. 1. Free energy schematic representation for the dissociation of trimeric cluster ions $[M_R{\cdot}I{\cdot}S_2]^+$ and $[M_S{\cdot}I{\cdot}S_2]^+$.

and occurs by competitive ligand loss to produce dimeric ions: $[M_R{\cdot}I{\cdot}S]^+$ and $[I{\cdot}S_2]^+$; by contrast, dissociation of $[M_S{\cdot}I{\cdot}S_2]^+$ generates $[M_S{\cdot}I{\cdot}S]^+$ and $[I{\cdot}S_2]^+$. The abundance A of the dimeric ions reflects the free energy diagram of Fig. 1. The small differences in steric interactions in the diastereomeric cluster ions $[M_R{\cdot}I{\cdot}S]^+$ and $[M_S{\cdot}I{\cdot}S]^+$ are recognized by easily measured differences in branching ratios for dissociation of the $[M_R{\cdot}I{\cdot}S_2]^+$ and $[M_S{\cdot}I{\cdot}S_2]^+$ complexes.

The chiral selectivity R_{chiral} is defined as:

$$R_{\text{chiral}} = \frac{R_{\text{homo}}}{R_{\text{hetero}}} = \frac{A(M_S)/A(S)_1}{A(M_R)/A(S)_2} \quad (9)$$

if the *S*-enantiomer of the chiral selector S is employed. In Eq. (9), the $A(S)_1$ and $A(S)_2$ terms refer to the $[I{\cdot}S_2]^+$ abundances from dissociation of $[M_R{\cdot}I{\cdot}S_2]^+$ and $[M_S{\cdot}I{\cdot}S_2]^+$, respectively. The R_{chiral} term serves as a numerical indication of the degree of chiral distinction achieved in a particular system and is the ratio of the individual intensity ratios of the fragment ions from the homochiral $[M_S{\cdot}I{\cdot}S_2]^+$ and the heterochiral $[M_R{\cdot}I{\cdot}S_2]^+$ precursor (if the *S*-enantiomer of the chiral selector S is employed). The farther R_{chiral} is from unity, the higher is the degree of chiral recognition. When $R_{\text{chiral}} < 1$, the heterochiral $[M{\cdot}I{\cdot}S]^+$ complex is more stable than the homochiral analog. The reverse is true if $R_{\text{chiral}} > 1$. When $R_{\text{chiral}} = 1$, no chiral discrimination occurs, which means that the particular combination of I and S fails to create stereochemically dependent interactions with the M enantiomers under the observation conditions used. The above discussion deals with the recognition of chirally pure compounds by the kinetic method. In cases in which the analyte is a mixture of the *R*- and *S*-enantiomers, a $R = [A(M_R) + A(M_S)]/A(S)$ term can be defined which falls between R_{homo} and R_{hetero}, measured with the pure enantiomers. The $\ln R_{\text{chiral}}$ is linearly related to the enantiomeric purity of the analyte, which allows quantitative chiral analysis.

The relative stability, $\Delta(\Delta G)$, of the homo $[M_S{\cdot}I{\cdot}S]^+$ versus the hetero $[M_R{\cdot}I{\cdot}S]^+$ cluster ion is calculated from the following equation, provided that the competing reactions

(5) have negligible reverse barriers:

$$\ln R_{\text{chiral}} = \frac{\Delta(\Delta G)}{RT_{\text{eff}}} \tag{10}$$

where R is the gas constant. The free energy quantity, $\Delta(\Delta G)$, reflects the different attractive electrostatic and repulsive steric interactions operating in the diastereomeric $[M_S{\cdot}I{\cdot}S]^+$ and $[M_R{\cdot}I{\cdot}S]^+$ clusters: negative $\Delta(\Delta G)$ values indicate that the heterochiral complexes are more stable than the homochiral analogues, and vice versa.

Cooks' kinetic method has been extensively applied for the chiral discrimination of amino acid ($M_{R/S}$) mixtures, using an amino acid of defined configuration as chiral selector S. The proton-bound trimers $[M{\cdot}H{\cdot}S_2]^+$ give rise to the $[M{\cdot}H{\cdot}S]^+$ and $[H{\cdot}S_2]^+$ fragments upon CID or MIKE decay (Eq. (5)). Their formation is accompanied by fragmentation of $[M{\cdot}H{\cdot}S_2]^+$ to $[M{\cdot}H]^+$and $[H{\cdot}S]^+$ (Eqs. (11) and (12)). The relative gas-phase basicities (GB) of the molecular pairs $[M{\cdot}S]^+$ and $[S_2]$ can be derived from Eqs. (13) and (14).

$$[M \cdot H \cdot S_2]^+ \rightarrow [M \cdot H]^+ + 2S \qquad (k'_F) \tag{11}$$

$$[M \cdot H \cdot S_2]^+ \rightarrow [H \cdot S]^+ + S + M \quad \text{(doubly degenerate)} \quad (k''_F) \tag{12}$$

$$\ln\frac{[H \cdot S_2]^+}{[M \cdot H]^+} = \ln\frac{k_2}{k'_F} = \frac{(GB(S_2) - GB(M))}{RT_{\text{eff}}} \tag{13}$$

$$\ln\frac{[M \cdot H \cdot S]^+}{[H \cdot S_2]^+} = \ln\frac{k_1}{2k''_F} = \frac{(GB(MS) - GB(S_2))}{RT_{\text{eff}}} \tag{14}$$

The chiral discrimination factor, ΔR^{chiral}, is defined by Eq. (15). The $[M{\cdot}H{\cdot}S]^+/[H{\cdot}S_2]^+$ ratios from CID of various mixtures of chiral amino acids are reported in Table 3.

$$\Delta R^{\text{chiral}} = \frac{[M \cdot H \cdot S]^+_{\text{hetero}}/[H \cdot S_2]^+}{[M \cdot H \cdot S]^+_{\text{homo}}/[H \cdot S_2]^+} = \frac{\{[M \cdot H \cdot S]^+/[H \cdot S_2]^+\}_{DL} + \{[M \cdot H \cdot S]^+\}_{LD}/[H \cdot S_2]^+}{\{[M \cdot H \cdot S]^+/[H \cdot S_2]^+\}_{DD} + \{[M \cdot H \cdot S]^+\}_{LL}/[H \cdot S_2]^+} \tag{15}$$

Using Eqs. (13) and (14), the relative GB ($\Delta GB^{\text{chiral}}$) of the heterochiral versus homochiral proton-bound complexes can be expressed as in Eq. (16).

$$\Delta GB^{\text{chiral}} = GB([M \cdot S]_{\text{hetero}}) - GB([M \cdot S]_{\text{homo}}) = RT_{\text{eff}} \ln\{\Delta R^{\text{chiral}}\} \tag{16}$$

The relevant $\Delta GB^{\text{chiral}}$ values, calculated by using $T_{\text{eff}} = 970$ K [43], are listed in Table 3. According to the reported values, the heterochiral Trp/Pro and Phe/Ala complexes are more stable than the homochiral ones. The reverse is true for the Phe/Pro and Phe/Val complexes. By the same token, the chiral discrimination factor, ΔR^{chiral}, measured by ESI-MS^2 for 19 amino acids was found to vary between 0.3 and 3 [44]. The stereochemistry associated to the CID of diastereomeric peptides has been investigated using a similar approach. The results suggest that the secondary structure of protonated peptides may play an important role in their gas-phase behavior [45].

The kinetic method, described in Fig. 1, has been successfully employed for enantiodiscriminating important chiral residues from post-translationally modified proteins, such as *O*-phospho-α-amino acids and α-aminophosphonic acids. The CID decomposition of their mixed proton and Na^+-bound trimers, carried out in a ESI-MS^2 instrument as a function of the collision energy (4–14 eV), points to a greater stability of the heterochiral proton and Na^+-bound dimers between *O*-phospho-serine and (1-aminoethyl)phosphonic acid (or *O*-phospho-threonine) relative to the homochiral ones [46]. The stability trend of the proton-bound dimers of α-aminophosphonic acids, H_2O_3P–CH(NH_2)–R (R = CH_3, *i*-C_3H_7, and *n*-C_5H_{11}) is less evident and is found to depend critically on their structural features [47]. Thus, when the components of the dimers have the largest alkyl groups R = *i*-C_3H_7 and *n*-C_5H_{11}, no stability difference is observed. Instead, the heterochiral complex is more stable than the homochiral one when the R alkyl substituents have a different bulkiness, e.g., R = CH_3 and *i*-C_3H_7. The reverse is true with R = CH_3 and *n*-C_5H_{11}.

The kinetic method has been also employed for evaluating relative stability of diastereomeric complexes between some chiral selectors S = (*S*)-(+)-3-hydroxy-tetrahydrofuran (**16**$_S$) or methyl-(*R*)-(+)-2-chloro-propionate (**17**$_R$), and the conjugate bases ($(M_{RR} - H)^-$ and $(M_{SS} - H)^-$, respectively) and acids ($(M_{RR} + H)^+$ and $(M_{SS} + H)^+$ respectively) of M_{RR} = (2*R*, 3*R*)-2,3-butanediol (**18**$_{RR}$) and M_{SS} = (2*S*, 3*S*)-2,3-butanediol (**18**$_{SS}$) (Plate 3) [48,49].

This method is based on the CID of the diastereomeric complexes, e.g., [**16**$_S{\cdot}$(**18**$_{RR}$ − H)$^-$] and [**16**$_S{\cdot}$(**18**$_{SS}$ − H)$^-$], and the measurement of relative abundances of the corresponding fragment ions, i.e., (**18**$_{RR}$ − H)$^-$

Table 3
Fragment-ion abundance ratios from CID of proton-bound $[M{\cdot}H{\cdot}S_2]^+$ clusters

Amino acid, M	Selector, S	$[M{\cdot}H{\cdot}S_2]^+/[{\cdot}H{\cdot}S_2]^+$	ΔR^{chiral}	S.D. of ΔR^{chiral}	$\Delta GB^{\text{chiral}}$ (kcal mol^{-1})[a]
Trp	Pro	1.528(DD); 1.529(LL); 1.656(DL); 1.643(LD)	1.079	0.004	0.2
Pro	Trp	2.936(DD); 3.049(LL); 3.429(DL); 3.461(LD)	1.151	0.008	0.3
Phe	Ala	0.291(DD); 0.291(LL); 0.315(DL); 0.313(LD)	1.079	0.008	0.2
Phe	Pro	15.221(DD); 15.098(LL); 9.346(DL); 9.901(DL)	0.645	0.015	−0.8
Phe	Val	0.786(DD); 0.776(LL); 0.744(DL); 0.749(LD)	0.956	0.004	−0.1

[a] Positive values indicate higher basicity for the heterochiral complex.

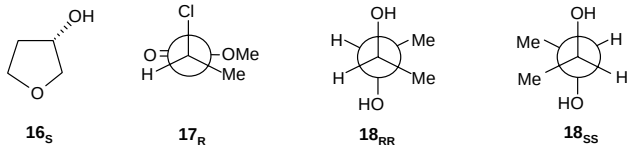

16$_S$ **17$_R$** **18$_{RR}$** **18$_{SS}$**

Plate 3.

(or $(\mathbf{18}_{SS} - \mathrm{H})^-$) and $(\mathbf{16}_S - \mathrm{H})^-$, which reflect the corresponding fragmentation rate constants k_{RR} (or k_{SS}) and (k'_S) (or k''_S).

$$(k'_S) \quad \mathbf{18}_{RR} + (\mathbf{16}_S - \mathrm{H})^- \leftarrow [\mathbf{16}_S \cdot (\mathbf{18}_{RR} - \mathrm{H})^-] \rightarrow (\mathbf{18}_{RR} - \mathrm{H})^- + 16_S \quad (k_{RR}) \tag{17}$$

$$(k''_S) \quad \mathbf{18}_{SS} + (\mathbf{16}_S - \mathrm{H})^- \leftarrow [\mathbf{16}_S \cdot (\mathbf{18}_{SS} - \mathrm{H})^-] \rightarrow (\mathbf{18}_{SS} - \mathrm{H})^- + \mathbf{16}_S \quad (k_{SS}) \tag{18}$$

$$\ln \frac{[(\mathbf{18}_{RR} - \mathrm{H})^-]}{[(\mathbf{16}_S - \mathrm{H})^-]} = \ln \frac{k_{RR}}{k'_S} = -\frac{\Delta(\Delta G)_{RR}}{RT_{\mathrm{eff}}} \tag{19}$$

$$\ln \frac{[(\mathbf{18}_{SS} - \mathrm{H})^-]}{[(\mathbf{16}_S - \mathrm{H})^-]} = \ln \frac{k_{SS}}{k''_S} = -\frac{\Delta(\Delta G)_{SS}}{RT_{\mathrm{eff}}} \tag{20}$$

Theoretical treatments lead to the approximate expression in Eqs. (17) and (18) [48], where T_{eff} is the effective temperature of the complexes, and the $\Delta(\Delta G)$'s are the differences in their dissociation free energies. If the entropy effects of the two competing fragmentation processes cancel, then the $\Delta(\Delta G)$'s can be substituted by the $\Delta(\Delta H)$'s.

The average effective temperature T_{eff}, which is a measure of excess internal energy content per degree of freedom of the ion–molecule complexes, was determined as 333 K from the slopes of the $1/RT$ dependence of the logarithm of the branching ratios similar to those of Eqs. (19) and (20) involving ions $(\mathbf{18}_{RR} - \mathrm{H})^-$, $(\mathbf{18}_{SS} - \mathrm{H})^-$, $(\mathbf{18}_{RR} + \mathrm{H})^+$, and $(\mathbf{18}_{SS} + \mathrm{H})^+$ and a number of reference molecules. With $T_{\mathrm{eff}} = 333$ K, the CID fragmentation ratios correspond to the $\Delta(\Delta G)$ values reported in Table 4, where A_{BD} represents the abundance of the conjugate bases and acids of 2,3-butanediols (i.e., $(\mathbf{18}_{RR} - \mathrm{H})^-$, $(\mathbf{18}_{SS} - \mathrm{H})^-$, $(\mathbf{18}_{RR} + \mathrm{H})^+$, and $(\mathbf{18}_{SS} + \mathrm{H})^+$) and A_S refers to the abundance of the conjugate bases and acids of the appropriate chiral selector S (i.e., $(\mathbf{16}_S - \mathrm{H})$ and $(\mathbf{17}_R + \mathrm{H})^+$, respectively).

The differences between the $\Delta(\Delta G)$ values of diastereomeric complexes $(\Delta\Delta(\Delta G) = \Delta(\Delta G)_{RR} - \Delta(\Delta G)_{SS}$ in Table 4) demonstrate that the kinetic method can be used to enantiodifferentiate chiral ions and molecules in the gas phase.

2.3. Metal-bound complexes

Chiral diols and tartrates have been studied as metal complexes as well. The enantiomers of 1,1′-bi-2-naphthol (**19**; Plate 4) and diisopropyltartrate (**1**($R_1 = R_2 = i$-C_3H_7); Plate 1) have been discriminated by generating their Li^+ complexes (using (*R*,*R*)-threohydrobenzoyn ($\mathbf{20}_{RR}$) as the chiral selector S) in the FAB source of a tandem mass spectrometer [50]. Unimolecular dissociation (MIKE) of the diastereomeric $[\mathbf{20}_{RR}\cdot\mathrm{Li}\cdot\mathbf{19}]^+$ (or $[\mathbf{20}_{RR}\cdot\mathrm{Li}\cdot\mathbf{1}]^+$) complexes yields the corresponding fragments $[\mathbf{20}_{RR}\cdot\mathrm{Li}]^+$ and $[\mathbf{19}\cdot\mathrm{Li}]^+$ (or $[\mathbf{1}\cdot\mathrm{Li}]^+$), whose relative abundance is taken as a measure of the relative stability of their precursor. According to kinetic energy release (KER) associated to the unimolecular fragmentation, this stability difference is attributed to the different structure of the diastereomeric $[\mathbf{20}_{RR}\cdot\mathrm{Li}\cdot\mathbf{19}]^+$ (or $[\mathbf{20}_{RR}\cdot\mathrm{Li}\cdot\mathbf{1}]^+$) complexes, rather than to their internal energy.

Statistically significant differences have been observed in the KER measurements of the fragments arising from MIKE dissociation of the transition-metal complex $[\mathrm{Co(acac)_2}\cdot\mathbf{1}]^+$, generated in FAB source of a tandem mass spectrometer from the diisopropyltartrate (**1**($R_1 = R_2 = i$-C_3H_7); Plate 1) enantiomers and cobalt trisacetonylacetonate ($\mathrm{Co(acac)_3}$) in the presence of the chiral selector S of defined configuration, either $\mathbf{19}_S$ or $\mathbf{19}_R$ of Plate 4 [51]. Indeed, different KER values were measured for the $[\mathrm{Co(acac)_2}\cdot\mathbf{1}]^+$ fragments, which have been considered to reflect different precursor $[\mathrm{Co(acac)_2}\cdot\mathbf{1}]^+$ ion structures. In these experiments, the chiral 1,1′-bi-2-naphthol selector S is thought to serve as a chemical kinetic resolving agent.

Accurate quantification of the optical isomers in mixtures of tartaric acid **1** and other α-hydroxy acids was performed by Cooks and coworkers by using the mass spectrometric kinetic method [52,53]. In a series of elegant studies, they used the same approach for enantiodiscriminating amino acids, peptides, pharmaceuticals, and drugs. Chiral recognition and quantitation of these molecules, recognized as building blocks in life sciences, are based on the competing fragmentation of the diastereomeric complexes $[\mathrm{M}_R\cdot\mathrm{I}\cdot\mathrm{S}_2\text{–}\mathrm{H}]^+$ and $[\mathrm{M}_S\cdot\mathrm{I}\cdot\mathrm{S}_2\text{–}\mathrm{H}]^+$ in which I is generally a divalent transition-metal ion, such as Cu(II), Zn(II), Ni(II), or Co(II), M are the chiral analytes, and S is the chiral selector of defined configuration Eq. (5) [54].

Table 4
Fragment-ion abundance ratios from CID of diasteromeric complexes

Diastereomeric complex	A_{BD}/A_S	$\Delta(\Delta G)$ (kcal mol^{-1})	$\Delta\Delta(\Delta G)$ (kcal mol^{-1})
$[\mathbf{16}_S\cdot(\mathbf{18}_{RR} - \mathrm{H})^-]$	$(\mathbf{18}_{RR} - \mathrm{H})^-/(\mathbf{16}_S - \mathrm{H})^- = 12.4$	−1.67	0.47
$[\mathbf{16}_S\cdot(\mathbf{18}_{SS} - \mathrm{H})^-]$	$(\mathbf{18}_{SS} - \mathrm{H})^-/(\mathbf{16}_S - \mathrm{H})^- = 25.6$	−2.14	
$[\mathbf{17}_R\cdot(\mathbf{18}_{RR} + \mathrm{H})^+]$	$(\mathbf{18}_{RR} + \mathrm{H})^+/(\mathbf{17}_R + \mathrm{H})^+ = 19.0$	−1.94	0.23
$[\mathbf{17}_R\cdot(\mathbf{18}_{SS} + \mathrm{H})^+]$	$(\mathbf{18}_{SS} + \mathrm{H})^+/(\mathbf{17}_R + \mathrm{H})^+ = 26.7$	−2.17	

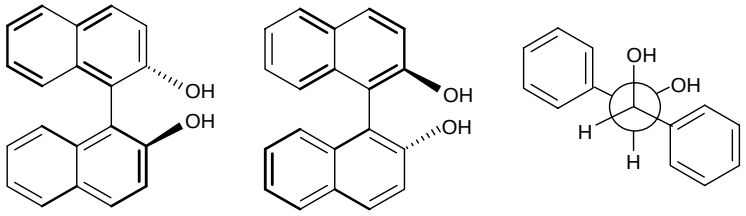

19_S 19_R 20_{RR}

Plate 4.

Using this procedure, D- and L-α amino acids have been enantiodifferentiated in the gas phase [55,56]. ESI of hydroalcoholic solutions of the amino acid and $CuCl_2$ into the source of an ion trap mass spectrometer reveals the presence of singly charged, covalently bound dimeric and trimeric ions. Table 5 reports the CID results of the diastereomeric complexes $[M_R{\cdot}Cu^{II}{\cdot}S_2{-}H]^+$ and $[M_S{\cdot}Cu^{II}{\cdot}S_2{-}H]^+$.

The degree of chiral discrimination is defined from the relative Cu(II) affinity $\Delta Cu(II)' = RT_{eff} \ln R_{chiral}$, with R_{chiral} as expressed in Eq. (9). The $\Delta Cu(II)'$ terms in Table 5 indicate that, irrespective of the chiral selector S used, the heterochiral complexes of most amino acids are more stable than the homochiral analogues ($R_{chiral} < 1$). The first 12 entries of Table 5 provide some insights into the effects of S on leucine, methionine, and tyrosine enantiodiscrimination. S = L-valine, L-serine, and L-proline give low enantioselectivity for leucine as analyte ($R_{chiral} \approx 1$). Instead, with S = aromatic selector, i.e., L-phenylalanine, high chiral selectivity is achieved. A similar behavior is observed for the methionine enantiodiscrimination. An excellent enantioselectivity is achieved for tyrosine with S = L-proline and L-tryptophan. The selectivity decreases dramatically when nonaromatic references are used. The great selectivity of aromatic S, such as L-phenylalanine or tryptophan, if compared to that of a rigid, nonaromatic S, like L-proline, is confirmed by extending the comparison to the corresponding Ala, Thr, and Asp systems.

Structural studies of the dimeric clusters $[M_R{\cdot}Me^{II}{\cdot}S{-}H]^+$ and $[M_S{\cdot}Me^{II}{\cdot}S_2{-}H]^+$, arising from CID of the corresponding $[M_R{\cdot}Me^{II}{\cdot}S_2{-}H]^+$ and $[M_S{\cdot}Me^{II}{\cdot}S{-}H]^+$ precursors,

Table 5
Fragment-ion abundance ratios in the MS^2 spectra of Cu(II)-bound trimer complexes

M	S	$[M_S{\cdot}Cu^{II}{\cdot}S_2{-}H]^+/[Cu^{II}{\cdot}S_2{-}H]^+$ [a]	$[M_R{\cdot}Cu^{II}{\cdot}S_2{-}H]^+/[Cu^{II}{\cdot}S_2{-}H]^+$ [a]	R_{chiral} [a]	$\Delta Cu(II)'$ (kcal mol^{-1}) [b]
Leu	L-Val	2.5	2.4	1.05	0.0
Leu	L-Pro	0.11	0.099	1.11	+0.1
Leu	L-Ser	10	9.5	1.05	0.0
Leu	L-Phe	0.41	0.96	0.43	−0.6
Met	L-Pro	33	60	0.50	−0.4
Met	4-OH-L-Pro	33	59	0.56	−0.4
Met	L-Glu	18	27	0.67	−0.3
Met	L-Trp	0.23	1.8	0.13	−1.4
Tyr	L-Met	0.90	2.8	0.32	−0.8
Tyr	L-Glu	8.0	16	0.50	−0.5
Tyr	L-Pro	4.7	43	0.11	−1.5
Tyr	L-Trp	0.02	0.21	0.09	−1.6
Phe	L-Pro	2.1	16	0.13	−1.4
Thr	L-Pro	0.88	0.89	1.00	0.0
Asp	L-Pro	3.2	4.5	0.71	−0.2
Ala	L-Phe	0.024	0.049	0.49	−0.5
Val	L-Phe	0.17	0.75	0.23	−1.0
Ile	L-Phe	0.36	1.7	0.21	−1.1
Pro	L-Phe	2.2	12	0.18	−1.2
Asp	L-Phe	1.1	3.0	0.37	−0.7
Glu	L-Phe	3.7	11	0.34	−0.8
Ser	L-Phe	0.18	0.28	0.64	−0.3
Thr	L-Phe	0.76	1.4	0.54	−0.4
Phe	L-Trp	0.013	0.11	0.12	−1.5
Asn	L-Trp	3.3	6.1	0.54	−0.4
Gln	L-Trp	7.3	50	0.15	−1.3
Trp	L-Asn	3.3	6.1	0.54	−0.4
His	L-Arg	0.046	0.022	2.09	+0.5
Lys	L-His	1.6	0.91	1.76	+0.4

[a] Chiral resolution factor, R_{chiral} as the ratio between the homochiral and the heterochiral ion abundance ratios.
[b] See text, $T_{eff} = 350$ K.

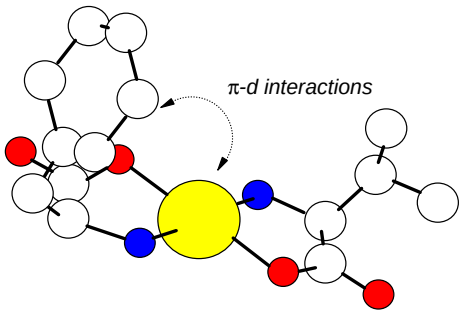

Fig. 2. π–d orbital interactions responsible for chiral distinction observed in the recognition of D,L-valine using Cu(II) with L-phenylalanine as the reference. Red, oxygen; white, carbon; blue, nitrogen; yellow, Cu(II) atom. The hydrogen atoms are omitted for the sake of clarity.

reveal that two ligands are covalently bound to the metal ion through multiple binding sites, which provide the basis for efficient chiral distinction [56,57]. In the case of amino acids, two of the interactions between the two ligands are Me(II)-mediated, resulting from the coordination of the amino and carboxylate groups to the central metal ion, whereas the third interaction involves the substituents at or near the asymmetric α-carbon of each of the two ligands (Fig. 2).

Although relatively weak, it is this last interaction that is essential for determining chiral discrimination. The superior chiral recognition achieved when S has an aromatic side chain (Table 5) suggests that π–d orbital interactions play an important role in the stereoselectivity. Evidence for such π–d orbital interaction is observed in the CID spectra of the dimeric $[M_R{\cdot}Me^{II}{\cdot}S{-}H]^+$ and $[M_S{\cdot}Me^{II}{\cdot}S{-}H]^+$ diastereomers, in which one ligand is an aromatic amino acid, and is supported by ab initio calculations. When an L-aromatic amino acid, such as L-phenylalanine, is used as S, these interactions are disrupted by the side group on the α-asymmetric carbon of the L-analyte, whereas the side-chain group in the D-analyte has little steric effect on the interaction because it is located at the opposite side of the square planar structure (Fig. 2). This interpretation is consistent with the observation that the heterochiral dimeric fragment ions are more stable than the homochiral analogues in cases where an aromatic amino acid is used as either analyte M or chiral selector S. As the size of the side-chain group on the analyte increases in the series: Ala < Leu < Val < Ile, the π–d orbital interactions between S = L-Phe and the side group on the α-asymmetric carbon of the L-analyte are more and more inhibited. An increasingly large preference for the heterochiral complexes over the homochiral ones should results as well as a decrease of the corresponding R_{chiral} values (Table 5).

In this connection, the nature of the metal ion is expected to play an important role and the experimental data indeed show intriguing effects [58]. In the case of amino acids, for example, Cu(II) offers much larger chiral selectivity than does Zn(II) or Ni(II), which is due to the formation of a square planar structure [59].

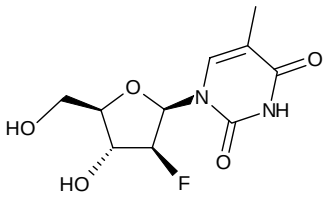

21

Plate 5.

The enantioselectivity factors in Table 5 indicate that amino acid samples with different enantiomeric excess (*ee*) should show differences in the $R = [A(M_R) + A(M_S)]/A(S)$ term. Indeed, $\ln R_{chiral}$ is linearly related to optical purity of the specimen and the relevant calibration curve can be established. Accordingly, it is possible to rapidly determine *ee* of an amino acid sample by a single measurement of $\ln R_{chiral}$ in a tandem mass spectrometer [55,56].

This behavior is typified by Clevudine (2′-fluoro-5-methyl-β,L-arabinofuranosyluracil **21**; Plate 5), a potent antiviral nucleoside against hepatitis B [58]. To optimize its chiral discrimination, several metal ions have been checked together with a variety of amino acids as chiral selectors S.

Differently from amino acid analytes which clearly prefer Cu(II) as metal ion center, **21** prefers transition metals as Co(II) and Zn(II) since these ions have a high affinity for its heteroaromatic ring which is distant from the stereocenters. Using *N*-acetyl-L-proline, as chiral selector S, and Co^{2+} as the metal ion, the data for various enantiomeric mixtures of **21** display a linear relationship between $\ln R_{chiral}$ and *ee* with a correlation coefficient, r^2, of 0.9995. This calibration curve is then used to measure the percent *ee* of various unknown samples. An average accuracy of 0.6% *ee* is obtained for this particular case from four unknown samples. Calibration curves can be constructed also by using slightly modified methods which require only one sample of the analyte with known optical purity [60]. They can be used for days, and the method can be applied to samples that contain only few percent of one enantiomer. Calibration curves can be established for the simultaneous chiral analysis of different amino acids in mixtures [61]. Quantitative enantiomeric determination of this sort can be made using protocols based not only on the kinetic method, but also on host–guest exchange reactions (*vide infra*). The same procedure has been applied to the chiral analysis of peptides [62–65], neurotrasmitters [66], thalidomite [67], and antibiotics [68].

2.4. Enantioselective self-assembling of amino acids

Homochirogenesis is at the basis of the abiogenic origin of homochirality and is an important step towards the explanation of the origin of life. It may be achieved by at least three fundamental mechanisms: (i) selective synthesis of only one enantiomer of a chiral molecule (symmetry breaking); (ii) preferential destruction of one enan-

tiomer of a heterochiral mixture (chiral enrichment); and (iii) separation of a racemic mixture into distinct homochiral parts (chiral transmission). Enantioselective self-assembling of chiral molecules may have important implications in the latter mechanism of homochirogenesis.

The term "self-assembling" describes a process, usually driven by thermodynamics, in which a larger, complex structure is formed from smaller building blocks in a specific manner. Binding sites must be present in just the right arrangement for the systems to assemble. With chiral building blocks, an enantioselective self-assembling process may take place in which the complex structure is constituted exclusively by a single enantiomeric form of a racemate.

The structure, the function, and the activity of biological molecules are greatly affected by hydrophobic, hydrogen-bonding, and electrostatic interactions between constituent amino acids, whose form in turn depends upon environmental conditions. In contrast with solution, the zwitterionic form of amino acids is destabilized in the gas phase due to the absence of solvation. For example, the N-terminus of glycine is not basic enough to deprotonate the carboxylic acid on its C-terminus [69,70], a result predicted by ab initio calculations [71–73]. By contrast, the high basicity of the guanidino side-chain functional group of arginine makes it a better candidate for a gas-phase stable zwitterion [74]. However, first experimental [75] and theoretical [76,77] evidence seem to exclude a stable zwitterionic from for an isolated arginine monomer in the gas phase. On the other hand, recent experiments, supported by theory [78], suggest that arginine in the presence of a net charge may exist in the zwitterionic state [79,80].

Theoretical calculations predict that, compared to other amino acids, arginine may dimerize and trimerize in the zwitterionic state [81]. ESI-MS experiments on the racemate of arginine, with one of the enantiomer isotopically labeled, reveal the formation of stable trimers with NO_3^- present as counterion. No preference for the chirality of the individual aminoacidic components is observed [82]. In the positive ion mode, ESI-MS of arginine solutions leads to abundant singly- and multiprotonated clusters [83]. The singly-protonated cluster $[(Arg)_n{\cdot}H]^+$ ($n = 4$) displays enhanced stability so as it is preferentially formed also by CID of larger clusters ($n > 4$). In the doubly-charged ion series, the dications $[(Arg)_n{\cdot}2H]^{2+}$ (n = 12–15) have enhanced stability relative to those of immediately smaller size.

As for arginine, ESI-MS analysis of serine solutions reveals unusually abundant protonated serine octamers $[(Ser)_8{\cdot}nH]^+$ (n = 1–3), which demonstrate a strong preference for homochirality [84]. In addition to them, the positive ion spectrum displays a series of Na^+ bound serine octamers $[(Ser)_8{\cdot}nNa]^{n+}$ (n = 1–3) [85]. CD of protonated and sodiated serine octamers provides some information on their structure. Thus, $[(Ser)_8{\cdot}nH]^{n+}$ (n = 1–3) show preferential fragmentation to the singly charged $[(Ser)_n{\cdot}H]^+$ ($n = 6$), with small contribution of $[(Ser)_n{\cdot}H]^+$ (n = 4, 5). By comparison, $[(Ser)_8{\cdot}nNa]^{n+}$ (n = 1–3) show inter alia the formation of a variety of multicharged fragments with $[(Ser)_n{\cdot}Na]^{n+}$ ($n = 6$) as only a minor one. These results suggest that $[(Ser)_8{\cdot}H]^+$ is composed of hydrogen-bonded dimers, stabilized by further extensive proton bonding. The final drum-shaped structure has incomplete hydrogen bonding, i.e., lone pairs on oxygen and amino hydrogens atoms available for further interactions. They can be regarded as "sticky ends" present on the top and bottom faces of the drum-shaped structure and are responsible of the formation of multicharged structures. The situation is rather different for $[(Ser)_8{\cdot}Na]^+$ which, instead, exhibits the Na^+ ion inside the octamer in a crown-ether-like structure. The formation of multicharged sodiated structures is due in this case to simple hydrogen bonding between two $[(Ser)_8{\cdot}Na]^+$ units. Density functional calculations and ion mobility experiments [86] support these models and show that the protonated homochiral octamer is energetically stabilized relative to its possible fragments (e.g., dimer plus protonated hexamer). The calculations also show that heterochiral octamers are less stable than homochiral octamers. For instance, $[(\text{L-Ser})_7\text{D-Ser}{\cdot}H]^+$ is 2.1 kcal mol^{-1} less stable than $[(\text{L-Ser})_8{\cdot}H]^+$.

Differently from serine, ESI-MS analysis of homoserine (HSer) solutions reveals an unusually abundant diprotonated homoserine octamer $[(HSer)_8{\cdot}2H]^{2+}$, but not the expected monoprotonated $[(HSer)_8{\cdot}H]^+$ one [86]. A 3/1 mixture of L-serine and L-homoserine yields abundant mixed serine octamers with the incorporation of one or two homoserine molecules into the cluster. CID of the isolated $[(Ser)_6(HSer)_2{\cdot}H]^+$ cluster leads to the preferential loss of two neutral serine molecules. Homoserine is always retained. The ESI-MS spectral patterns of threonine and allothreonine solutions is similar to that of homoserine. A 1/1 mixture of D-serine and D-threonine yields abundant mixed singly- and doubly-charged octamers incorporating from 2 to 6 threonine molecules. Their relative abundance indicates that threonine may incorporate freely into serine clusters because the additional methyl group does not interfere with the bonding of the cluster.

ESI-MS of cysteine solutions yields only the singly-protonated hexamer $[(Cys)_6{\cdot}H]^+$. No preference for the chirality of the individual aminoacidic components is observed [87]. Addition of cysteine to a serine solution yields an abundant homochiral mixed octamer $[(\text{L-Ser})_{8-m}(\text{L-Cys})_m{\cdot}H]^+$ (m = 0–2). No $[(\text{L-Ser})_{8-m}(\text{D-Cys})_m{\cdot}H]^+$ (m = 1, 2) octamers, but only $[(\text{L-Ser})_8{\cdot}H]^+$ is observed by using the wrong L-cysteine enantiomer. A similar picture is observed by replacing cysteine with other amino acid, such as aspartic acid, asparagine, leucine, and methionine. The enantioselective incorporation of these amino acids into the serine octamers represents an example of chiral transmission to elementary biomolecules and a possible way of chirality amplification on primitive earth.

A slight preference for the formation of homochiral dimers of 2-pentanol around Fe^+ ions has been detected in an ESI-FT-ICR instrument by measuring the rate constant ratios

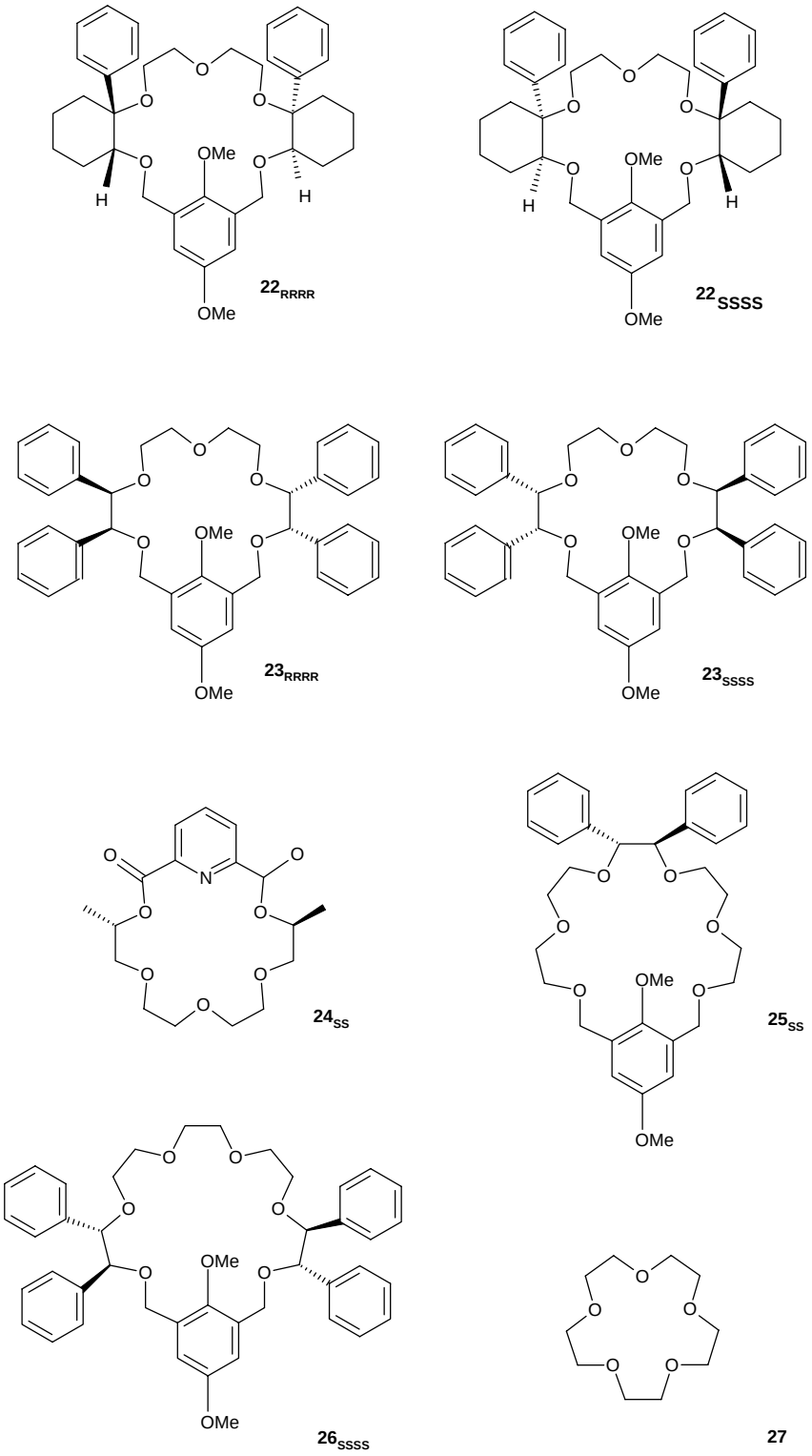

Plate 6.

for the uptake of a (*R*)-2-pentanol/(*S*)-(5,5,5)-trideutero-2-pentanol mixture by the $[(R)\text{-2-pentanol}\cdot\text{Fe}]^+$ ($k_{RR}/k_{RS} = 1.05 \pm 0.03$) and $[(S)\text{-(5,5,5)-trideutero-2-pentanol}\cdot\text{Fe}]^+$ ions ($k_{SS}/k_{SR} = 1.04 \pm 0.02$) [88]. Although in agreement with the above homochiral self-assembling examples, the magnitude of the observed effects is too small to draw any decisive conclusions. Quite obviously, the stereogenic centers in these adducts are too far apart from each other to bring about a more evident diastereoselectivity.

2.5. Host–guest inclusion complexes

Crown ethers reveal particularly suitable for enantiodiscriminating chiral ammonium ions under FAB-MS, ESI-MS, or FT-ICR conditions [5,6,8,10,13].

There are several methods to enantiodifferentiate chiral ammonium ions by FAB-MS. One is the so-called enantiomer-labeled (EL) guest method [89]. The method is based on the preparation of a mixture containing the enantiopure host (denoted as C) and the racemate of the guest. One of the guest enantiomers is isotopically labeled (e.g., $[M^*_S]^+$) and the other is not (e.g., $[M_R]^+$). Consequently, the signals for the two diastereomeric host–guest pairs (i.e., $[C{\cdot}M_R]^+$ and $[C{\cdot}M^*_R]^+$ of Eqs. (21) and (22)) appear at different *m/z* ratios.

$$C + [M_R]^+ \rightarrow [C \cdot M_R]^+ \tag{21}$$

$$C + [M^*_S]^+ \rightarrow [C \cdot M^*_R]^+ \tag{22}$$

If no thermodynamic isotope effect is operative, the relative stability of the diastereomeric $[C{\cdot}M_R]^+$ and $[C{\cdot}M^*_S]^+$ complexes can be represented approximately by their relative peak intensity (RPI), i.e., the IRIS value:

$$\text{IRIS} = \frac{[C \cdot M_R]^+}{[C \cdot M^*_S]^+} \tag{23}$$

Usually, isotope effects on noncovalent binding are small. However, both stereochemical and isotope effects can easily be separated by performing a control experiments using the other enantiomer of the host under the same conditions.

This experimental procedure has been applied to the crown ethers **22** and **23** of Plate 6, first with FAB as the ionization method [90,91], later with ESI-MS [92,93]. A number of amino acid methyl esters have been used as guests, including **28**, **29**, and **8** (Plate 7). For instance, the FAB spectra of **28**/**22**$_{RRRR}$ reveal that the host recognizes **28**$_R$ better than **28**$_S$ (over fivefold excess). Chiral recognition of **28** by **23**$_{SSSS}$ is much less pronounced. Quite surprisingly, the large 5.3:1 excess of **28**$_R$/**22**$_{RRRR}$ over **28**$_S$/**22**$_{RRRR}$ in the FAB spectra reduces to ca. 1.5:1, if ESI is used to generate the ionic complexes. This observation appears to be general for all host–guest pairs studied and it was attributed to the electrospray process, although no real explanation was advanced as to the observed ESI effect on stereochemistry [92,93]. Enantiomer labeling can also be applied to the host [93–95]. An enantiopure guest is combined with a 1:1 mixture of the enantiomers of the host, one of them isotopically labeled. This enantiomer-labeled host method has been applied using **23**$_{RRRR}$ and hexadeuterated **23**$^*_{SSSS}$ at the two methyl groups. After calibration, the method can also be used to determine the enantiomeric excess of an unknown mixture of the guest enantiomers. Extension of these methods to spiroacetal polyethers has been reported [96].

$$C + [M]^+ \rightarrow [C \cdot M]^+ \tag{24}$$

$$C_{ref} + [M]^+ \rightarrow [C_{ref} \cdot M]^+ \tag{25}$$

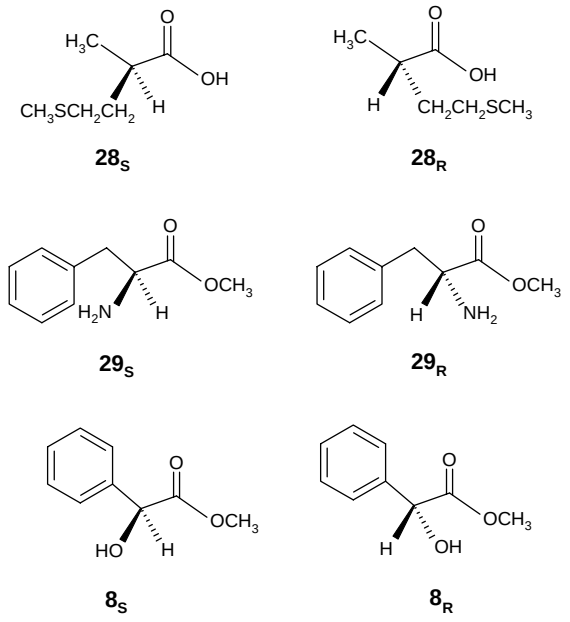

Plate 7.

$$C + [C_{ref} \cdot M]^+ \leftrightarrow C_{ref} + [C \cdot M]^+,$$
$$\text{RPI} = \frac{[C \cdot M]^+[C_{ref}]}{[C_{ref} \cdot M]^+[C]} \tag{26}$$

$$M + [C]^+ \rightarrow [C \cdot M]^+ \tag{27}$$

$$M_{ref} + [C]^+ \rightarrow [C \cdot M_{ref}]^+ \tag{28}$$

$$M + [C \cdot M_{ref}]^+ \leftrightarrow M_{ref} + [C \cdot M]^+,$$
$$\text{RPI} = \frac{[C \cdot M]^+[M_{ref}]}{[C \cdot M_{ref}]^+[M]} \tag{29}$$

Another method for enantiodifferentiating chiral ammonium ions by FAB-MS is called the RPI method. It does not require labeling procedures, but rather it is based on two independent measurements of each host enantiomer (i.e., C_R and C_S), with a given guest (M) relative to an achiral reference host (C_{ref}) or guest (M_{ref}) (Eqs. (24)–(26) and (27)–(29), respectively). According to Eq. (26), the RPI value, derived from the combination of Eqs. (24) and (25), can be regarded as a measure of the degree of M^+ cation transfer equilibria 26. Two RPI values (RPI_R and RPI_S) can be measured, depending upon the configuration of the guest (i.e., M_R and M_S). Because C_{ref} is achiral, the relationship $RPI_R/RPI_S = [C{\cdot}M_R]^+/[C{\cdot}M_S]^+$ holds, provided that $[C]/[C_{ref}]$ remains constant in the two sets of experiments. In a similar way, the RPI value, derived from the combination of Eqs. (27) and (28), can be regarded as a measure of the degree of C^+ cation transfer equilibria (29). Again, two RPI values (RPI_R and RPI_S) can be measured, depending upon the configuration of the chiral guest (i.e., M_R and M_S). Because M_{ref} is achiral, the relationship $RPI_R/RPI_S = [C \cdot M_R]^+/[C{\cdot}M_S]^+$ holds, provided that $[M_R]/[M_{ref}] = [M_S]/[M_{ref}]$ in the two sets of experiments.

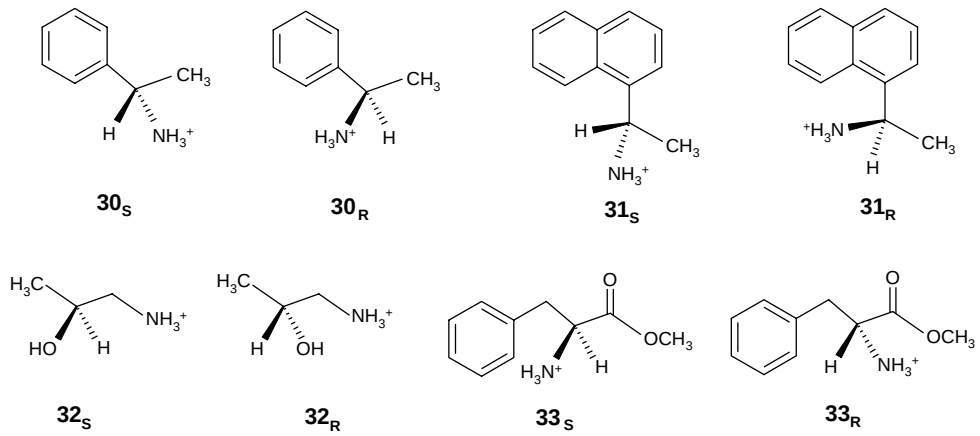

Plate 8.

These methods have been used to study chiral recognition properties of crown ether $\mathbf{24}_{SS}$ with several ammonium ions (M_R and M_S) including **30** and **31** (Plate 8). The method has been extended to a variety of other crown ethers (Plate 6) [97–101]. A 1.17-fold preference of $\mathbf{31}_R$ over $\mathbf{31}_S$ was observed with $\mathbf{24}_{SS}$, which further increases to 1.70:1 ratio upon replacement of the two methyl groups of $\mathbf{24}_{SS}$ with phenyl substituents [97].

Chiral selectivity factors, $RPI_R/RPI_S = [C{\cdot}M_R]^+/[C{\cdot}M_S]^+$ as defined in Eq. (26), for a variety of host–guest inclusion complexes are reported in Table 6 [99,100]. Thus, chiral crown ethers $\mathbf{25}_{SS}$ and $\mathbf{23}_{RRRR}$ bind the (*R*)-enantiomers of the selected guests more strongly than the (*S*)-enantiomers. In contrast to $\mathbf{23}_{RRRR}$, crown ether $\mathbf{26}_{SSSS}$ shows no chiral differentiation. This result is rationalized in terms of structural complementarity of the relevant host–guest complex ions. The larger size of the crown ring and the accompanying shift of the attached phenyl groups (chiral barriers) result in looser intermolecular complementarity with the guest ammonium ion, even if a sterically bulky naphthyl unit exists.

The studies discussed in this section use M_S in order to compare chiral recognition as it occurs in a medium (a solvent in ESI-MS, a matrix in FAB-MS). Although one might argue that the only difference is the stereochemistry and, thus, the solvent and the ionization conditions should not have a distinct influence, the differences between FAB- and ESI-determined chiral selectivity should be a clear warning. Consequently, clear-cut determinations of intrinsic chiral recognition in the gas phase must rely on true gas-phase equilibrium and kinetic studies. Such investigations with hosts **24** and, among others, **30** and **31** as guests have been performed [102,103]. Both procedures in Eqs. (24)–(29) were used in these studies. The protonated host ions were generated in the ESI source of a FT-ICR mass spectrometer and were allowed to react with the chiral amine and an achiral reference until equilibrium was reached. A second experiment with the other enantiomer of the chiral guest provides the chiral selectivity factor, $RPI_R/RPI_S = [C \cdot M_R]^+/[C{\cdot}M_S]^+$ as defined in Eqs. (26) and (29), wherefrom the difference in the free energies of binding for the two guests can be estimated.

Table 6
Chiral selectivity factors $RPI_R/RPI_S = [C{\cdot}M_R]^+/[C{\cdot}M_S]^+$ (Eq. (26)) for diasteremomeric complexes between crown ethers and alkylammonium ions (C_{ref} = **27**).

C	M	$RPI_R/RPI_S = [C{\cdot}M_R]^+/[C{\cdot}M_S]^+$
$\mathbf{25}_{SS}$	**32**	1.0
$\mathbf{25}_{SS}$	**31**	1.2
$\mathbf{25}_{SS}$	**30**	1.1
$\mathbf{25}_{SS}$	**33**	0.9
$\mathbf{23}_{RRRR}$	**31**	1.2
$\mathbf{23}_{RRRR}$	**33**	1.5
$\mathbf{26}_{SSSS}$	**31**	1.0
$\mathbf{26}_{SSSS}$	**33**	1.1

The procedure has been applied to the gas-phase exchange equilibria of ligands **30** between chiral $\mathbf{24}_{SS}$ and the achiral 18-crown-6, as reference (C_{ref}) [102]. The achiral crown ether C_{ref} displays an affinity for ligands **30** which is higher than that of the chiral crown ether $\mathbf{24}_{SS}$. The equilibrium constants for reaction (26) with ligands $\mathbf{30}_R$ and $\mathbf{30}_S$ amount to 130 ± 15 and 567 ± 68, respectively, which correspond to a difference of 1.0 ± 0.1 kcal mol^{-1} between the stability of the heterochiral [$\mathbf{24}_{SS}{\cdot}\mathbf{30}_R$] complex and the homochiral [$\mathbf{24}_{SS}{\cdot}\mathbf{30}_S$] one. This stability difference is greater than that measured in methanol solution (0.5 kcal mol^{-1}), but similar to that seen in CD_2Cl_2 (1.1 kcal mol^{-1}) [104]. This provides experimental support to the concept that solvation moderates those short-range intracomplex forces that play a major role in chiral discrimination, such as the π–π stacking interactions between guests **30** and the host $\mathbf{24}_{SS}$.

With the same methodology, it was possible to quantify the gas-phase exchange equilibria of the (*R*)-enantiomer of the chiral amines (M_R), i.e., $\mathbf{34}_R$, $\mathbf{35}_R$, $\mathbf{14}_R$, $\mathbf{36}_R$ and with protonated $\mathbf{24}_{SS}$ or its (*R*,*R*)-enantiomer ($\mathbf{24}_{RR}$) (Plate 9) [103]. One of the selected chiral amines was introduced together with a reference achiral amine (M_{ref}), i.e., **37** or **38**, into the FT-ICR cell, where they react with $[H{\cdot}\mathbf{24}_{SS}]^+$ or $[H{\cdot}\mathbf{24}_{RR}]^+$ to form the corresponding

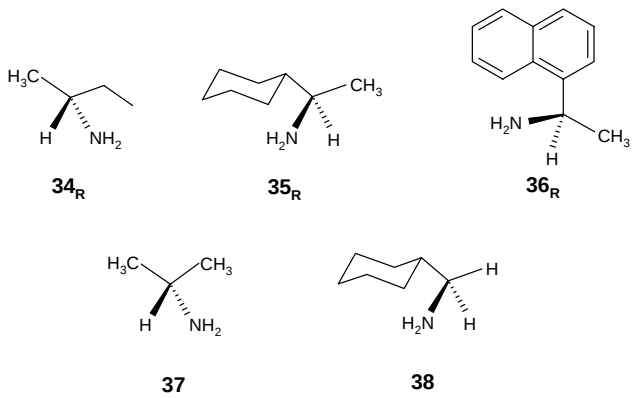

Plate 9.

$[M_R{\cdot}H{\cdot}\mathbf{24}_{SS}]^+$ and $[M_R{\cdot}H{\cdot}\mathbf{24}_{RR}]^+$ adducts. The equilibrium constant for the exchange of the chiral and the achiral amine guests Eq. (29) was determined from the relevant $RPI_S = [M_R \cdot H \cdot \mathbf{24}_{SS}]^+/[M_R{\cdot}H{\cdot}M_{ref}]^+$ and $RPI_R = [M_R \cdot H \cdot \mathbf{24}_{RR}]^+/[M_R{\cdot}H{\cdot}M_{ref}]^+$ ratios and the enantioselectivity of the process was inferred from their $RPI_R/RPI_S = [M_R \cdot H \cdot \mathbf{24}_{RR}]^+/[M_R{\cdot}H{\cdot}\mathbf{24}_{SS}]^+$ ratios. As observed before, binding of the guest with the absolute configuration opposite to that of the stereocenters of the host is invariably preferred. The enantiomeric preference of $[H{\cdot}\mathbf{24}_{SS}]^+$ or $[H{\cdot}\mathbf{24}_{RR}]^+$ towards M_R is expressed by the relevant $\Delta\Delta G^\circ = \Delta G^\circ([M_R \cdot H \cdot \mathbf{24}_{RR}]^+) - \Delta G^\circ([M_R \cdot H \cdot \mathbf{24}_{SS}]^+)$ terms which amount to 0.07 ± 0.10 kcal mol^{-1} ($M_R = \mathbf{34}_R$), 0.21 ± 0.05 kcal mol^{-1} ($M_R = \mathbf{35}_R$), 0.57 ± 0.12 kcal mol^{-1} ($M_R = \mathbf{14}_R$), and 0.84 ± 0.14 kcal mol^{-1} ($M_R = \mathbf{36}_R$). This trend corroborates the hypothesis that the stacking interactions between the guest and the host as well as the steric hindrance to complexation represent main intrinsic factors for chiral recognition.

With $M_{ref} = \mathbf{38}$, the data for various enantiomeric mixtures of **36** display a linear relationship between RPI_R/RPI_S and *ee*. Enantiomeric impurities as small as about 2% can currently be detected with this method [105]. Variable-temperature FT-ICR-MS measurements of the ligand exchange equilibria on the diastereomeric complexes $[M_R{\cdot}H{\cdot}\mathbf{24}_{SS}]^+$and $[M_R{\cdot}H{\cdot}\mathbf{24}_{RR}]^+$ ($M_R = \mathbf{14}_R$ or $\mathbf{36}_R$) by $M_{ref} = \mathbf{38}$ allowed to establish the enthalpy and entropy contribution to their thermodynamic stability [106]. The heterochiral $[M_R{\cdot}H{\cdot}\mathbf{24}_{SS}]^+$ complexes appear more stable than the homochiral $[M_R{\cdot}H{\cdot}\mathbf{24}_{RR}]^+$ complexes by: -1.6 ± 0.2 kcal mol^{-1} ($M_R = \mathbf{14}_R$); -2.4 ± 0.3 kcal mol^{-1} ($M_R = \mathbf{36}_R$). Entropy disfavors the heterochiral complexes by -3.5 ± 0.5 cal mol^{-1} K^{-1} ($M_R = \mathbf{14}_R$) and by -4.8 ± 0.9 cal mol^{-1} K^{-1} ($M_R = \mathbf{36}_R$). Enthalpy–entropy compensation is evident. Although theoretical calculations correctly conform to the observed heterochiral > homochiral stability trend, nevertheless they failed to reproduce the experimental finding that enantiodiscrimination of **36** is greater than that of **14**.

Cyclodextrins (CDs) are a group of cyclic oligosaccharides composed of α(1,4)-linked glucopyranose units. The most common have six, seven, and eight units with the common names α-, β-, and γ-CD, respectively. The utility of CDs stems from their truncated-cone molecular shape with a sizable inner cavity (Plate 10). In water, CDs are believed to form inclusion complexes that are mostly stabilized by hydrophobic interactions between the unpolar surface inside the CD cavity and the surface of the guest. In the gas phase, the energetics that benefit from this arrangement do not exist any more, because there is no water that surrounds the complex. Consequently, there are no benefits from hydrophobic interactions in the gas phase. Rather, van der Waals' forces and, if possible, hydrogen bonding remain. However, the gas-phase complexes are ions, usually positive ions generated by MALDI, FAB, or ESI. For example, the higher basicity of an amino group will lead to the generation of CD complexes with the ammonium form of an amino acid. Strong interactions can be expected for a host with so many hydroxy dipoles that may arrange in a favorable fashion around the cationic guest. For a maximization of the number of such interactions, it is likely that the guest is located inside the cavity to provide a geometrically reasonable fit between guest and cavity. The conclusion from these considerations is that the complexes exist in solution as well as in the gas phase, but for different reasons.

Because of their asymmetry, CDs exhibit chiral effects towards chiral molecules under FAB [107] and MALDI [108] conditions. The main ambiguity of these studies remains regarding the environment in which chiral recognition occurs, whether in the bulk matrix, in the selvedge vaporization region, or in the gas phase. Besides, neither MALDI nor FAB ensure attainment of purely kinetic or equilibrium conditions so as that quantitative interpretation of the MS patterns in terms of relative stability of diastereomeric host/guest intermediates or transition structures is precluded. For this reason, the problem of gas-phase CDs enantioselectivity was tackled by Lebrilla et al. from the kinetic side by using an FT-ICR methodology [9,109]. Protonated β-cyclodextrin/amino acid complexes ($[\beta\text{-MeCD}{\cdot}H{\cdot}A]^+$), isolated in the reaction cell of an FT-ICR instrument, react with gaseous alkylamine (B) to undergo the gas-phase guest-exchange reaction.

$$[\beta\text{-MeCD} \cdot H \cdot A]^+ + B \rightarrow [\beta\text{-MeCD} \cdot H \cdot B]^+ + A \quad (30)$$

The rate of reaction (30) is found to be sensitive to the configuration of the guest A, making β-MeCD a gas-phase chiral selector. Its enantioselectivity, defined by the measured k_D/k_L ratio, is as large as far k_D/k_L is from unit. Table 7 indicates that the β-MeCD enantioselectivity increases with the size of the A side chain (cf. alanine ($k_D/k_L = 0.62$) with valine ($k_D/k_L = 32$), leucine ($k_D/k_L = 0.28$), isoleucine ($k_D/k_L = 0.26$), and *allo*-isoleucine ($k_D/k_L = 0.24$)) [109–111]. A similar trend is observed even when A contains a hydroxyl group in the side chain (cf. HSer, Thr, and AThr with Ser in Table 7). Proline and *cis*-4-hydroxyproline (HPro) exhibit low selectivities because of their rigidity and compactness. Aromatic A with relatively bulky side

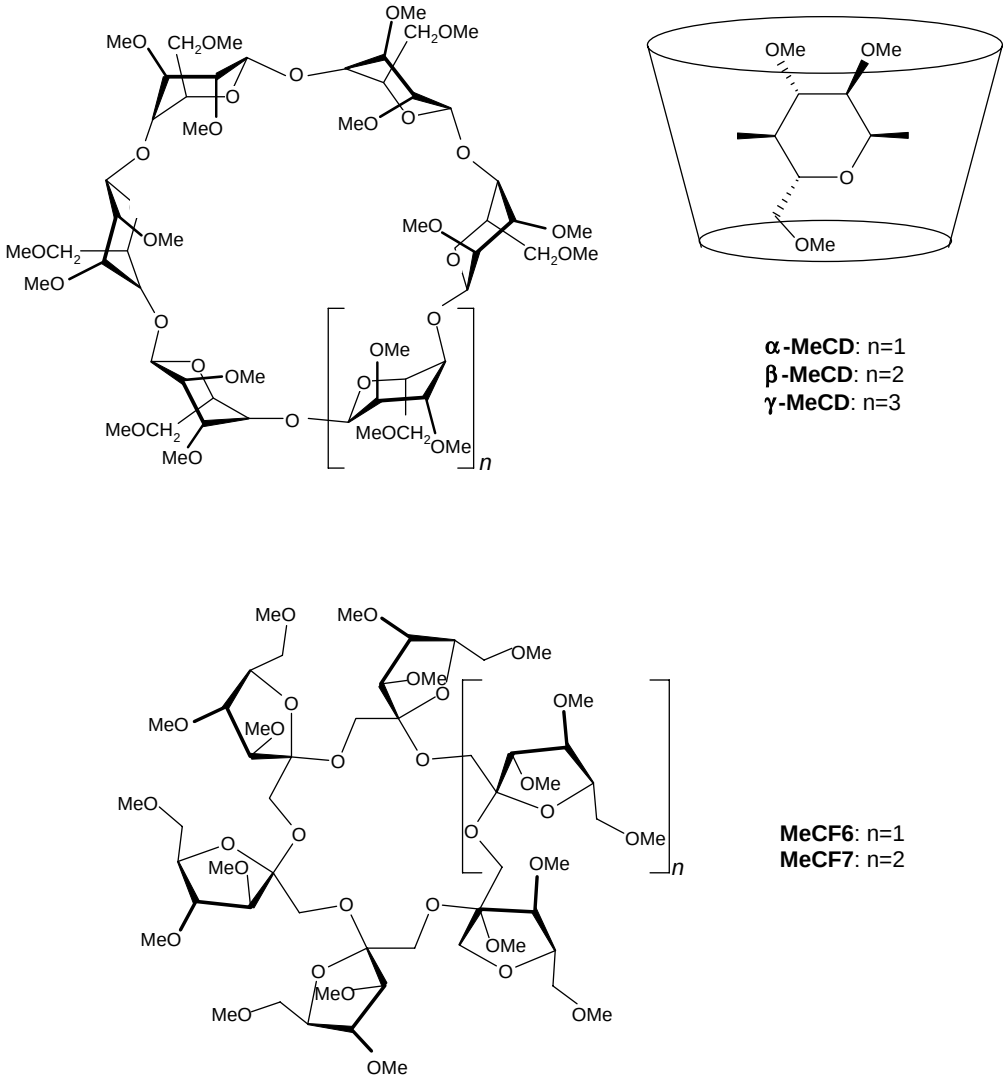

Plate 10.

chains, such as phenylalanine ($k_D/k_L = 1.22$) and tyrosine ($k_D/k_L = 1.49$), exhibit significantly smaller enantioselectivities (open diamonds in Fig. 3). Similar trends are obtained when more basic alkylamines B are used, including 2-butylamine (**34**) and 1-amino-2-propanol [112].

According to molecular modeling [110,111], the different enantioselectivities of Table 7 can be accounted for by the structure of the relevant $[\beta\text{-MeCD}\cdot H\cdot A]^+$ complexes. Leucine, isoleucine, and *allo*-isoleucine with four carbons in the side chain have the optimal size to fit into the β-MeCD cavity, while phenylalanine and tyrosine with seven carbons are too large to fit into the same cavity. Noticeable differences in the interactions of the two enantiomers of A with the β-MeCD host are observed. Chiral differentiation occurs when the access to the protonated amino group of A is limited either by its alkyl side chain or by the methoxy groups of the host that are drawn in by hydrogen-bonding interactions. These differences in binding translate to differences in reaction rates.

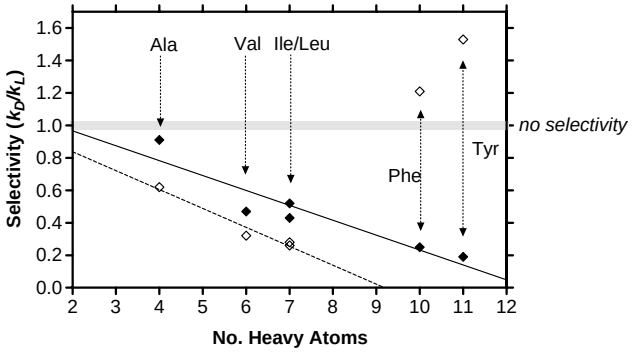

Fig. 3. Plot of the ligand exchange enantioselectivity (k_D/k_L) as a function of the number of non-hydrogen atoms on the amino acid guest. Hosts: permethylated β-CD (open diamonds); permethylated maltoheptaose (full diamonds); reagent base: 1-propylamine.

Table 7
Reaction selectivity of various protonated β-MeCD/amino acid complexes with 1-propylamine (B)

Amino acid (A)	k_L ($\times 10^{11}$ cm^3 molecule^{-1} s^{-1})	k_D/k_L
Ala	2.4	0.62
Cys	3.4	0.45
Glu	0.011	0.53
Ile	1.0	0.26
Alle[a]	1.9	0.24
Leu	0.50	0.28
Met	0.014	2.70
Phe	1.4	1.22
Pro	1.2	0.67
HPro[b]	0.031	0.71
Ser	0.64	0.83
HSer	0.35	0.45
Thr	0.12	1.59
AThr[c]	0.18	0.045
Val	3.1	0.32

[a] *allo*-Isoleucine.
[b] *cis*-4-Hydroxyproline.
[c] *allo*-Threonine.

Phenylalanine behaves differently from valine in β-MeCD. Both L- and D-phenylalanine interact in the same way. In fact, the predominant interaction of both the ammonium and the carboxylic acid group of phenylalanine forces its phenyl group to remain inside the cavity. The similarity in the binding of the two enantiomers is responsible for the observed small enantioselectivity ($k_D/k_L = 1.22$). In contrast, both the ammonium and the carboxylic acid group of L-valine interacts preferentially with the narrow rim of β-MeCD, whereas only the ammonium of D-valine interacts in the same way and its carboxylic acid group interacts preferentially with the wider rim of the host. Such a difference in the binding of the two enantiomers accounts for the observed high (and reverse) enantioselectivity ($k_D/k_L = 0.32$) (open diamonds in Fig. 3).

Additional experiments were performed to examine the role of the molecular size on the host enantioselectivity. Since the methyl groups in β-MeCD orient themselves toward the center of the cavity, it is expected that decreasing the extent of methyl derivatization in β-CD from 21 (β-MeCD) to 14 methyl groups increases the effective size of the cavity [110]. As a matter of fact, the enantioselectivity of valine ($k_D/k_L = 0.32$ with β-MeCD) increases to $k_D/k_L = 0.18$ with 14-methyl-β-CD. No significant effect of the cavity size is observed with the smaller alanine.

Another way to increase the host cavity is by using exchange reactions in γ-MeCD (diameter of the cavity from 7.5 to 8.3 Å) instead of β-MeCD (diameter of the cavity from 6.0 to 6.5 Å) [110]. The larger cavity size of γ-MeCD decreases (and inverts) the enantioselectivity of valine from $k_D/k_L = 0.32$ to $k_D/k_L = 1.14$ and that of isoleucine from $k_D/k_L = 0.26$ to $k_D/k_L = 2.28$. This observation indicates that the three amino acids have optimal enantioselectivity with β-MeCD. Conversely, phenylalanine increases in selectivity from $k_D/k_L = 1.2$ (with β-MeCD) to $k_D/k_L = 1.8$ (with γ-MeCD). This observation suggests that the larger cavity of γ-MeCD allows each enantiomer of the larger amino acid to find more distinct interactions with the larger host.

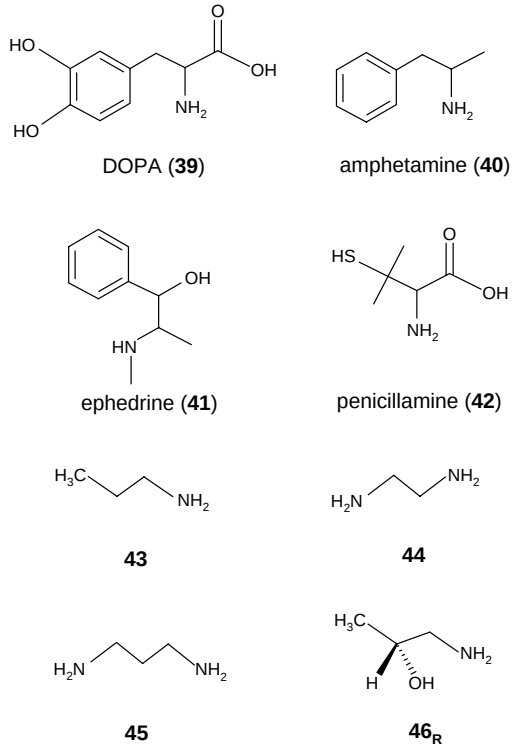

Plate 11.

The gas-phase guest-exchange reaction (30) has been employed to probe the enantioselectivity of β-MeCD for pharmacologically important compounds, such as DOPA (**39**), amphetamine (**40**), ephedrine (**41**), and penicillamine (**42**) (Plate 11) [113]. A variety of alkyl amines B, including 1-propylamine (**43**), ethylene diamine (**44**), 1,3-diaminopropane (**45**), and (*R*)-1-amino-2-propanol (**46**$_R$) have been used as reactants.

The guest exchange kinetic results are reported in Table 8. The presence of more than one reacting [β-MeCD·H·A]$^+$ structure is observed with **39** and **42** as guests ("fast" and "slow" in Table 8). The results have been rationalized in terms of specific interaction in the relevant inclusion complexes which determine their structure and relative stability.

Closely related analogues of cyclodextrins are the cyclofructans (CFs), depicted in Plate 10. Permethylated six ($MeCF_6$) and seven-membered CFs ($MeCF_7$) exhibit an appreciable enantioselectivity towards a number of amino acid isopropyl esters using the FAB-MS-EL (amino ester) guest method [114–116]. The relevant IRIS values are reported in Table 9 and compared with those obtained by using CDs and crown ethers, as selectors. Relative to these, $MeCF_6$ shows a higher enantioselectivity for the esters of tryptophan and *tert*-leucine, while $MeCF_7$ for the esters of phenylglycine, serine, and proline.

Table 8
Selectivities for the β-MeCD host ($k \times 10^{11}$ cm^3 molecule^{-1} s^{-1})

Guest		Alkyl amine			
		43	**46**$_R$	**44**	**45**
39	k_D	$<10^{-15}$	$<10^{-15}$	0.0024	Fast: 0.131; slow: 0.014
	k_L	$<10^{-15}$	0.0047	0.0021	Fast: 0.122; slow: 0.0131
	k_D/k_L	–	–	0.20	Fast: 1.07; slow: 0.46
40	k_D	0.27	1.34	–	–
	k_L	0.40	1.78	–	–
	k_D/k_L	0.68	0.75	–	–
41	$k_{(+)}$	0.031	0.53	–	–
	$k_{(-)}$	–	0.64	–	–
	$k_{(+)}/k_{(-)}$	–	0.83	–	–
42	k_D	Fast: 1.80; slow: 0.55	–	–	–
	k_L	3.4	–	–	–
	k_D/k_L	Fast: 0.53; slow: 0.16	–	–	–

Table 9
$I_R/I_{S\text{-dn}}$ values of permethylated cyclic oligosaccharide hosts with amino acid ester hydrochloride guests

Guest (counterion: Cl^-)	$MeCF_6$	$MeCF_7$	α-MeCD	β-MeCD	γ-MeCD	18-C-6
[Trp-O-Pr^i]$^+$	1.38	1.29	1.29	1.23	1.17	0.98
[Pgly-O-Pr^i]$^+$	0.99	0.76	0.94	0.91	0.89	0.99
[Phe-O-Pr^i]$^+$	1.00	1.01	1.02	1.01	1.00	1.02
[Tle-O-Pr^i]$^+$	1.18	1.00	0.95	0.94	0.93	0.97
[Met-O-Pr^i]$^+$	1.04	0.95	0.91	0.91	0.92	0.96
[Ser-O-Pr^i]$^+$	1.01	1.18	0.95	1.15	0.99	0.96
[Pro-O-Pr^i]$^+$	1.08	1.16	1.07	1.07	1.14	0.96
[Gly-O-Pr^i]$^+$	1.01	0.99	0.97	0.98	–	0.99

The maltose-based oligomers are exact linear analogues of CDs. For example, maltoheptaose is composed of seven α(1–4)-linked sugar units such as β-MeCD. Its linear chain is sufficiently flexible to wrap around guest molecules and form "quasi-inclusion" complexes in the gas phase [112].

Phenomenological chiral discrimination of various permethylated linear oligosaccharides toward organic amines has been examined by using the FAB-MS-EL guest method [116–119]. As shown in Table 10, permethylated fructo-oligosaccharides, especially the permethylated 1^F-fructonystose (MeFruNys in Plate 12), display a remarkable chiral discrimination ability [117]. If compared to $MeCF_6$ [115,120,121], linear permethylated fructo-oligosaccharides exhibit a much greater enantioselectivity due to their low molecular symmetry and high flexibility. The dynamic conformation changes of linear fructo-oligosaccharides emphasize the difference in the host–guest complex stability.

Along this line, several new linear hosts and flexible cyclic hosts having a C_2-symmetry axis (bisDPGP, bisTAGP, and bisTMGP; Plate 12) have been designed and synthesized based on the structural feature of the highly selective MeFruNys [122]. However, these tailor-made flexible hosts prove less effective than MeFruNys as chiral selector (Table 10).

Exchange experiments of amino acids "wrapped" in permethylated linear oligosaccharides were carried out in an ESI-FT-ICR instrument [112]. Table 11 lists the k_D/k_L values for the exchange reactions of a selected group of amino acids complexed to permethylated maltoheptaose and

Table 10
Chiral discrimination ability ($I_R/I_{S\text{-dn}}$ values) of permethylated cyclic and acyclic oligosaccharide hosts toward amino acid 2-propyl ester salts

Guest	MeKes	MeNys	MeFruNys	$MeManFru_3$	$MeGlc^6Fru_3$	$MeSorFru_3$	$MeCF_6$	bisDPGP	bisTAGP	bisTMGP
[Ala-O-Pr^i]$^+$	1.11	1.16	0.45	1.09	0.60	0.80		1.43	1.46	1.40
[Val-O-Pr^i]$^+$	1.19	0.87	0.14	0.84	0.49	0.51		0.85	1.39	1.18
[Met-O-Pr^i]$^+$	1.18	1.54	0.28	1.28	0.79	0.83	1.04	1.33	1.50	1.27
[Phe-O-Pr^i]$^+$	1.15	1.08	0.18	0.98	0.64	0.67	1.00	1.78	1.88	0.85
[Trp-O-Pr^i]$^+$	1.18	1.28	0.56	1.25	0.84	0.77	1.38	2.64	2.09	1.91
[Pro-O-Pr^i]$^+$	1.16	1.19	1.23	1.06	1.16	1.16	1.08	1.98	1.77	1.09
[Pgly-O-Pr^i]$^+$	0.93	1.56	0.26	1.20	0.79	0.72	0.99	0.76	0.96	0.55
[Tle-O-Pr^i]$^+$	1.23	0.85	0.33	0.98	0.40	0.40	1.18	1.03	1.57	1.63

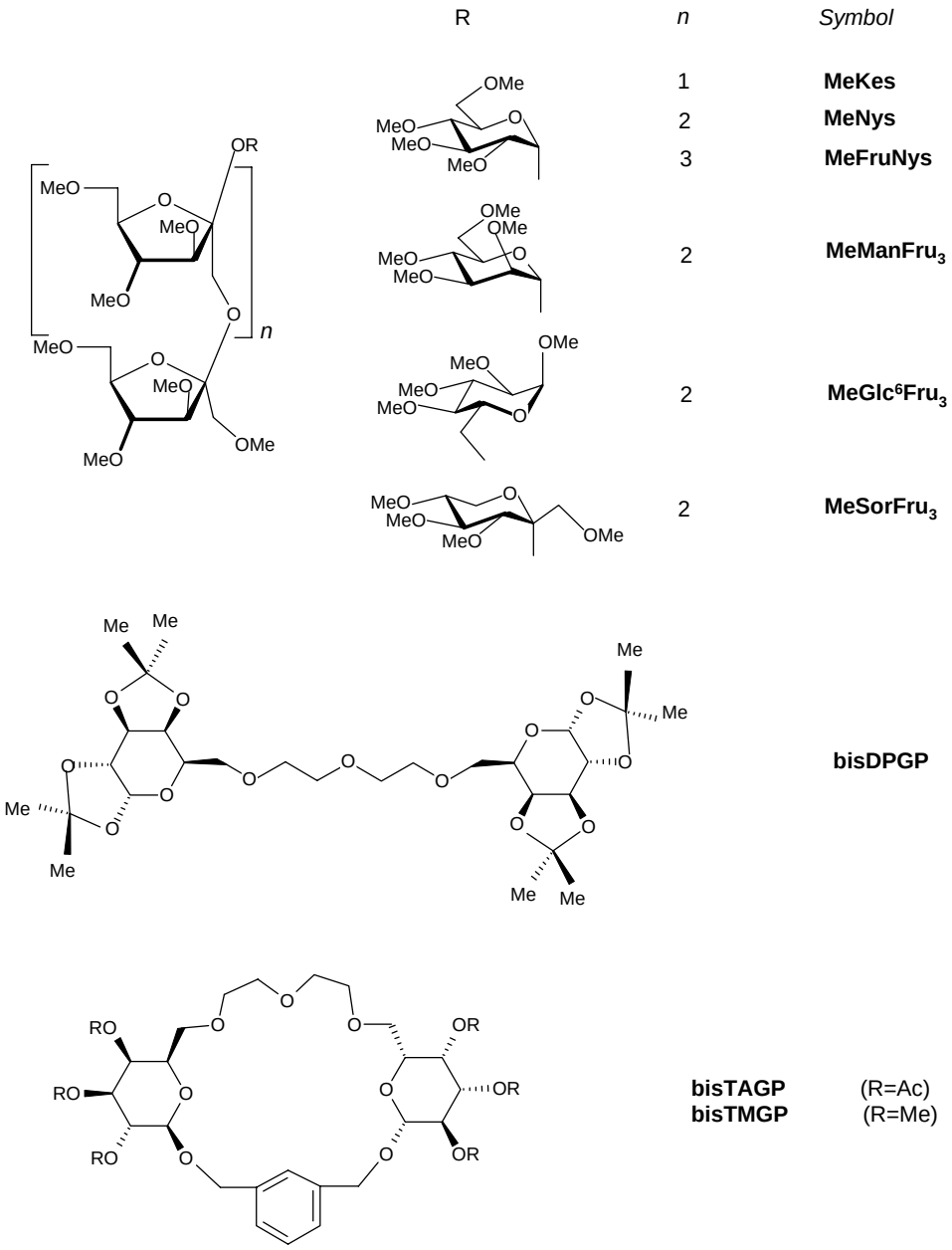

Plate 12.

reacted with **43**. The enantioselectivities of the exchange reactions are slightly less that those with β-MeCD for most amino acids. However, the same trend is observed as a function of the side-chain size of the guests. Remarkably, the reaction on the maltoheptaose complexes with tyrosine and phenylalanine exhibits a significantly greater enantioselectivity relative to β-MeCD. For example, the k_D/k_L value for phenylalanine decreases from 1.21 with β-MeCD to 0.25 with maltoheptaose. Using this latter as host, a linear plot is now obtained for k_D/k_L as a function of the A side chain (full diamonds in Fig. 3).

Molecular modeling calculations give important insight into the origin of such observation. Unlike the rigid β-MeCD, the linear maltoheptaose allows each enantiomer of phenylalanine to find the most favorable conformation. The phenyl group of L-phenylalanine is oriented towards the C6 center of the hosts, while that of D-phenylalanine is oriented towards the C2 and C3 centers of the hosts. Smaller linear hosts, such as maltohexaose and maltopentaose, show lower enantioselectivities (Table 11). Molecular modeling calculations predict that these hosts are too small to fully envelop the guest and create an environment for high enantioselectivity.

Calixarene and their resorcinarene relatives are similar to CDs with respect to their ability to form a concave cavity in which guests can bind. Calixarenes are conformationally more flexible than the resorcinarenes and, depending on the substituents attached to their wider upper rim or to the

Table 11
Rate constants ($k \times 10^{11}$ cm^3 molecule^{-1} s^{-1}) and selectivities (k_D/k_L) of selected amino acids with β-MeCD and linear permethylated oligosaccharides

Amino acids		β-MeCD	Met-heptaose	Met-hexaose	Met-pentaose
Ala	k_D	1.5	3.1	–	3.9
	k_L	2.4	3.4	–	4.2
	k_D/k_L	0.62	0.91	–	0.93
Val	k_D	1.1	1.6	–	3.1
	k_L	3.4	3.4	–	3.2
	k_D/k_L	0.32	0.47	–	0.97
Ile	k_D	0.26	1.3	–	1.1
	k_L	1.0	3.0	–	1.6
	k_D/k_L	0.26	0.43	–	0.69
Leu	k_D	0.14	1.3	2.1	0.85
	k_L	0.50	2.5	2.9	1.5
	k_D/k_L	0.28	0.52	0.72	0.57
Phe	k_D	1.7	0.14	0.89	0.69
	k_L	1.4	0.63	1.1	0.86
	k_D/k_L	1.21	0.25	0.81	0.77
Tyr	k_D	0.029	0.005	–	–
	k_L	0.019	0.026	–	–
	k_D/k_L	1.53	0.19	–	–

narrower lower rim, they may exist in a highly-symmetric bowl-shaped, so-called cone conformation or in several other conformations that do not exhibit an as perfect cavity as does the cone conformation (Plate 13). Cationic guests, such as alkali metal or ammonium ions, bind quite strongly inside the cavity mostly by electrostatic interactons with the n- or π-centers of the host.

Chiral recognition by calixarenes in the gas phase is virtually unknown [123–125]. To date, only a few very recent gas-phase studies on this subject can be retrieved from the literature, including, (i) a gas-phase study on the displacement of several amino acids A from the chiral amino [4] resorcinarene **49** (Plate 13) carried out by Speranza and coworkers using an electrospray-ionization Fourier-transform ion cyclotron resonance (ESI-FT-ICR) mass spectrometer [126,127], and (ii) Lebrilla and coworkers' study on the ability of the achiral calix[4]arene **47** and calix[6]arene **48** to form inclusion complexes with natural amino acids under matrix-assisted laser desorption ionization (MALDI) conditions [124].

$$[\mathbf{49} \cdot \mathrm{H} \cdot \mathrm{A}]^+ + \mathrm{B} \rightarrow [\mathbf{49} \cdot \mathrm{H} \cdot \mathrm{B}]^+ + \mathrm{A} \quad (31)$$

The molecular asymmetry of **49** is due to the four axial pendants containing the chiral L-valine group. The efficiency of the phase exchange reaction (31), where A are representative amino acids and B is either (*S*)-(+)-(**34**$_S$) or (*R*)-(−)-2-butylamine (**34**$_R$) is appreciably affected by the configuration of both A and B. The guest exchange kinetic results are reported in Table 12. The presence of more than one reacting $[\mathbf{49}{\cdot}\mathrm{H}{\cdot}\mathrm{A}]^+$ structure is observed with A = **39**. A similar behavior was observed with β-MeCD as the host [113].

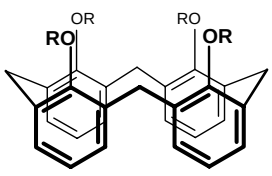

47

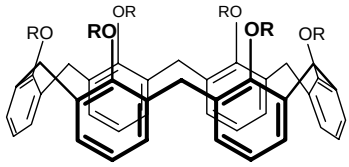

48

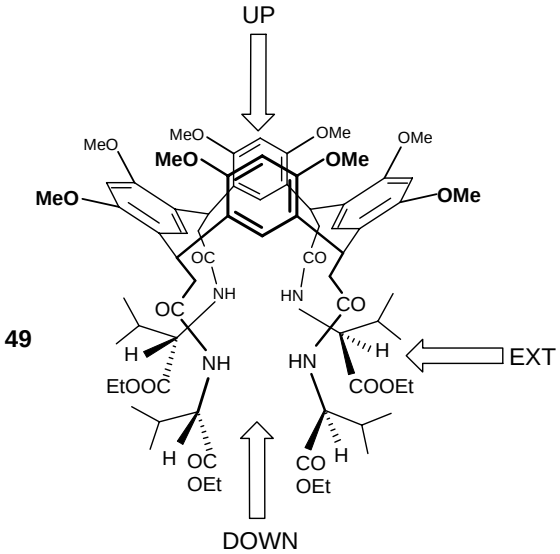

49

Plate 13.

Table 12
Rate constants of the displacement reaction (31)[a]

Amino acid (A)	PA (*A*) (kcal mol^{-1})	(*R*)-(−)-$C_4H_9NH_2$ (**34**$_R$)		(*S*)-(+)-$C_4H_9NH_2$ (**34**$_S$)		S_B	Reaction efficiency	
		k_R[a]	$S_A{}^R$	k_S[a]	$S_A{}^S$		k_R/k_{coll}	k_S/k_{coll}
D-Ala	215.5[b]	7.69 ± 0.12	1.52 ± 0.05	7.06 ± 0.11	1.20 ± 0.04	1.09 ± 0.03	0.69	0.63
L-Ala		5.05 ± 0.10		5.89 ± 0.09		0.86 ± 0.03	0.45	0.53
D-Ser	218.6[c]	4.59 ± 0.06	0.67 ± 0.02	3.70 ± 0.06	0.49 ± 0.01	1.24 ± 0.05	0.41	0.34
L-Ser		6.87 ± 0.05		7.56 ± 0.06		0.91 ± 0.02	0.62	0.68
D-Leu	218.6[b]	3.76 ± 0.02	1.33 ± 0.02	4.68 ± 0.05	1.29 ± 0.05	0.80 ± 0.02	0.34	0.42
L-Leu		2.82 ± 0.02		3.64 ± 0.10		0.77 ± 0.03	0.25	0.32
D-DOPA	221.0[d]	2.28 ± 0.06	0.76 ± 0.04	1.26 ± 0.05	0.69 ± 0.11	1.81 ± 0.12	0.20	0.11
L-DOPA		3.00 ± 0.09		1.82 ± 0.20		1.65 ± 0.24	0.27	0.16
D-DOPA		0.073 ± 0.008	0.73 ± 0.14	0.064 ± 0.008	0.81 ± 0.19	1.14 ± 0.28	0.006	0.006
L-DOPA		0.100 ± 0.008		0.079 ± 0.009		1.27 ± 0.25	0.009	0.007
D-Pro	224.9[e]	1.51 ± 0.01	0.92 ± 0.01	1.38 ± 0.02	0.92 ± 0.03	1.09 ± 0.03	0.13	0.12
L-Pro		1.64 ± 0.01		1.50 ± 0.03		1.09 ± 0.03	0.15	0.14
D-Pip	225.6[e]	0.147 ± 0.002	0.91 ± 0.02	0.117 ± 0.002	0.74 ± 0.04	1.26 ± 0.04	0.013	0.010
L-Pip		0.161 ± 0.003		0.157 ± 0.003		1.02 ± 0.04	0.014	0.014

[a] $k \times 10^{-10}$ cm^3 molecule^{-1} s^{-1}.
[b] P.B. Armentrout, J. Am. Soc. Mass Spectrom. 11 (2000) 371.
[c] http://webbook.nist.gov/chemistry/name-ser.html.
[d] Taken as equal to the PA of tyrosine.
[e] A.F. Kuntz, A.W. Boynton, G.A. David, K.E. Colyer, J.C. Poutsma, J. Am. Soc. Mass Spectrom. 13 (2002) 72.

The results of Table 12 indicate that the efficiency of the gas-phase exchange reaction (31) is affected by the nature and the configuration of both the amino acid guest (k_D/k_L) and the configuration of the amine B (k_R/k_S). The emerging selectivity picture, discussed in the light of molecular mechanics and molecular dynamics calculations, points to chiral recognition by **49** as determined by the effects of the host asymmetric frame upon the structure, stability, and rearrangement dynamics of the diastereomeric [**49**·H·A]$^+$ complexes and the orientation of the amine reactant B in the encounters with [**49**·H·A]$^+$. Indeed, docking (MM) and molecular dynamics (MD) calculations on several [**49**·H·A]$^+$ (A = aianine, serine, and DOPA) complexes points to three regions of the host as most suited for hosting the amino acid A, i.e., (i) inside the achiral upper tim cavity (UP); (ii) among the four chiral pendants in correspondence of its chiral lower rim cavity (DOWN); and (iii) in the external position in proximity of two adjacent pendants (EXT) (Plate 13).

MD simulations on low-energy [**49**·H·A]$^+$ (A = alanine) docking geometries point to EXT as the thermodynamically most favored structures at room temperature. The relevant diastereomeric structures are almost equally stable. Therefore, the observed enantioselectivity has to be attributed to specific stabilization of the exchange transition structures. In this view, the small effects of the configuration of B (k_R/k_S in Table 12) indicates that the B amine displaces alanine from the relevant EXT structure without getting completely into the chiral cavity of the host.

Docking and molecular dynamics calculations on [**49**·H·A]$^+$ (A = serine) complexes point to DOWN as the most favored hosting region for both L- and D-serine, although the complex with L-serine is ca. 6 kcal mol^{-1} less stable than with D-serine. In addition, while DOWN with D-serine persists unchanged up to 20 ns, that with L-serine rearranges to the quasi-degenerate EXT within the same lapse of time. Accordingly, the pronounced effect of the serine configuration on the exchange reaction (31) (k_D/k_L in Table 12) is accounted for by the greater stability of $[\mathbf{49} \cdot \mathrm{H} \cdot \mathrm{A}]^+_{\mathrm{DOWN}}$ (A = D-serine) relative to $[\mathbf{49} \cdot \mathrm{H} \cdot \mathrm{A}]^+_{\mathrm{EXT}}$ (A = L-serine). This latter complex exhibits a limited effect of the B configuration (k_R/k_S in Table 12), much like that measured with the $[\mathbf{49} \cdot \mathrm{H} \cdot \mathrm{A}]^+_{\mathrm{EXT}}$ (A = alanine) complexes. This coincidence reflects a common exchange mechanism in which amine B pushes away the guest A from EXT without getting completely into the chiral cavity of the host. In contrast, the comparatively large effect of the B configuration on the slower reaction between B and $[\mathbf{49} \cdot \mathrm{H} \cdot \mathrm{A}]^+_{\mathrm{DOWN}}$ (A = D-serine) (Table 12) reflects the involvement of a more congested, higher-energy transition structures with B partially inside the host chiral cavity while pushing D-serine away from it.

MC/MD simulations on $[\mathbf{49} \cdot \mathrm{H} \cdot \mathrm{A}]^+_{\mathrm{DOWN}}$ (A = DOPA) complexes indicate that DOPA, irrespective of its configuration, can be permanently trapped not only into the chiral DOWN region of the host, but also onto its achiral UP region. The relevant diastereomeric structures are almost equally stable, with the DOWN structures ca. 5 kcal mol^{-1} more stable than the UP ones. This computational result is consistent with the formation of more than one reacting [**49**·H·A]$^+$ (A = DOPA) structures, the most reactive corresponding to UP and the less reactive to DOWN. The UP structure displays the highest effect of the B configuration (k_R/k_S in

Table 12). This implies that the B amine must get completely inside the empty chiral cavity of $[\mathbf{49} \cdot H \cdot A]^+_{UP}$ (A = DOPA) to displace the guest. In contrast, the slower exchange reaction with $[\mathbf{49} \cdot H \cdot A]^+_{DOWN}$ (A = DOPA) exhibits a much smaller effect of the B configuration which is similar to that accompanying the reaction with $[\mathbf{49} \cdot H \cdot A]^+_{DOWN}$ (A = D-serine). This observation indicates the involvement of a congested, high-energy transition structures with B not fully inserted into the host chiral cavity which, therefore, may exert only in part the effects of its asymmetry toward it. The above results represent the first attempt to a dynamic model of chiral recognition of biomolecules by enzyme mimics in the unsolvated state.

Chiral recognition of phenylglycine methyl ester by antibiotic host nonactine **50** and monensin methyl ester **51** (Plate 14) was detected and evaluated using the FAB-MS-EL (amino ester) guest method [91]. The relevant IRIS = 0.54 value was essentially on the same line

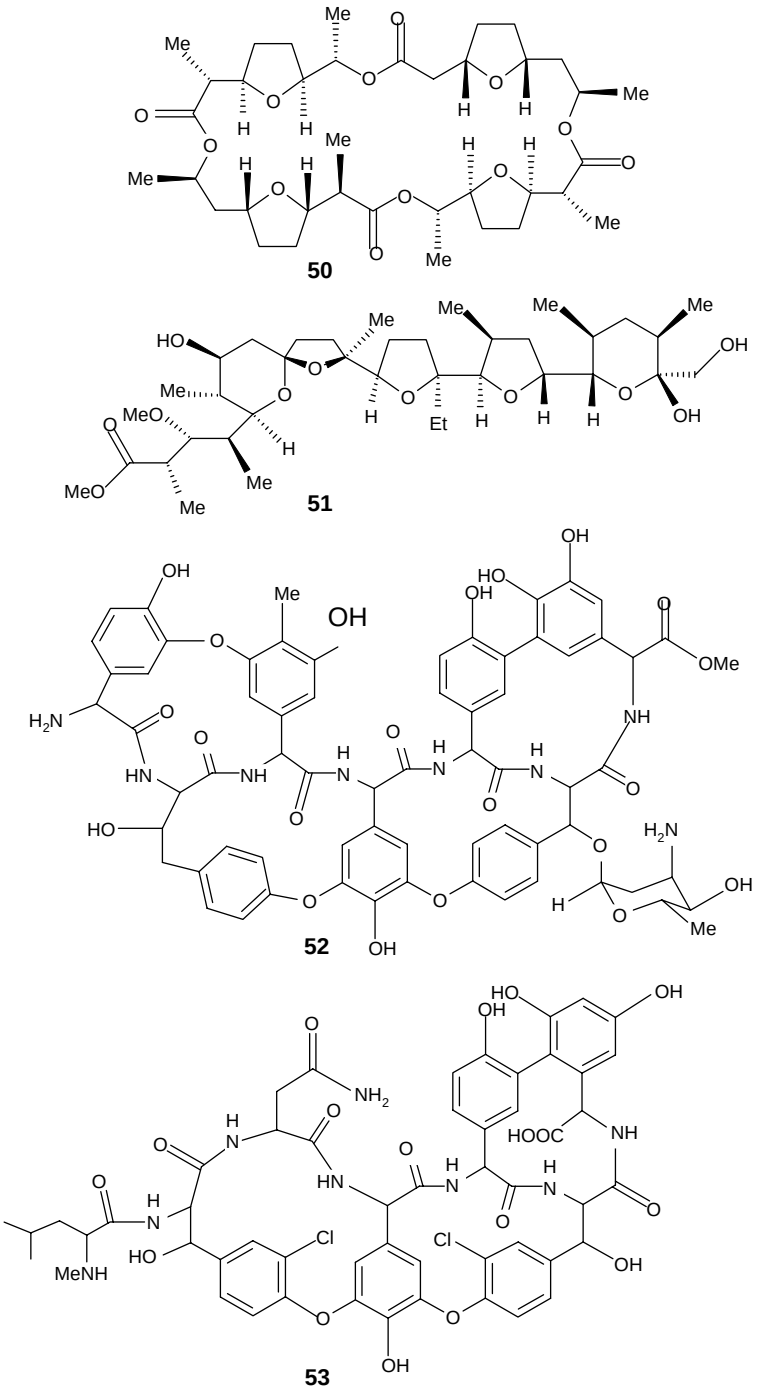

Plate 14.

as the results derived independently from the ion-selective electrode method in water [128]. No distinct selectivity of the aglycones of ristocetin A **52** and vancomycin **53** has been observed toward the cell wall analog peptide *N*-acetyl-D-ala-D-ala and *N*-acetyl-L-ala-L-ala [129]. The same study has been repeated by using the ESI-MS^2-EL (amino ester) guest method [130]. CID experiments have been carried out to probe the gas-phase stability of isomeric 1:1 noncovalent complexes formed between vancomycin and tripeptide stereoisomers. In the negative ion mode, the CID results show that a complex between vancomycin and ligands with the (−)-L-Ala-L-Ala terminus dissociate more readily than a complex formed between vancomycin and ligands with the (−)-L-Ala-L-Ala terminus. The difference in gas-phase stability is in agreement with what would be expected if the noncovalent complexes had retained their structural specific interactions from living cells to the gas phase. In positive ion mode, no significant difference in the gas-phase stabilities of the isomeric complexes is observed. This is attributed to protonation of the C-terminus of the peptide ligand which destroys the specific interaction between antibiotic and peptide ligand.

The proton transfer from multiply charged [cytochrome $c]^{n+}$ (n = 7–9) to (*S*)-(+)-(**34**$_S$) or (*R*)-(−)-2-butylamine (**34**$_R$) show significant enantioselectivity [131,132]. Ions [cytochrome $c]^{n+}$ (n = 7–9) were produced by ESI and introduced into the analyzer cell of a FT-ICR containing an alkylamine, i.e., **34**$_S$, **34**$_R$, **43**, or tert-butylamine (**54**). Rate constants for the proton transfer are listed in Table 13.

Proton transfer to **34**$_R$ is invariably faster than that to **34**$_S$, irrespective of the charge state of cytochrome *c*. In any instances, the reaction is very inefficient (0.1–0.001%) due to the endoergonicity of the process and the large steric interactions in the corresponding transition structures. The decay of the [cytochrome $c]^{9+}$ ions with reaction time is best represented by a single rate constant, while that of the [cytochrome *c*] (n = 7, 8) ions is best represented by two rate constants ("fast" and "slow" in Table 13). This is indicative of a single conformer for [cytochrome $c]^{9+}$ and of two conformers for [cytochrome $c]^{n+}$ (n = 7, 8) [133]. The relative amounts of these conformers (percent in Table 13) are the same for **34**$_S$ and **34**$_R$. (*S*)-2-Butylamine **34**$_S$ exhibits decreasing reactivity with decreasing n, as expected from purely Coulombic considerations. In this regard, **43** and **54** behave in the same manner. With **34**$_R$, the rate constant with n = 9 and the highest rates with n = 7, 8 are approximately equal, suggesting a possible reactive site for the three charged states. Comparison of the rate constants of Table 13 indicates that **43** is approximately as reactive as **34**$_S$, despite the 1.6 kcal mol^{-1} lower basicity. Toward [cytochrome $c]^{n+}$ (n = 8, 9), **54** is one order of magnitude less reactive than **43**, despite the 2.9 kcal mol^{-1} higher basicity. These findings are interpreted in terms of the strong influential role of steric effects in the highly specific arrangement of the alkylamine toward the multiply charged protein.

3. Enantioselectivity in chiral ion–molecule reactions

As pointed out above, MS is the tool of choice for determining the intrinsic factors affecting the stability of diastereomeric INC in the gas phase and for evaluating how much they can be influenced by solvation in the condensed phase. The next step is to determine the factors governing the evolution of diastereomeric INC to products and their sensitivity to environmental conditions (kinetic enantioselectivity).

MS normally operates at extremely low pressures, i.e., under conditions approaching the collision-free limit and thus ensuring against radiationless dispersal of the INC internal energy acquired in its formation. It is this energy which is used to overcome the INC → products activation barrier.

3.1. Stereospecific nucleophilic substitutions

Nucleophilic substitution is a cornerstone reaction of organic chemistry studied for more than 100 years [134]. Remarkable progress has been made in the 20th century in unveiling how this reaction occurs A major contribution is due to gas-phase studies which provided the deepest insight into the mechanistic details of a reaction normally conducted in solution. In addition, these studies revealed the critical effects of the solvent not only on the reaction coordinate but

Table 13
Rate constants for the proton transfer from [cytochrome $c]^{n+}$ (n = 7–9) to alkylamines[a]

[Cytochrome $c]^{n+}$		**34**$_R$ (GB, 211.7)		**34**$_S$ (GB, 211.7)		**43** (GB, 210.1)	**54** (GB, 213.0)
n	Type	k_R[b]	Percent	k_S[b]	Percent	k[b]	k[b]
9		1.5 ± 0.3 (−11)		2.5 ± 0.2 (−12)		2.2 (−12)	6.1 (−13)
8[c]		2.3 ± 0.5 (−12)		4.6 ± 1.1 (−13)		2.9 (−13)	3.8 (−14)
8	Fast	1.0 ± 0.3 (−11)	45	1.9 ± 0.4 (−12)	46	3.1 (−13)	3.7 (−13)
8	Slow	1.4 ± 0.l (−12)	55	3.7 ± 1.0 (−13)	54		
7[c]		2.3 ± 0.1 (−13)		8.4 ± 3.6 (−14)		7.2 (−14)	
7	Fast	1.1 ± 0.1 (−11)	21	1.4 ± 0.3 (−12)	30	1.4 (−13)	5.1 (−14)
7	Slow	1.3 ± 1.11 (−13)	79	1.4 ± 1.9 (−13)	70		

[a] k in cm^3 molecule^{-1} s^{-1}.
[b] The figures in parentheses refer to the power of 10. GB, gas-phase basicity (kcal mol^{-1}).
[c] Further reaction of the lower charged state arising from proton transfer.

also on the actual topography of the PES [135]. The most serious limitation of MS studies in this area is the almost complete lack of information on the stereochemistry of the process and the structure of their neutral products. For these reasons, most of the gas-phase investigations on the mechanism of nucleophilic substitutions have been carried out using alternative experimental techniques, such as stationary radiolysis or electron bombardment flow (EBF) radiolysis, which allow for the isolation of the reaction products and their structural identification.

The first MS contribution in this area was provided by a sophisticated trapped ICR experiment by Lieder and Brauman [136], who elucidated the stereochemistry of a single negative-ion substitution reaction between Cl^- and *cis*- and *trans*-4-bromocyclohexanols. Identification and structural discrimination of the substituted neutral products, i.e., *cis*- and *trans*-4-chlorocyclohexanols, were based on their positive-ion pattern after switching the apparatus from negative to positive ion mode. The results indicate that nucleophilic Cl-to-Br displacement on *cis*-4-bromocyclohexanol involves 91 ± 14% inversion of configuration, whereas the same reaction on *trans*-4-bromocyclohexanol involves 86 ± 19% inversion of configuration.

The pronounced stereoselectivity of gas-phase nucleophilic substitutions was found helpful for discriminating the enantiomeric and diastereomeric forms of menthols ((1*R*,2*S*,5*R*)-(−)-**55**, (1*S*,2*R*,5*S*)-(+)-**55**, and (1*R*,2*R*,5*S*)-(−)-**55** in Plate 15) by reaction with (*S*)-2-amino-l-butanol (**56**$_S$) under CIMS conditions [137]. Self-protonation of **56**$_S$ under CIMS conditions (0.5 Torr, 100 °C) leads to the predominant formation of the corresponding ammonium ion [**56**$_S$·H]$^+$ which is able to react with menthols **55** yielding the corresponding adducts [**55**·H·**56**$_S$]$^+$ and substituted ionic products [(**55**·H·**56**$_S$)-H_2O]$^+$.

The MIKE/CID spectra of the substituted products [(**55**·H·**56**$_S$)-H_2O]$^+$ exhibit an appreciable dependence on the configuration of **55**. The origin of substituted products [(**55**·H·**56**$_S$)-H_2O]$^+$ has been investigated and attributed to a stereospecific bimolecular S_N2 process (33):

$$\mathbf{55} + [\mathbf{56}_S \cdot \mathrm{H}]^+ \leftrightarrows [\mathbf{55} \cdot \mathrm{H} \cdot \mathbf{56}_S]^+ \quad (32)$$

$$[\mathbf{55} \cdot \mathrm{H} \cdot \mathbf{56}_S]^+ + \mathbf{56}_S \rightarrow [(\mathbf{55} \cdot \mathrm{H} \cdot \mathbf{56}_S) - \mathrm{H_2O}]^+ + \mathbf{56}_S + \mathrm{H_2O} \quad (33)$$

The exclusive loss of H_2O from MIKE/CID of [(**55**·H·**56**$_S$)-H_2O]$^+$ indicates that its formation process (33) is also regioselective in the sense that it is the amino group of the **56**$_S$ nucleophile that exclusively attacks the activated [**55**·H·**56**$_S$]$^+$ precursor. Steric interactions in the isomeric [(**55**·H·**56**$_S$)-H_2O]$^+$ ions are responsible for the differences observed in the relevant MIKE/CID spectra (Plate 15).

The same approach has been employed for enantiodiscriminating isopinocampheols (1*S*,2*S*,3*S*,5*R*)-(+)-**57** and (1*R*,2*R*,3*R*,5*S*)-(−)-**57** [138] and mandelic acids **10**$_R$ and **10**$_S$ [139] (Plate 16). Several chiral reagent gases were used, including (*R*)-2-amino-1-propanol (**15**$_R$), (*S*)-2-amino-1-butanol (**56**$_S$), (*S*)-2-pyrrolidinemethanol (**58**$_S$) and (*S*)-(14$_S$) and (*R*)-1-phenylethylamine (**14**$_R$).

The reactivity of protonated acetylated (*R*)- and (*S*)-2-butyl acetate (**59**), its dimeric forms $(CH_3COOsBu)_2H^+$ (**60**), and acetylated (*R*)- and (*S*)-2-butyl acetate (**61**), towards (*S*,*S*,*S*) tri-*sec*-butylborate (**62**$_{SSS}$) has been measured by FT-ICR-MS. The relevant ion patterns are shown in

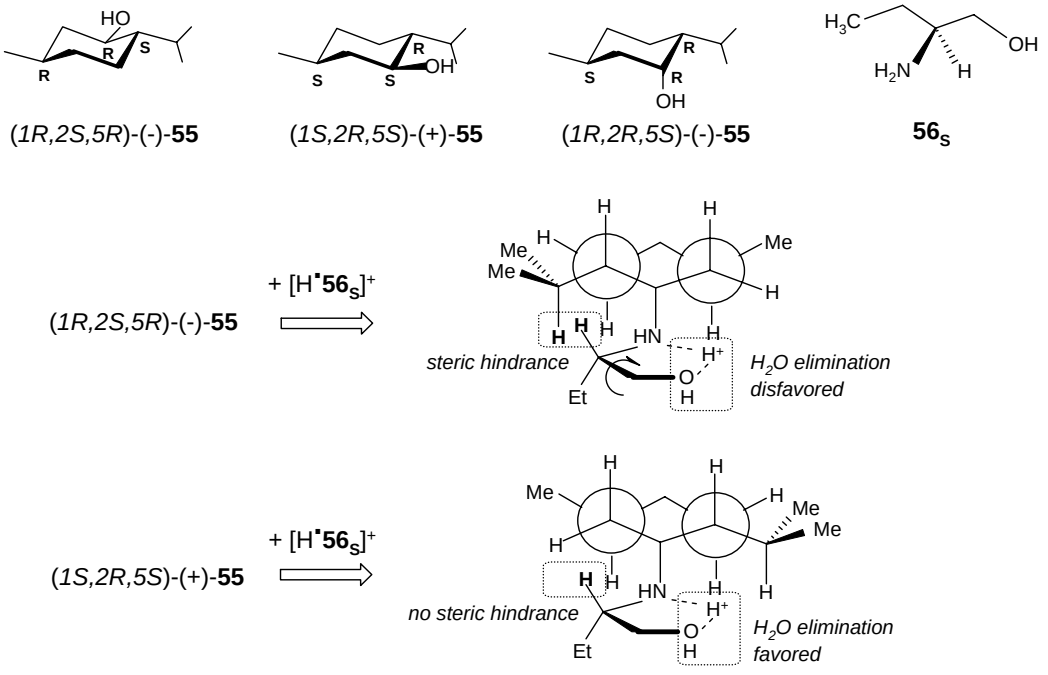

Plate 15.

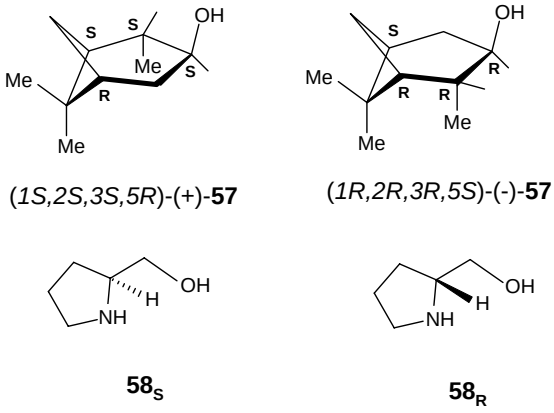

Plate 16.

Scheme 1 [140]. The kinetic data of Table 14 reveal some differences in both the overall reactivity of chiral ions **59**–**61** toward $\mathbf{62}_{SSS}$ (k_{tot}, k'_{tot} and k_v) and the relative extent of the competing addition/elimination (k_i and k_{iv}), proton transfer (k_{ii}), and ligand exchange (k_{iii}) channels. They clearly indicate that $\mathbf{62}_{SSS}$ reacts more efficiently with the homochiral (*S*)-2-butyl acetate ions $\mathbf{59}_S$, $\mathbf{60}_S$, and $\mathbf{61}_S$ than with their heterochiral counterparts $\mathbf{59}_R$, $\mathbf{60}_R$, and $\mathbf{61}_R$. As expected, the reaction efficiency of the racemate (±)-2-butyl acetate ions $\mathbf{59}_{R/S}$, $\mathbf{60}_{R/S}$, and $\mathbf{61}_{R/S}$ falls in between.

Independent evidence for backside attack in gas-phase acid-induced nucleophilic substitutions was provided by a number of studies, carried out using stationary radiolysis [141–150]. Further confirmation was provided by Morton and coworkers [151], who investigated the stereochemistry of the proton-induced nucleophilic substitution on (*S*)-(+)-($\mathbf{63}_S$) and (*R*)-(−)-2-butanol ($\mathbf{63}_R$) in the gas phase at 10^{-3} Torr in their 70 eV EBF radiolysis reactor. In the presence of a strong base, i.e., tri-*n*-propylamine (PA = 226 kcal mol^{-1}), the formation over sixfold of the (*R*,*S*)-di-2-butyl ether ($\mathbf{64}_{RS}$) vs. the (*R*,*R*)- and (*S*,*S*)-forms ($\mathbf{64}_{RR}$ and $\mathbf{64}_{SS}$, respectively) is attributed to a simple backside displacement in the proton-bound adduct of the starting 2-butanol enantiomer with inversion of configuration of the reaction site and loss of a molecule of water. When tri-*n*-propylamine is replaced by the less basic NH_3 (PA = 193 kcal mol^{-1}), fast neutralization of the proton-bound dimers of the starting 2-butanol is prevented and, therefore, they can grow, producing aggregates that resemble solution microenvironments in which S_N1 pathways may be accessible as well. As a consequence, the stereospecificity of the process is lost and predominant racemization is observed ([$\mathbf{64}_{RS}$]/[$\mathbf{64}_{RR}$ (or $\mathbf{64}_{SS}$)] = 1.2).

Table 14
Phenomenological rate constants (×10^{10} cm^3 molecule^{-1} s^{-1}) and efficiencies (eff = k_{obs}/k_{coll}) (in parentheses) of the reaction of chiral 2-butylacetate ions with (*S*,*S*,*S*)-tri-*sec*-butylborate ($\mathbf{62}_{SSS}$, Scheme 1)

Ionic reactant	k_{tot}	k_i	k_{ii}	k_{coll}
$\mathbf{59}_R$	4.89 (0.36)	3.47 (0.29)	1.42 (0.12)	11.89
$\mathbf{59}_S$	6.26 (0.52)	3.95 (0.33)	2.31 (0.19)	11.89
$\mathbf{59}_{R/S}$	5.12 (0.43)	3.81 (0.32)	1.31 (0.11)	11.89
	k_{tot}'	k_{iii}	k_{iv}	
$\mathbf{60}_R$	0.07 (0.007)	0.03 (0.003)	0.04 (0.004)	9.73
$\mathbf{60}_S$	0.08 (0.008)	0.03 (0.003)	0.05 (0.005)	9.73
$\mathbf{60}_{R/S}$	0.08 (0.008)	0.03 (0.003)	0.05 (0.005)	9.73
	k_v			
$\mathbf{61}_R$	4.44 (0.41)			10.80
$\mathbf{61}_S$	5.37 (0.50)			10.80
$\mathbf{61}_{R/S}$	5.35 (0.49)			10.80

3.2. High-pressure enantioselective reactions

In order to determine the effects of solvation and ion-pairing on the course of an ionic reaction in solution, the same reaction should be investigated in the gas phase under conditions ensuring thermal equilibration for all the transient species involved. To achieve this important condition, the reaction must be performed in the gas phase at sufficiently high pressures where the internal energy acquired by ion–molecule complexation is efficiently removed by unreactive collisions with the bulk gas prior to reaction. The ion–molecule encounter complexes are thermally coupled with the gaseous environment much like with the solvent in solution [151–155].

Under such conditions, the INC evolution may be accompanied by the rearrangement of its components or simply by their mutual re-orientation before reaction or dissociation. Thus, the knowledge of the structure, the configuration, and the initial orientation of the components of the microsolvated systems is crucial for understanding its reaction stereochemistry. This section deals with the stereochemistry of representative addition and substitution reactions taking place within gaseous complexes $[AH \cdot B]^+$, wherein AH^+ is the formally charged moiety generated by stationary γ-radiolysis and B is a nucleophilic molecule. The systems investigated involve: (i) protonated (*R*)-(−)-2-chlorobutane and an arene [156]; (ii) deuterated 2-butyl/toluene pair from protonated (*S*)-(+)-1-D_1-3-(*para*-tolyl)butane [157]; (iii) chiral oxonium ions and methanol [158,159]; (iv) chiral phenonium ions and ROH (R = H, CH_3) [160,161]; (v) prochiral allyl cation and ROH (R = H, CH_3) [162–164]; (vi) prochiral methyl benzyl cation and methanol [165,166]; and (vii) an O-protonated (*R*)-(+)-1-arylethanol and ^{18}O-methanol [167].

Complexes $[AH{\cdot}B]^+$ are generated in an inert gaseous medium at pressures high enough (700–750 Torr) to allow their complete thermal equilibration. A tailor-made procedure has been used which ensures that the reaction products arise exclusively from the intracomplex reorganization of $[AH{\cdot}B]^+$. Thus, adducts $[AH{\cdot}B]^+$ are generated by intracomplex proton transfer in the $[AH{\cdot}B]^+$ adduct obtained by coordination of molecule A around ion BH^+ Eq. (34).

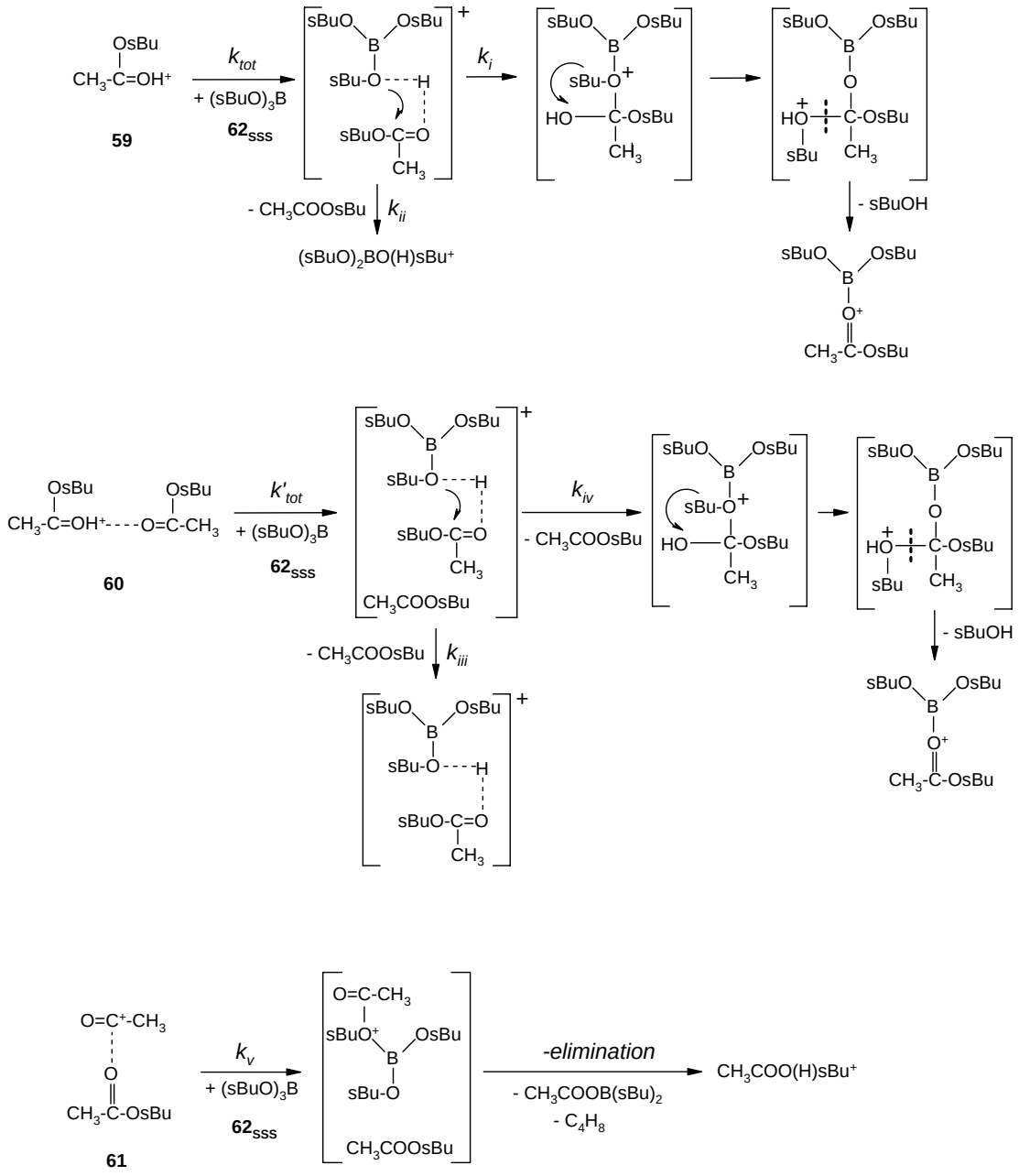

Scheme 1.

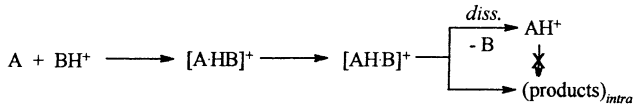

(34)

The BH^+ precursor is prepared by a route excluding the presence of its conjugate base B. For instance, the $[AH{\cdot}B]^+$ complex with AH^+=O-protonated (*R*)-(+)-1,2-propene oxide and B=$CH_3{}^{18}OH$ is generated by intracomplex proton transfer within the adduct between (*R*)-(+)-1,2-propene oxide (A) with $CH_3{}^{18}OH_2{}^+$ (BH^+). Ions $CH_3{}^{18}OH_2{}^+$ are in turn formed in the gas phase by methylation of $H_2{}^{18}O$ with the $(CH_3)_2F^+$ ions obtained in known yields by γ-radiolysis of CH_3F. In this way, ions $CH_3{}^{18}OH_2{}^+$ are generated in complete absence of their conjugate $CH_3{}^{18}OH$ base and, hence, their reaction products, i.e., the ^{18}O-labeled 1-methoxy-2-propanols, are bound to arise exclusively from the intracomplex substitution on the incipient O-protonated (*R*)-(+)-1,2-propene oxide by the putative $CH_3{}^{18}OH$ molecule.

$$\mathrm{A} + \mathrm{H}^+ \rightarrow \mathrm{AH}^+$$
$$\mathrm{AH}^+ + \mathrm{B} \rightleftarrows [\mathrm{AH} \cdot \mathrm{B}]^+ \rightarrow (\mathrm{products})_{\mathrm{extra}} \qquad (35)$$

In some instances, the outcome of the intracomplex process (34) is confronted with that of the direct reaction between unsolvated AH^+ ion (or its rearranged form) and an external B molecule (reaction sequence (35)). Taking again the above example, AH^+=O-protonated (*R*)-(+)-1,2-propene oxide is simply obtained by protonation of (*R*)-(+)-1,2-propene oxide with $C_nH_5^+$ ($n = 1$, 2) ions, formed by γ-radiolysis of gaseous CH_4. The "extracomplex" sequence (35) takes place by coordination of the so-formed O-protonated (*R*)-(+)-1,2-propene oxide with external $CH_3{}^{18}OH$ molecules, present as a massive additive in the irradiated mixture.

3.3. Intracomplex reactions in arenium ion/(R)-(−)-2-chlorobutane pairs

A crucial question concerns the chemical identity and the relative spatial arrangement of the components of a microsolvated system, two features of paramount importance to assess the kinetic and the mechanistic role of the corresponding ion–dipole pairs in solution. In the example reported in this section, Cacace and coworkers consider the INC involved in the classical Friedel–Crafts alkylation of arenes [156]. At 300 K and under FT-ICR conditions, the benzenium ion $C_6H_7^+$ reacts with 2-chlorobutane C_4H_9Cl to give the $C_{10}H_{15}^+$ ion with a rate constant of 5×10^{-11} cm^3 molecule^{-1} s^{-1}, corresponding to a collision efficiency of 2.5% [168].

$$C_6H_7^+ + C_4H_9Cl \rightarrow [C_6H_7^+ \cdot C_4H_9Cl] \rightarrow [C_6H_6 \cdot C_4H_9ClH^+] \rightarrow C_{10}H_{15}^+ + HCl \quad (36)$$

$$C_6H_7^+ + C_4H_9Cl \rightarrow [C_6H_7^+ \cdot C_4H_9Cl] \rightarrow [C_6H_6 \cdot C_4H_9^+ \cdot HCl] \rightarrow C_{10}H_{15}^+ + HCl \quad (37)$$

No information is available from this experiment as to the detailed path of formation of $C_{10}H_{15}^+$, whether via Eqs. (36) and (37). Besides, no information is available as to the spatial relationship and the dynamics of the species present in the second complexes of Eqs. (36) and (37). To answer these questions, the $^{12}C_6H_6D$ arenium ion was prepared in the gas phase by deuteronation of $^{12}C_6H_6$ with radiolytic $C_nD_5^+$ ($n = 1$, 2) ions. Similarly, the $^{12}C_6H_6CH_3^+$ arenium ion was generated in the gas phase by methylation of $^{12}C_6H_6$ with radiolytic $(CH_3)_2F^+$. Both arenium ions were allowed to react at 700–750 Torr with (*R*)-(−)-2-chlorobutane. The corresponding 2-arylbutanes, recovered among the radiolytic products, display complete racemization which points to their formation as proceeding exclusively via Eq. (37). This implies that alkylation follows a S_N1 mechanism, i.e., a process wherein covalent bond breaking precedes covalent bond formation as in the three-body adduct of Eq. (37) whose individual components are not constrained in a fixed geometry, but are free to re-orientate or to rearrange before addition (Plate 17).

3.4. Intracomplex reaction in 2-bulyl ion/toluene pairs

As pointed out in the previous section, key INC features, such as the mutual orientation of their components and their evolution dynamics, usually escape precise determination because of intrinsic limitations of the available experimental methodologies. This lack of information is particularly unsatisfactory since, in principle, the nature and the

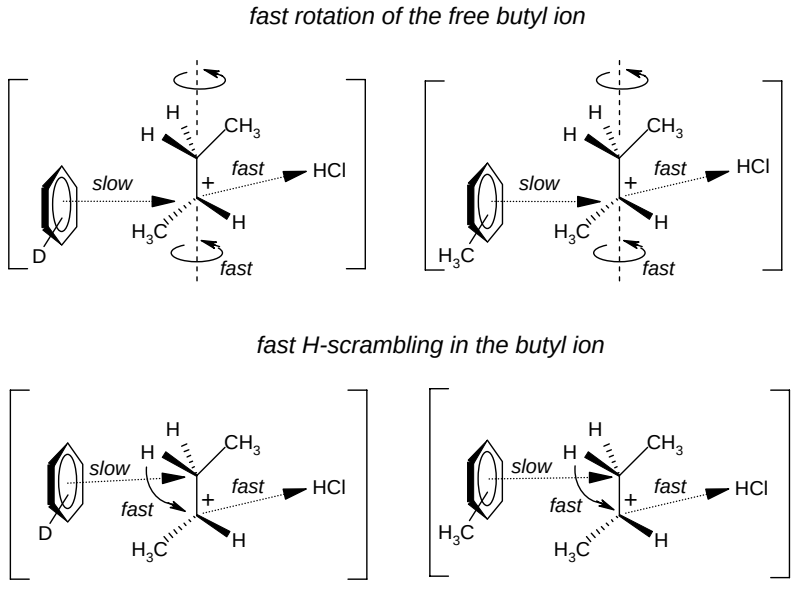

Plate 17.

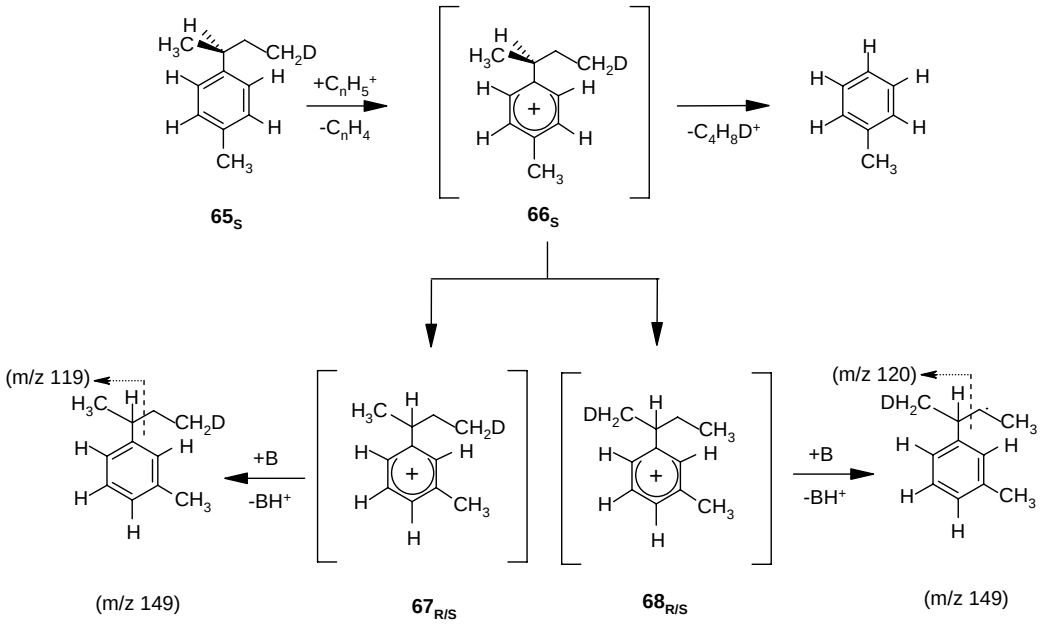

65$_S$ **66$_S$** **67$_{R/S}$** **68$_{R/S}$**

Scheme 2.

dynamics of INC may determine its evolution to products and, thus, the reaction selectivity. Filippi and coworkers [157] recently provided novel indications of the factors governing the positional selectivity in a representative gas-phase electrophilic aromatic substitution, i.e., the *sec*-butylation of toluene, based on a careful investigation of the nature and the dynamics of a tailor-made INC.

Ring-protonated (*S*)-(+)-1-D$_1$-3-(*para*-tolyl)butane (**66**$_S$) was generated by attack of radiolytic $C_nH_5^+$ ($n = 1, 2$) ions on (*S*)-(+)-1-D$_1$-3-(*para*-tolyl)butane (**65**$_S$) and its isomerization kinetics and stereochemistry investigated in the gas phase at 70 Torr and $T = 100$–$160\,^\circ$C (Scheme 2). The process leads to the exclusive formation of the relevant meta isomer (**67**$_{R/S}$) with complete racemization and partial 1,2-H shift in the migrating 2-butyl group (**68**$_{R/S}$). These results, together with the relevant activation parameters ($\Delta H^* = 10.3 \pm 1.2$ kcal mol^{-1}, $\Delta S^* = -5.3 \pm 3.6$ cal mol^{-1} K^{-1}), point to the occurrence of tightly bound, isomeric 2-butyl ion/toluene complexes of defined structure and stability placed ca. 10 kcal mol^{-1} below the classical electrostatically bound π-complexes on the relevant PES. The existence and the η^1-type structure of these low-energy intermediates are confirmed by ab initio calculations (Fig. 4).

Formation of the tightly-bound η^1-type complexes in the isomerization of **66**$_S$ rises some questions about the role of these intermediates in determining the substrate and positional selectivity of the gas-phase ionic alkylation of arenes. Indeed, the classical mechanistic model of gas-phase aromatic alkylations involves the preliminary formation of all electrostatically bound π-complex acting as a microscopic reaction "vessel" wherein the reactants are confined by electrostatic forces. The substrate selectivity of the alkylation reaction essentially reflects the competition between the collisional stabilization of the individual π-complexes and their back-dissociation. The positional selectivity reflects instead the different activation free energies for the conversion of the π-complex to isomeric σ-bonded arenium ions.

Filippi and coworkers' discovery of tightly-bound, isomeric η^1-type complexes on the 2-butyl ion/toluene PES put into question this widely accepted model [157]. Indeed, their occurrence provides a rationale for the significant pressure effect on the isomeric product pattern observed in the gas-phase *sec*-butylation of toluene ($T = 24\,^\circ$C) [169]. This pressure effect can be explained only by acknowledging the intermediacy of isomeric η^1-type complexes with lifetimes comparable with their collision time with the bulk gas at 70–710 Torr (5×10^{-10}/5×10^{-11} s).

In this frame, the positional selectivity of the gas-phase *sec*-butylation of toluene, a model reaction for electrophilic aromatic substitutions, is determined by the relative population of isomeric η^1-type complexes and the activation free energies for their conversion to the relevant σ-bonded arenium ions. At high pressure, where collisional cooling of the η^1-type complexes is efficient, the reaction is essentially controlled by enthalpy factors favoring formation of the *ortho* and *para* η^1-type isomers and their conversion to the corresponding σ-arenium intermediates. At low pressures, where collisional cooling of the, η^1-type complexes is less efficient, their relative population and conversion to the corresponding arenium ion can be significantly altered by the contribution of the entropic factors.

3.5. Acid-induced ring opening of chiral alkene oxides

The mechanism and the stereochemistry of acid-induced ring opening in 1,2-epoxides are heavily affected in solution by environmental factors. For instance, depending upon the pH of the reaction medium, alcoholysis of epoxides may

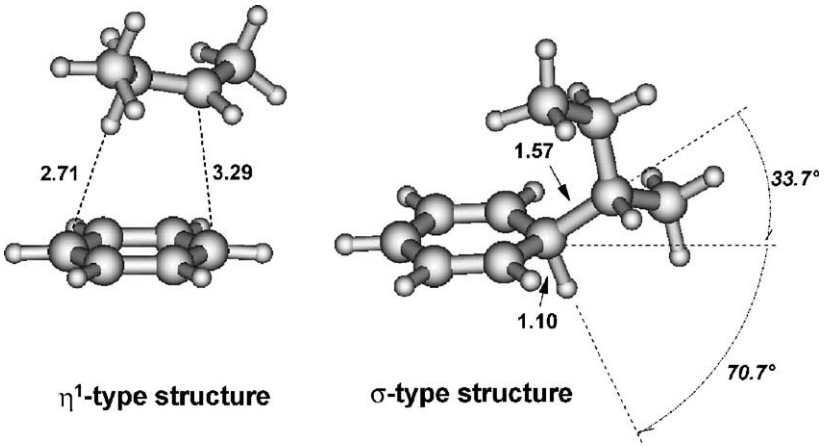

Fig. 4. HF/6-31+G** optimized structures and main geometrical parameters of the stable σ and, η^1-type complexes located on the potential energy surface (PES) of protonated *sec*-butyl benzene (bond lengths in (Å); angles in (°)).

follow either a unimolecular or a bimolecular pathway with a stereochemistry ranging from complete retention to complete inversion of configuration. Discrimination between intrinsic structural and environmental factors on ring opening of epoxides arises from a detailed investigation of the reaction in the gas phase.

Gas-phase acid-induced ring opening of enantiomerically pure 1,2-propene (**69**$_R$ and **69**$_S$) and styrene oxides (**70**$_R$ and **70**$_S$) has been investigated at room temperature using $CH_3{}^{18}OH$, CD_3OH, and $H_2{}^{18}O$, as nucleophiles, and $C_nH_5{}^+$ ($n = 1, 2$) and $(CH_3)_2F^+$, as gaseous acids, generated by γ-radiolysis of CH_4 and CH_3F (720 Torr), respectively (Scheme 3) [158,159]. No racemization of the starting chiral epoxide is observed under all experimental conditions. Therefore, the ring opening takes place on the O-protonated (or O-methylated) **69**–**70** retaining the original configuration of their precursors. Ring opening proceeds via two different reaction pathways. In the $CH_3F/H_2{}^{18}O$ systems, the reaction follows the intracomplex mechanism depicted in Eq. (34). It involves protonation of the oxygen of the epoxide by the $CH_3{}^{18}OH_2{}^+$ ion, generated in the gaseous mixture by $(CH_3)_2F^+$-methylation of $H_2{}^{18}O$. The neutral $CH_3{}^{18}OH$ molecule, arising from the proton transfer, moves around the oxonium ions ($k < 10^8\ s^{-1}$) before attacking their ring carbons. The attack exclusively occurs at the α carbon of **72** with slightly predominant inversion of the configuration (55–67%). With **71**, instead, the attack takes place at both ring carbons ($\alpha/\beta = 0.72 \pm 0.05$) with exclusive inversion of their configuration.

In the $CH_4/CH_3{}^{18}OH$ systems, the intracomplex pathway is preceded by the extracomplex attack of an external $CH_3{}^{18}OH$ molecule (sequence (35)). Both the intracomplex

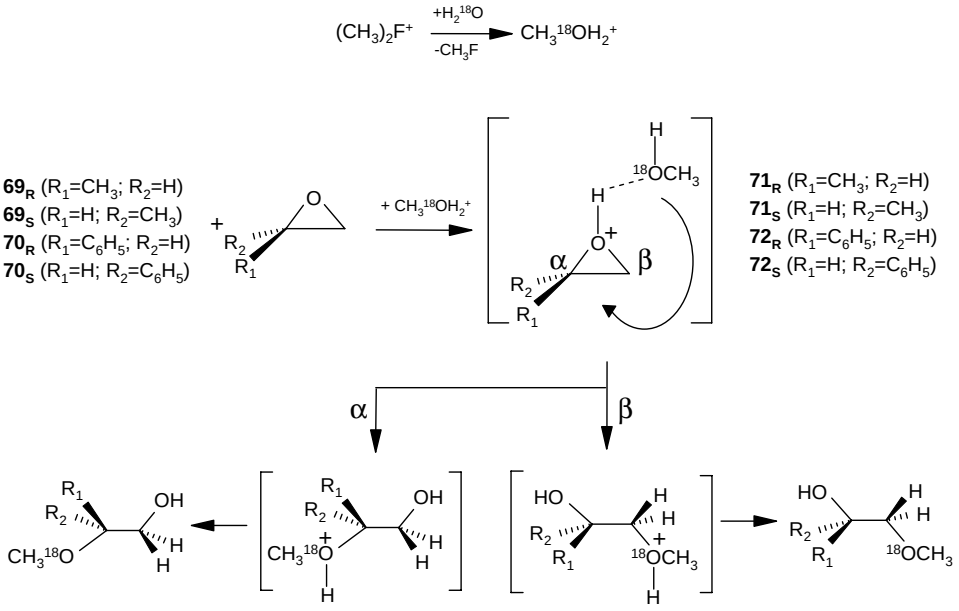

Scheme 3.

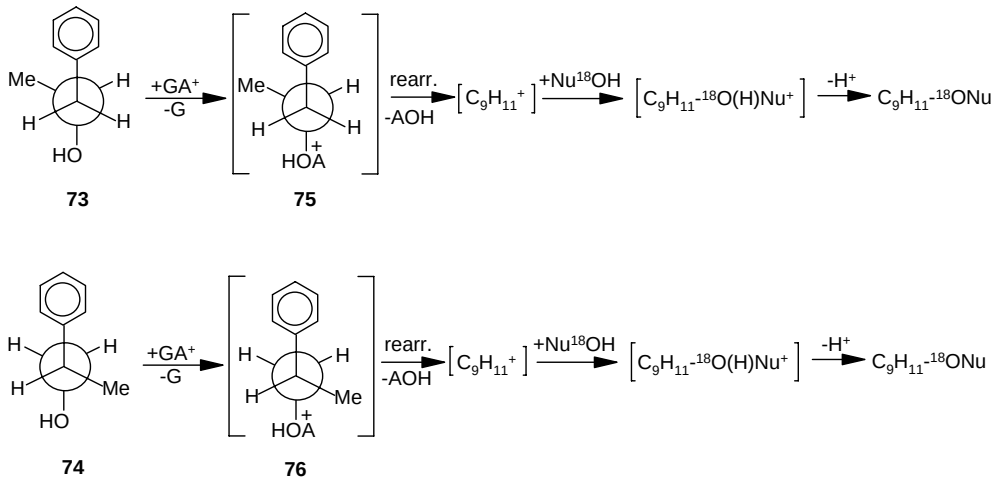

Scheme 4.

and the extracomplex pathways display the same regio- and stereoselectivity. The different regio- and stereoselectivity observed for **71** and **72** is explained in terms of a different extent of C_α–O bond rupture in the relevant TS. Ring-opening of **72** involves a loose TS characterized by extensive C_α–O bond cleavage promoted by conjugative delocalization of the C_α positive charge over the phenyl ring. The same stabilization mechanism is not operative in the ring opening of **71** whose TS is therefore characterized by a much less advanced C_α–O cleavage.

3.6. Acid-induced Wagner–Meerwein rearrangements in chiral alcohols

In the frame of a comprehensive investigation of gas-phase analogues of solvolytic reactions [152,155], some efforts have been directed to the study of Wagner–Meerwein rearrangements in cationized β-arylalkyl systems. In particular, the study was focused on the assessment of the kinetics and the stereochemistry of the unimolecular AOH loss from the chiral oxonium ions **75** and **76** (A = H or CH_3; Scheme 4) [160,161].

Ions **75** and **76** are generated from the corresponding chiral alcohols **73** and **74** by reaction with gaseous acids (GA^+), either $C_nH_5^+$ (n = 1, 2) (A = H) or $(CH_3)_2F^+$ (A = CH_3), formed respectively by γ-radiolysis of CH_4 and CH_3F (750 Torr). The reaction sequences of Scheme 4 have been investigated in the temperature range 25–140 °C, in the presence of $CH_3{}^{18}OH$ or $H_2{}^{18}O$, as nucleophiles (Nu ^{18}OH). The experimental results conform to the unimolecular loss of H_2O from **75** and **76** (A = H), anchimerically assisted by all the groups adjacent to the leaving moiety (Scheme 5). Anchimeric assistance to the CH_3OH loss from **75** and **76** (A = CH_3) appears much less effective.

The linear Arrhenius plots of the $k_{Ph}^{back}/k_{Ph}^{front}$, k_{Ph}^{back}/k_H and k_{Ph}^{front}/k_H ratios and of the k_{Ph}/k_{Me}, k_{Ph}/k_H, and k_{Me}/k_H, ratios (Scheme 5), taken in the 25–140 °C interval, obey to the differential activation parameters listed in Table 15. From the reported values, the absolute activation energy for the backside phenyl, frontside phenyl, methyl, and hydrogen participation to the H_2O loss in **75** and **76** (A = H) can be estimated as ranging around 9, 8, 4, and 2 kcal mol^{-1}, respectively.

Analysis of Table 15 indicates that, in the 25–140 °C temperature interval, the neighboring-group assistance in **75** and **76** (A = H) is mainly controlled by entropic, rather than enthalpic factors. Furthermore, the counterintuitive observation that the frontside phenyl-group participation involves an activation barrier lower than that of the competing backside participation finds a rationale in the *gauche-anti* conformation of the oxonium ion **75***ga* (A = H), most favored in the gas phase, and on the stabilizing electrostatic interactions between the leaving H_2O moiety and the ring of the phenonium ion in the transition structure **82** (Plate 18).

Table 15
Differential Arrhenius parameters for the competing neighboring group participation to the unimolecular H_2O loss in the chiral oxonium ions **75** and **65** (A = H)

Reaction	Arrhenius equation (x = 1000/2.303RT)	Correlation coefficient
77 ← **75** → **79**	$\log(k_{Ph}^{back}/k_H) = (5.0 \pm 0.3) - (7.0 \pm 0.3)x$	0.960
78 ← **75**→ **79**	$\log(k_{Ph}^{front}/k_H) = (3.2 \pm 0.3) - (5.6 \pm 0.3)x$	0.964
77 ← **75** → **78**	$\log(k_{Ph}^{back}/k_H^{front}) = (1.7 \pm 0.5) - (1.3 \pm 0.5)x$	0.927
77 ← **76** → **79**	$\log(k_{Ph}/k_{Me}) = (4.7 \pm 0.2) - (5.7 \pm 0.2)x$	0.997
77 ← **76** → **81**	$\log(k_{Ph}/k_H) = (6.0 \pm 0.2) - (7.1 \pm 0.2)x$	0.997
79 ← **76** → **81**	$\log(k_{Me}/k_H) = (1.3 \pm 0.5) - (1.4 \pm 0.5)x$	0.906

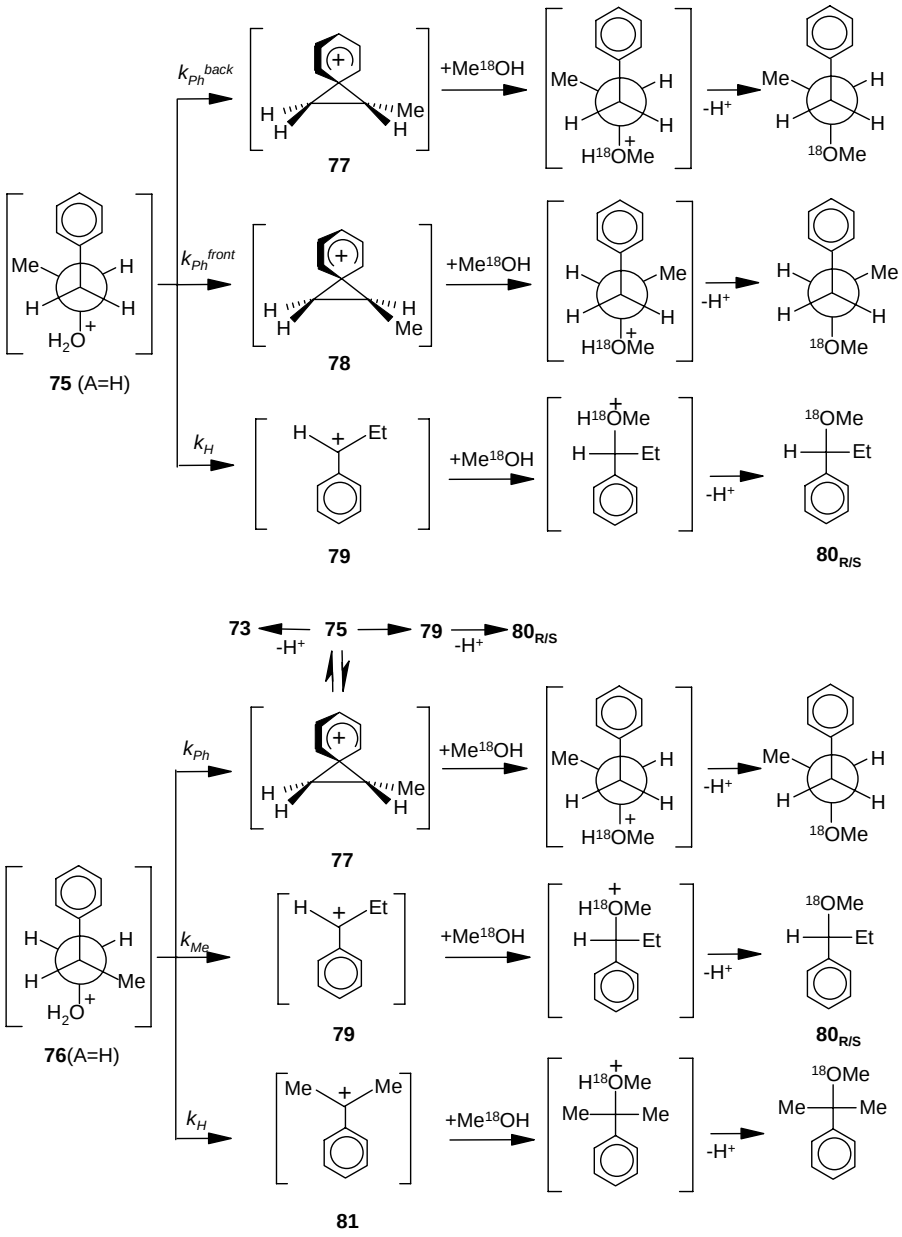

Scheme 5.

Closer insights into the transition structures involved in the anchimeric assistance to H_2O loss from **75** and **76** (A = H) are obtained by the measurement of the relevant deuterium primary and secondary kinetic effects.

3.7. Intracomplex rearrangements in allyl cation/ROH (R = H, CH_3) pairs

Bimolecular nucleophilic displacements in allylic compounds are known to proceed via the four possible pathways shown in Scheme 6.

The existence itself of the S_N2' mechanism, the question of its concertedness, and the origin of its stereochemistry, have been matter of lively debate for the last half-century. The controversy was continuously sustained by the paucity of firm proofs of the S_N2' mechanism in solution and by the coincidence of the S_N2' products with those arising from alternative competing mechanisms, i.e., S_N1, unimolecular rearrangement of the starting alcohol before substitution and of its derivatives after S_N2 substitution, etc.

This ambiguity has been removed by the results of a comprehensive investigation on the gas-phase acid-induced nucleophilic substitution on several allylic alcohols showing that the concerted S_N2' reaction competes with the classical S_N2 pathway in the absence of solvation and ion-pairing factors [170–172]. Assessment of the stereochemistry of the gas-phase S_N2' reactions in these systems requires a detailed knowledge of the extent of conceivable rearrangements

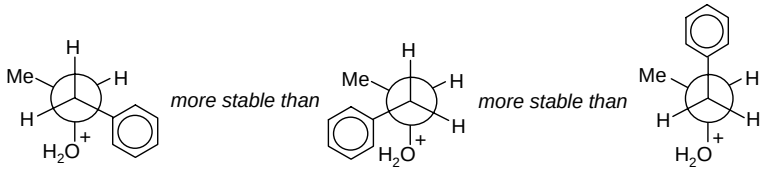

75*ga* **75***gg* **75***ag*

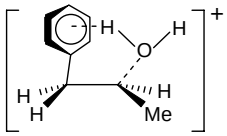

82

Plate 18.

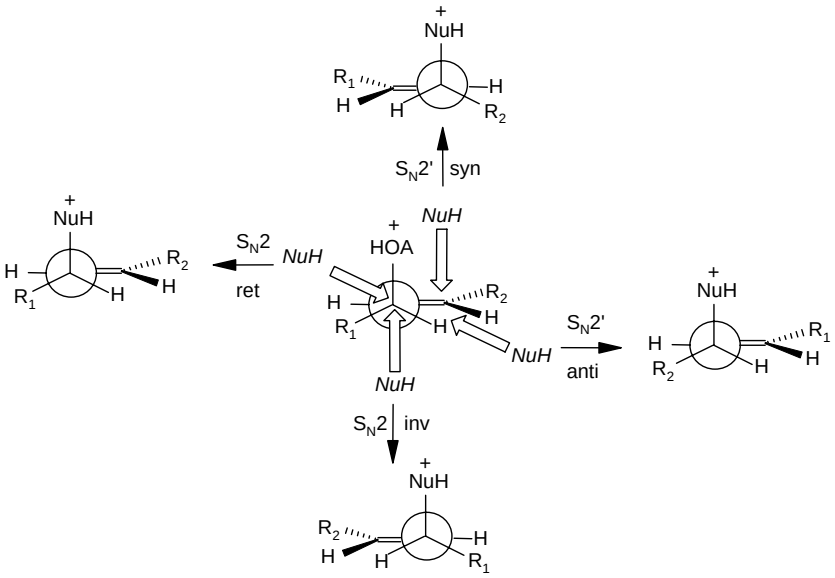

Scheme 6.

in the starting intermediate **83** prior to nucleophilic attack (Scheme 7).

To this purpose, the oxonium ion **83** (A = H; R_1 = C_2H_5; R_2 = CH_3) has been generated in the gas phase (720 Torr) by protonating the corresponding allylic alcohol with $C_nH_5^+$ (n = 1, 2) and $sC_3H_7^+$, obtained respectively by γ-radiolysis of CH_4 and C_3H_8. Ion **83** was found to undergo appreciable inversion to **84** (A = H; R_1 = C_2H_5; R_2 = CH_3) and isomerization to racemate **85**, (A = H; R_1 = C_2H_5; R_2 = CH_3) in yields (Y_{racem} and Y_{isom}, respectively), which depend on the temperature of the gaseous mixture (40–120 °C) and on the reaction time t. This is defined by the concentration of the powerful $(CH_3)_3PO_4$ base (proton affinity PA = 212 kcal mol^{-1}) [162] deliberately added to the system. The experimental results, combined with ab initio calculations on the model [$C_3H_5^+/H_2O$] system, point to the rearrangement of **83** as proceeding through structurally distinct intermediates **86** and **87** characterized by site-specific hydrogen bonding (Scheme 7). If the probabilities of conversion of complex **86** to the **83**/**84** enantiomeric pair and to isomer **85** are equal, the rate constant for the formation of **86** from **83** can be expressed by $k_{isom} = t^{-1} \ln(1 - 2Y_{isom})^{-1}$ and that for the formation of **87** by $k_{isom} = t^{-1} \ln[1 - 2(Y_{racem} - 0.5Y_{isom})]$. The relevant values are respectively plotted in Fig. 5 as a function of the reaction temperature.

The observation that essentially the same rate constants are measured in methane (circles and triangles) and propane (diamonds and squares) at 40 and 100 °C demonstrates that the starting oxonium ion **83** is in thermal equilibrium with the bulk gas and that its unimolecular rearrangement depends exclusively on the reaction temperature.

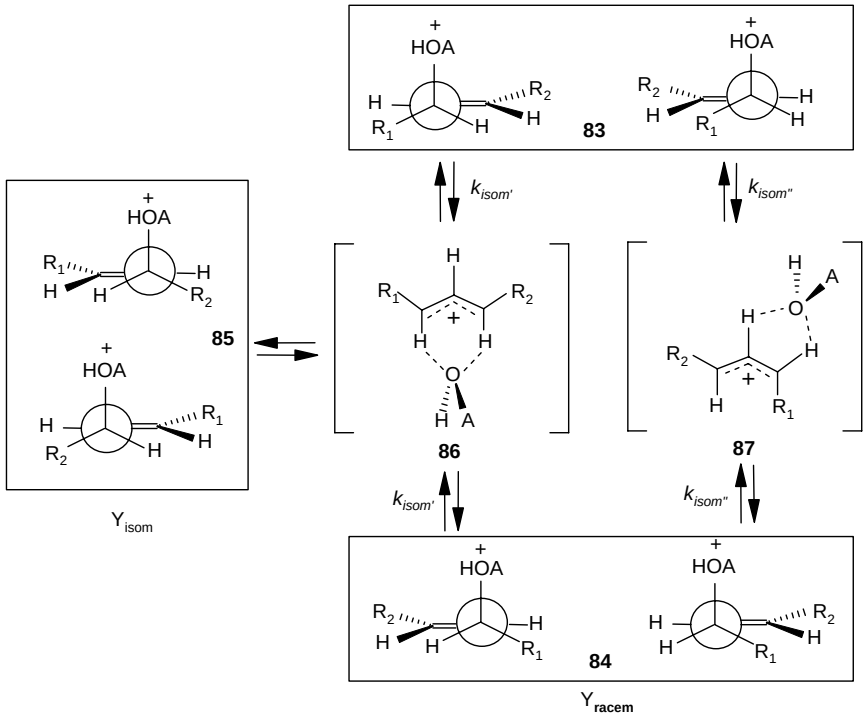

Scheme 7.

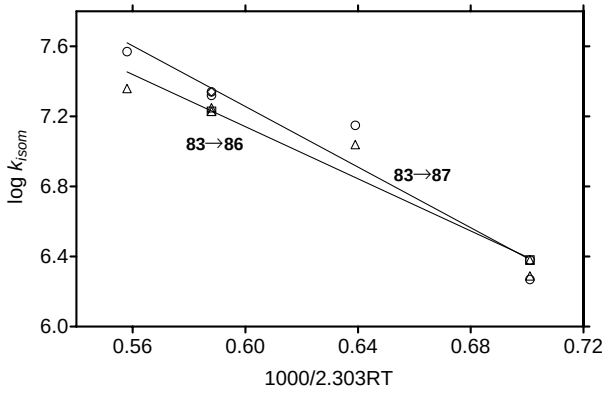

Fig. 5. Arrhenius plots for the **83** isomerization reaction in 720 Torr of methane (**83** → **86** (triangles); **83** → **87** (circles)) and propane (**83** → **86** (squares); **83** → **87** (diamonds)).

Similar plots have been obtained for the gas-phase rearrangement of **83** (A = CH_3; R_1 = C_2H_5; R_2 = CH_3) and **84** (A = CH_3; R_1 = CH_3; R_2 = C_2H_5) in 720 Torr methyl chloride in the temperature range from 40 to 120 °C [163]. Regression ana1ysis of the relevant Arrhenius curves leads to the activation parameters listed in Table 16.

The activation parameters of Table 16 suggest that the energy, the charge distribution, and the location of the relevant transition structures (TS) along the reaction coordinate depend significantly on the nature of the moving AOH moiety. When A = H, the racemization and isomerization TS are located early on the reaction coordinate, whereas they are late with A = CH_3 and are characterized by comparatively stronger H-bond interactions.

The limited extent of intramolecular rearrangements undergone by the chiral oxonium ions **83** and **84** at 720 Torr and at 40 °C (Table 16) allows their use for probing the regio- and stereochemistry of the displacement reactions of Scheme 6. In this case, the allylic alcohol, precursor of the chiral oxonium ions **83** and **84**, acts as the nucleophile NuH [164]. The relevant results are condensed in Plate 19.

They are fully consistent with modern concepts [173–175] pointing to concerted acid-catalyzed S_N2' reactions which are feasible in the gas phase and which efficiently compete

Table 16
Arrhenius parameters for the gas-phase racemization and isomerization of chiral ions **83** and **84**

Reaction	Arrhenius equation ($x = 1000/2.303RT$)	Correlation coefficient (r)	ΔH^* (kcal mol^{-1})	ΔS^* (cal mol^{-1} K^{-1})
83(A = H; R_1 = C_2H_5; R_2 = CH_3) → **86**	$\log k_{isom} = (11.6 \pm 0.4) - (7.4 \pm 0.5)x$	0.960	6.7 ± 0.5	−7.9 ± 2.4
83(A = H; R_1 = C_2H_5; R_2 = CH_3) → **87**	$\log k_{isom} = (12.5 \pm 0.4) - (8.7 \pm 0.6)x$	0.963	8.0 ± 0.6	−3.7 ± 2.8
83(A = CH_3; R_1 = C_2H_5; R_2 = CH_3) → **86**	$\log k_{isom} = (10.6 \pm 0.4) - (5.4 \pm 0.5)x$	0.978	4.7 ± 0.5	−12.4 ± 2.1
83(A = CH_3; R_1 = C_2H_5; R_2 = CH_3) →**87**	$\log k_{isom} = (10.1 \pm 0.4) - (6.3 \pm 0.5)x$	0.960	5.6 ± 0.5	−14.6 ± 2.1
84(A = CH_3; R_1 = CH_3; R_2 = C_2H_5) → **86**	$\log k_{isom} = (10.9 \pm 0.4) - (5.8 \pm 0.5)x$	0.987	5.1 ± 0.5	−11.2 ± 1.9
84(A = CH_3; R_1 = CH_3; R_2 = C_2H_5) → **87**	$\log k_{isom} = (10.3 \pm 0.4) - (6.5 \pm 0.6)x$	0.988	5.8 ± 0.6	−13.6 ± 2.1

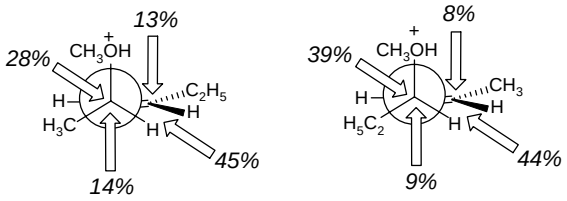

Plate 19.

with the classical S_N2 processes. According to these concepts, a preferred *anti* relationship between the NuH and the leaving group is observed in gas-phase S_N2'. The relevant TS is only marginally influenced by stereoelectronic factors, while it is strongly favored by the lack of the nonbonding and repulsive Coulombic interactions between NuH and leaving group, which usually play a critical role in the gas phase.

3.8. Intracomplex rearrangements in chiral benzyl cation/CH_3OH pairs

The rate of ^{18}O exchange between water and the chiral-labeled alcohols as a function of racemization has been extensively used as a criterion for discriminating the S_N2 from the S_N1 solvolytic mechanisms in solution. The expected ratio of exchange versus racemization rate is 0.5 for the S_N2 mechanism and 1.0 for a pure S_N1 process [176]. With chiral ^{18}O-enriched 1-phenylethanol in aqueous acids, this ratio is found to be equal to 0.84 ± 0.05. This value has been interpreted in terms of the kinetic pattern of Scheme 8 involving the reversible dissociation of the oxonium ion **88**$_S$ (XOH=$H_2{}^{18}O$) to the chiral intimate ion-dipole pair **89** ($k_{-1} > k_{inv}$). In **89**$_S$, the leaving $H_2{}^{18}O$ molecule

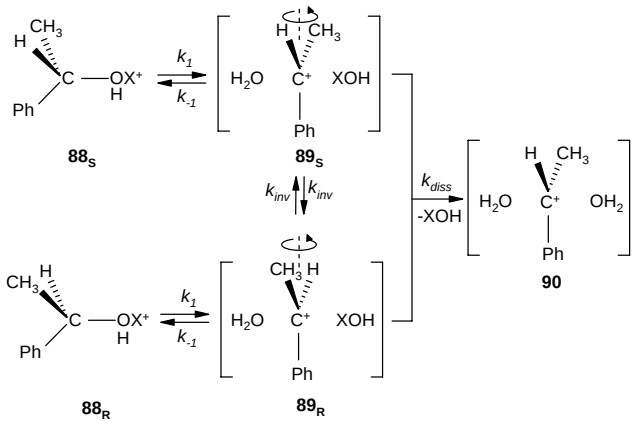

Scheme 8.

does not equilibrate immediately with the solvent (i.e., $H_2{}^{16}O$), but remains closely associated with the ion. This means that k_{inv} is of the same order of magnitude of k_{diss} [177,178]. In contrast, the rate constant ratio of exchange versus racemization of chiral 1-phenyl-1-methoxyethane in acidic acetonitrile–water solutions is as large as 0.99. The closeness of this value to that of a pure S_N1 mechanism indicates that, in Scheme 8 (XOH=CH_3OH), either k_{inv} is many orders of magnitude lower than k_{diss} or, if not, that internal return is negligible ($k_{-1} \ll k_{inv}$) [179]. This kinetic ambiguity prevents identification of the actual factors hindering inversion in **89**$_S$ (XOH=CH_3OH).

Removal of this ambiguity was due to Speranza and coworkers [165] who prepared the chiral oxoniun ion **88**$_S$ (XOH=CH_3OH) in the gas phase by methylation of *S*-(−)-1-phenylethanol (**91**$_S$) with $(CH_3)_2Cl^+$ ions (Scheme 9).

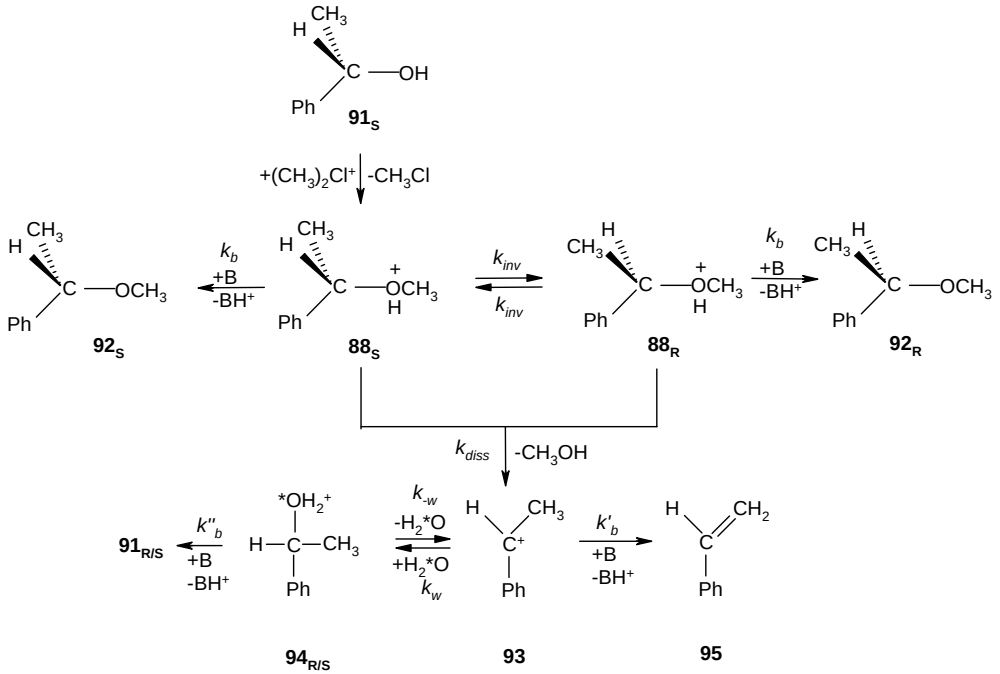

Scheme 9.

The latter ions are generated by γ-radiolysis of CH_3Cl, present as bulk component (720 Torr; 25–160 °C) of gaseous mixtures containing traces of **91**$_S$, of $H_2{}^{18}O$, of a radical scavenger (i.e., O_2), and of a powerful base (i.e., $(C_2H_5)_3N$).

Detailed information on the reorganization dynamics of the intimate ion-dipole **89**$_S$, arising from **88**$_S$ by C–O bond dissociation, is inferred from the kinetic study of the intracomplex inversion of configuration of **88**$_S$ versus its dissociation to α-methylbenzyl cation (**93**) and CH_3OH. The results point to k_{inv} values that are anything but negligible relative to k_{diss} rate constants within the entire temperature range investigated (25–160 °C). Indeed, k_{inv} are just two to four time lower than k_{diss}. This implies that, in acidic media, the hindered inversion of **88**$_S$ (XOH=CH_3OH) has to be ascribed to the lack of appreciable **89**$_S$ → **88**$_S$ (and **89**$_R$ → **88**$_R$) internal return ($k_{-1} < k_{inv}$; Scheme 8), rather than to k_{inv} negligible relative to k_{diss} [179]. Accordingly, the difference in the behavior of **89**$_S$ (and **89**$_R$) in acidic solution essentially reduces to $k_{-1} > k_{diss}$, when XOH=$H_2{}^{18}O$, and $k_{-1} \ll k_{diss}$ when XOH=CH_3OH.

Quantum-chemical calculations at the B3LYP/6-31G* level of theory have been employed to gather some insights into the reasons for this dual behavior. The calculations qualitatively indicate that the **88**$_S$ ⇆ **88**$_R$ (XOH=CH_3OH) transition structures are placed late along the reaction coordinate. The CH_3OH moiety is enough removed from the benzyl ion moiety to start interacting with the solvent cage. These interactions favor **89**$_S$ → **90** dissociation and prevent efficient **89**$_S$ → **88**$_S$ internal return ($k_{-1} < k_{diss}$; Scheme 8) [175]. The **88**$_S$ ⇆ **88**$_R$ (XOH=$H_2{}^{18}O$) transition structures are instead placed much earlier along the reaction coordinate so as to resemble the starting **88**$_S$ ion. In them, the moving $H_2{}^{18}O$, less basic than CH_3OH, sits nearby the departure face of the still flexible benzylic residue and does not appreciably interact with its acidic hydrogens. A surplus of energy is needed to remove the $H_2{}^{18}O$ moiety far enough to establish appreciable interactions with the solvent cage and to promote **89**$_S$ → **90** dissociation. As a consequence, **89**$_S$ → **88** internal return can efficiently compete with $H_2{}^{18}O$ diffusion to the aqueous cage ($k_{-1} > k_{diss}$). Besides, the shielding effect of the $H_2{}^{18}O$ leaving group accounts for the observed prevalence of the inversion of configuration in the H_2O-to-$H_2{}^{18}O$ exchange in solution [177,178].

Using the same experimental approach, a family of enantiomerically pure oxonium ions, i.e., O-protonated 1-aryl-1-methoxyethanes (aryl = 4-methylphenyl (**96**$_S$); 4-chlorophenyl (**97**$_S$); 3-(α,α,α-trifluoromethyl)phenyl (**98**$_S$); 4-(α,α,α-trifluoromethyl)phenyl (**99**s); 1,2,3,4,5-pentafluorophenyl (**100**$_R$) and 1-phenyl-1-methoxy-2,2,2-trifluoroethane (**101**$_R$)), has been generated in the gas phase by $(CH_3)_2Cl^+$ methylation of the corresponding 1-arylethanols [167]. Some information on their reaction dynamics was obtained from a detailed kinetic study of their inversion of configuration (k_{inv}) and dissociation (k_{diss}) as a function of temperature. The relevant Arrhenius plots are given in Figs. 6 and 7, respectively. The relevant linear curves obey the equations reported in Tables 17 and 18, respectively. The corresponding activation parameters were calculated from the transition-state theory.

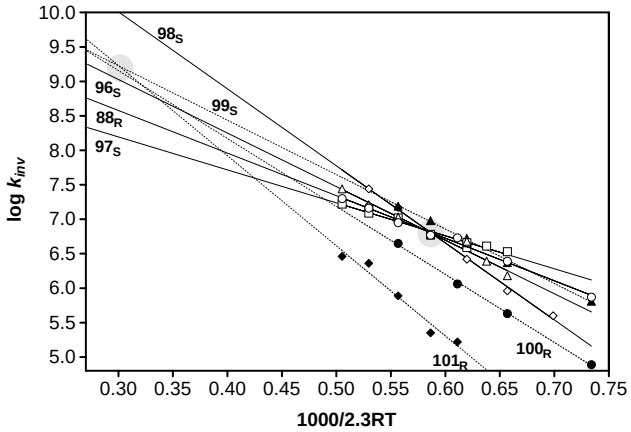

Fig. 6. Arrhenius plots for the inversion of configuration of O-protonated 1-aryl-1-methoxyethanes.

The activation parameters of the inversion reaction are found to obey two different isokinetic relationships (IKR) depending upon the nature and the position of the substituents in the oxonium ions (Fig. 6). In contrast, the activation parameters of the dissociation reaction obey a single isokinetic relationship (Fig. 7). The linear correlations of Fig. 8 show the existence of two different enthalpy–entropy compensation effects on the gas-phase inversion of and **88**$_R$ and **96**$_S$–**101**$_R$ ions related to the nature and the position of the substituent(s) in their structure, i.e., the F family (**96**$_S$, **97**$_S$, **98**$_S$, and **88**$_R$) and the G family (**99**$_S$, **100**$_R$ and **101**$_R$). In contrast, the curve of Fig. 9 points to the existence of a single enthalpy–entropy compensation in the gas phase dissociation of the same ions, i.e., the E family (**97**$_S$, **98**$_S$, **99**$_S$, **100**$_R$, and **88**$_R$).

The definition of IKR implies that, at the isokinetic temperature(T_{iso}), $\Delta G^* = \Delta H^* - T_{iso}\Delta S^* =$ constant. Therefore, the slopes of the linear curves of Figs. 8 and 9

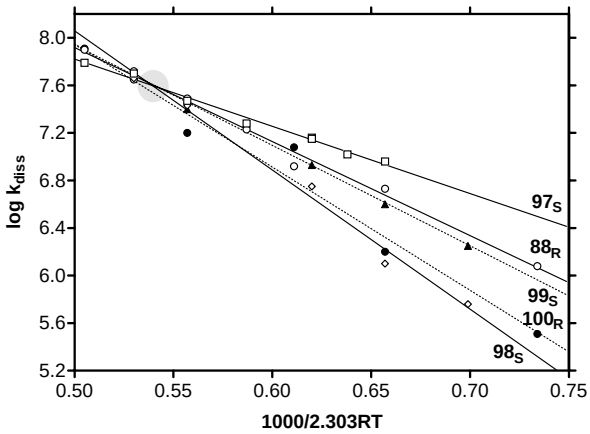

Fig. 7. Arrhenius plots for the dissociation of O-protonated 1-aryl-1-methoxyethanes.

Table 17
Arrhenius parameters for the gas-phase intracomplex inversion of O-protonated 1-aryl-1-methoxyethanes

Process	Arrhenius equation ($y = 1000/2.303RT$)	Correlation coefficient (r^2)	ΔH^*_{inv} (kcal mol^{-1})	ΔS^*_{inv} (cal mol^{-1} K^{-1})
96$_S$ → **96**$_R$	$\log k_{inv} = (11.3 \pm 0.3) - (7.8 \pm 0.5)y$	0.978	7.0 ± 0.5	−9.0 ± 0.9
97$_S$ → **97**$_R$	$\log k_{inv} = (9.6 \pm 0.2) - (4.8 \pm 0.3)y$	0.973	4.0 ± 0.4	−16.9 ± 0.9
98$_S$ → **98**$_R$	$\log k_{inv} = (13.3 \pm 0.2) - (11.1 \pm 0.3)y$	0.997	10.4 ± 0.3	+0.1 ± 1.1
88$_R$ → **88**$_S$	$\log k_{inv} = (10.4 \pm 0.1) - (6.2 \pm 0.2)y$	0.994	5.4 ± 0.3	−13.3 ± 1.0
99$_S$ → **99**$_R$	$\log k_{inv} = (11.7 \pm 0.1) - (8.0 \pm 0.2)y$	0.998	7.3 ± 0.3	−7.4 ± 0.8
100$_R$ → **100**$_S$	$\log k_{inv} = (12.0 \pm 0.1) - (9.7 \pm 0.2)y$	0.999	8.9 ± 0.2	−5.4 ± 0.5
101$_R$ → **101**$_S$	$\log k_{inv} = (13.1 \pm 0.8) - (13.0 \pm 1.5)y$	0.964	12.3 ± 1.5	−0.9 ± 1.0

Table 18
Arrhenius parameters for the gas-phase dissociation of O-protonated 1-aryl-1-methoxyethanes

Process	Arrhenius equation ($y = 1000/2.303RT$)	Correlation coefficient (r^2)	ΔH^*_{diss} (kcal mol^{-1})	ΔS^*_{diss} (cal mol^{-1} K^{-1})
97$_S$ → pClC$_6$H$_4$CHCH$_3^+$ + MeOH	$\log k_{diss} = (10.6 \pm 0.1) - (5.7 \pm 0.2)y$	0.989	4.9 ± 0.3	−12.2 ± 0.7
98$_S$ → mCF$_3$C$_6$H$_4$CHCH$_3^+$ + MeOH	$\log k_{diss} = (13.9 \pm 0.4) - (11.7 \pm 0.7)y$	0.990	10.9 ± 0.6	2.6 ± 2.0
88$_R$ → C$_6$H$_5$CHCH$_3^+$ + MeOH	$\log k_{diss} = (11.9 \pm 0.3) - (7.9 \pm 0.2)y$	0.992	7.1 ± 0.3	−6.7 ± 1.2
99$_S$ → pCF$_3$C$_6$H$_4$CHCH$_3^+$ + MeOH	$\log k_{diss} = (12.1 \pm 0.3) - (8.4 \pm 0.5)y$	0.990	7.7 ± 0.5	−5.4 ± 1.4
100$_R$ → C$_6$F$_5$CHCH$_3^+$ + MeOH	$\log k_{diss} = (13.1 \pm 0.7) - (10.3 \pm 1.1)y$	0.965	9.6 ± 1.1	−0.9 ± 1.9

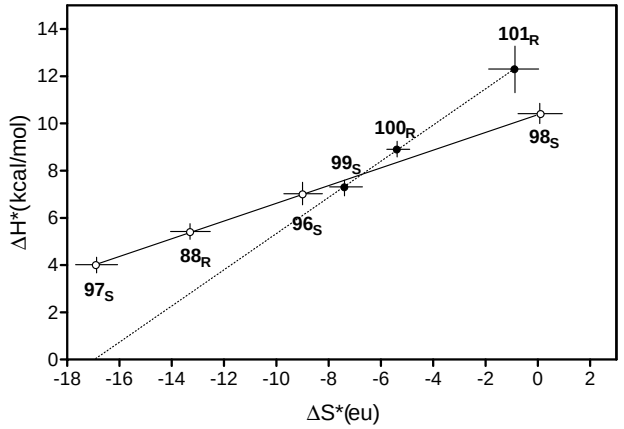

Fig. 8. Enthalpy–entropy compensation plots for the inversion of configuration of O-protonated 1-aryl-1-methoxyethanes (F family: **88**$_R$, **96**$_S$, **97**$_S$, and **98**$_S$; G family: **99**$_S$, **100**$_R$, and **101**$_R$).

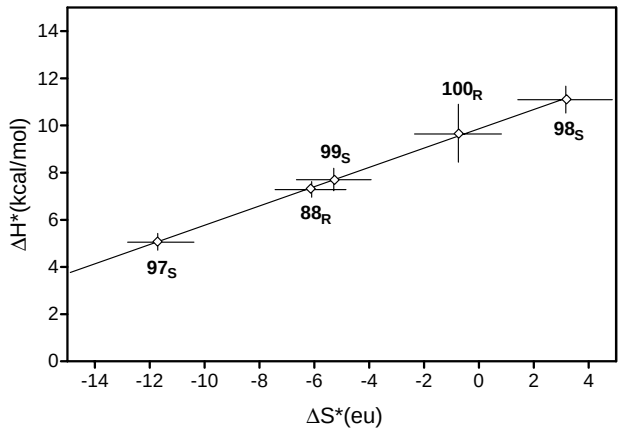

Fig. 9. Enthalpy–entropy compensation plot for the dissociation of O-protonated 1-aryl-1-methoxyethanes (the E family).

provide the relevant T_{iso}values, while the Y-intercepts give an estimate of the corresponding ΔG^*_{iso} terms. Accordingly, the isokinetic parameters for the F inversion reactions are $T_{iso} = 376 \pm 2$ K, $\Delta G^*_{iso} = 10.37 \pm 0.02$ kcal mol^{-1}, and $\log k_{iso} = 6.84$, whereas those for the G inversion reactions are $T_{iso} = 767 \pm 10$ K, $\Delta G^*_{iso} = 13.00 \pm 0.05$ kcal mol^{-1} and $\log k_{iso} = 9.35$. Similarly, the isokinetic parameters for the E dissociations are $T_{iso} = 409 \pm 5$ K, $\Delta G^*_{iso} = 9.89 \pm 0.04$ kcal mol^{-1}, and $\log k_{iso} = 7.61$.

The origin of IKR can be interpreted in terms of Linert's model [180]. The rate constant of a given reaction taking place in a constant-temperature "heat bath" (HB) depends on the collision number between the reacting system (M) and HB molecules, the energy barrier height of the given process, the temperature of the "heat bath," and the quantum–mechanical transition probability between any reactant level and the transition structure. When the "heat bath" contains energy stored in the form of vibrational degrees, the transition probabilities for vibrational–vibrational energy transfer is expressed by $P_{l,m} = l \exp(\omega/\nu)$ (where m is the HB vibrational level associated with ν and l is that associated with M) and reach the maximum value for a resonant vibrational–vibrational coupling, i.e., when $\nu m = \omega l$. In the condensed phase, cooperative supramolecular effects normally make available a quasi-continuum of HB vibrational frequencies (ν). In this case, the only variable parameter for a family of reactions is (ω) and, therefore, the IKR can be expressed mathematically as $d \ln k(\omega)/d\omega = 0$ at T_{iso}. Accordingly, for a homogeneous family of reactions, such as those involving O-protonated 1-aryl-1-methoxyethanes, a single T_{iso} should be expected whose value (in Kelvin degrees) is related to the characteristic vibrational frequency ν (in cm^{-1}) predominantly exchanging energy in HB by the $T_{iso} = h\nu/2k_B$ equation, where k_B is Botzmann constant and h is Planck constant.

While this is the case for the gas-phase E dissociation (Figs. 7 and 9), the observation in the same gaseous HB (CH_3Cl at 720 Torr) of two isokinetic temperatures for the inversion of configuration of the F and G families (Figs. 6 and 8) underlines the existence of a point of discontinuity in the ν/ω coupling which may be peculiar for gaseous media where cooperative supramolecular effects are negligible and, thus, the variable parameters for a family of reactions are both ν and ω [180].

In this frame, the two IKR of Fig. 8 can be rationalized in terms of Larsson's selective energy transfer (SET) model [181], which introduces in Linert's model the notion of possible switchovers in the resonant ν/ω coupling. Thus, in the assumption of full ν/ω resonance ($T_{iso} = h\nu/2k_B$), $T_{iso} = 376 \pm 2$ K for the inversion of configuration of the F family corresponds to a vibrational frequency ν_F predominantly exchanging energy of $523 \pm 3\,cm^{-1}$, while $T_{iso} = 767 \pm 10$ K for the inversion of the G family to a predominant vibrational frequency $\nu_G = 1067 \pm 14$ cm. According to theory, these frequencies should correspond to intense absorption bands of the vibrational spectrum of gaseous CH_3Cl. As a matter of fact, the IR spectrum of gaseous CH_3Cl shows characteristic vibrational bands around $1015\,cm^{-1}$, assigned to its ν_6(e) CH_3-rocking mode. On the contrary, none of the characteristic absorption bands of the CH_3Cl spectrum can account for $T_{iso} = 372 \pm 2$ K obtained for the F series. Rather, this T value reflects the activation of the F ions by a more intimate mechanism involving their transient complexation with a CH_3Cl molecule. Indeed, HF/6-31G* calculations of a model complex between O-protonated benzyl methyl ether and CH_3Cl indicate the presence of nine vibrational frequencies over those characteristic of the two isolated components. Among these, that related to the out-of-plane C–Cl···H–O bending mode falls at $572\,cm^{-1}$, a value which is close to the experimental $\omega_F = 523 \pm 3\,cm^{-1}$ one. The same $572\,cm^{-1}$ vibrational mode coincides with the critical ($\omega_{diss} = 569\,cm^{-1}$) value for the dissociation of the E family ($T_{iso} = 409 \pm 5$ K).

It is concluded that the inversion of configuration of the selected family of O-protonated 1-aryl-1-methoxyethanes obeys two different reaction dynamics driven by the activation dynamics from the bulk gas (CH_3Cl). Thus, if activation predominantly proceeds through a resonant energy exchange with ν_6(e) $= 1015\,cm^{-1}$ CH_3-rocking mode of the unperturbed molecule of the bath gas (CH_3Cl), the inversion reaction proceeds through the dyamically most accessible TS involving unassisted C_α–O bond rupture (the G family). If, instead, activation involves the out-of-plane C–Cl···H–O bending vibration developed in the intimate encounter complex between CH_3Cl and the oxonium ions, the inversion reaction proceeds through the energetically most accessible TS where the CH_3OH motion is assisted by coordination with the acidic hydrogens of the benzylic residue (the F family). The same vibrational mode is active in promoting the dissociation of most of members of the selected oxonium ions family, irrespective of their belonging to the F or G sets.

3.9. Intracomplex substitution in (R)-(+)-1-arylethanol/$CH_3{}^{18}OH_2{}^+$ adducts

It is well established that bimolecular S_N2 reactions generally involve predominant inversion of configuration of the reaction center. Unimolecular S_N1 displacements instead proceed through the intermediacy of free carbocations and, therefore, usually lead to racemates. However, many alleged S_N1 solvolyses do not give fully racemized products. The enantiomer in excess often, but not always, corresponds to inversion. Furthermore, the stereochemical distribution of products may be highly sensitive to the solvolytic conditions [182]. These observations have led to the concept of competing [183–185] or mixed [185–187] S_N1–S_N2 mechanisms. More recently, the existence itself of S_N1 reactions has been put into question [188].

Some obscure facets of this intricate picture have been unveiled by Filippi and Speranza who investigated the stereochemistry and the intimate mechanism of a model "solvolytic" reaction taking place in an ion-dipole pair in the gaseous phase [168]. Adducts $\mathbf{103}_R$ and $\mathbf{104}_R$ are obtained in the gas phase by association of the relevant chiral alcohols, i.e., (*R*)-(+)-1-phenyl-ethanol ($\mathbf{91}_R$) and (*R*)-(+)-1-(pentafluorophenyl) ethanol ($\mathbf{102}_R$), with the $CH_3{}^{18}OH_2{}^+$ ion, generated by γ-radiolysis of $CH_3F/H_2{}^{18}O$ mixtures (Scheme 10). As mentioned above, the absence of neutral nucleophile molecules, i.e., $CH_3{}^{18}OH$, in the reaction medium ensures that the ^{18}O-labeled ethers **92** and **105** of Scheme 10 arise exclusively from the intracomplex "solvolysis" of $\mathbf{103}_R$ and $\mathbf{104}_R$, respectively.

The experimental results point to intracomplex "solvolysis" in $\mathbf{103}_R$ and $\mathbf{104}_R$ as proceeding through the intermediacy of the relevant benzyl cation (a pure S_N1 mechanism). "Solvolysis" of $\mathbf{103}_R$ leads to complete racemization at $T > 50\,^\circ$C, whereas at $T < 50\,^\circ$C the reaction displays a preferential retention of configuration. Predominant retention of configuration is also observed in the intracomplex "solvolysis" of $\mathbf{104}_R$. The exothermic intracomplex displacement in $\mathbf{103}_R$ proceeds through TS's characterized by noncovalent interactions between the stable benzyl cation and the nucleophile/leaving group pair (an S_N1 process). The formation of the $\mathbf{92}^*_{R/S}$ racemate from $\mathbf{103}_R$ at $T > 50\,^\circ$C is entirely consistent with this view. In this frame, the slight predominance of retained $\mathbf{92}^*_R$ over the inverted $\mathbf{92}^*_S$ observed at $T < 50\,^\circ$C, is accounted for by a free rotation of the benzylic moiety of complex **103** (Plate 20) slower than its bonding to $CH_3{}^{18}OH$. In fact, the procedure adopted to generate $\mathbf{103}_R$ in the gas phase requires that the $CH_3{}^{18}OH$ moiety resides initially in the same region of space containing the leaving group. In the absence of any intracomplex rotation of the benzylic moiety of **103**, $CH_3{}^{18}OH$ is spatially situated to attack from the frontside (a "troposelective" reaction) [168]. At higher temperatures, this

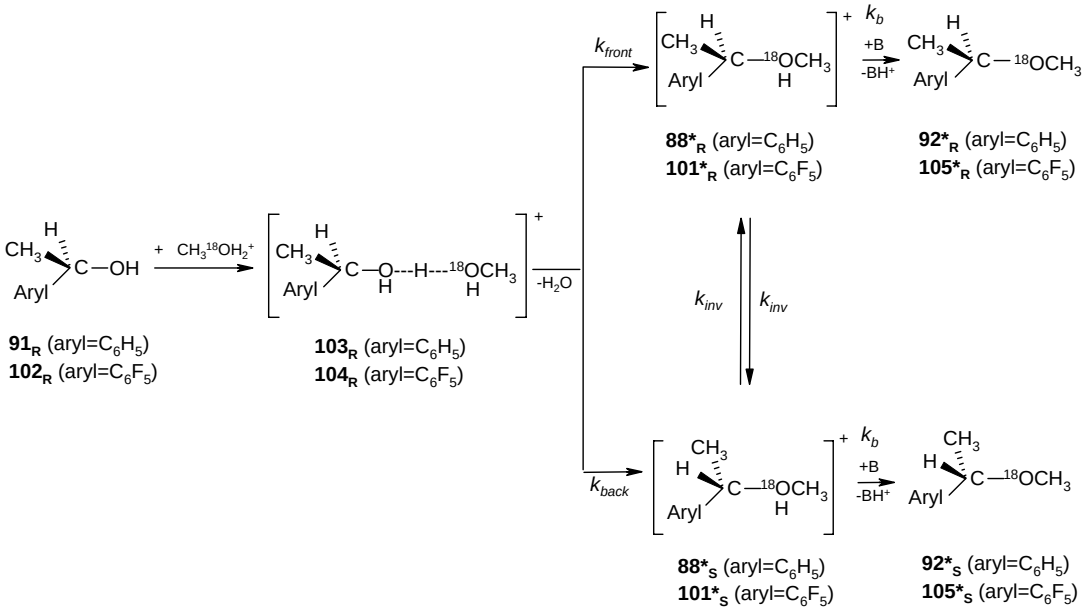

Scheme 10.

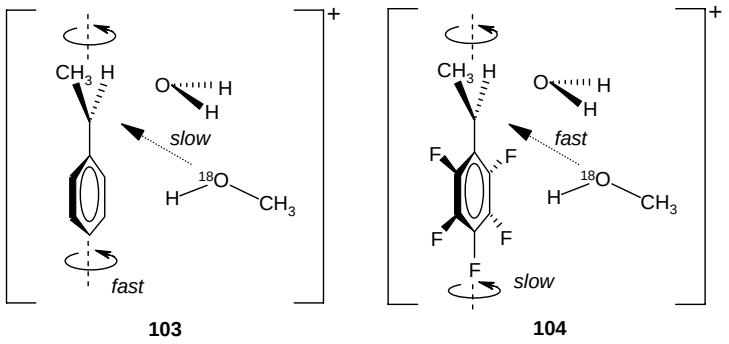

Plate 20.

positional advantage is annulled and the $\mathbf{92}^*_{R/S}$ racemate is formed.

The intracomplex "solvolysis" of $\mathbf{102}_R$ can be considered highly troposelective since it involves predominant retention of configuration (88% at 25 °C). Inductive and resonance effects of the ring fluorine substituents reduce appreciably the stabilization energy of α-methyl pentafluorobenzyl cation relative to the unsubstituted homologue. This implies that the interactions between the nucleophile/leaving group and benzylic moiety in complex **104** (Plate 20) are stronger than those operating in adduct **103**. As a consequence, free rotation of benzylic moiety in $\mathbf{104}_R$ is slow relative to covalent bonding with $CH_3{}^{18}OH$.

The above gas-phase picture may represent a guideline for understanding the mechanism and the stereochemistry of substitution reactions in the solvent cage. The results of gas-phase $\mathbf{91}_R$ "solvolysis" demonstrate the existence of a pure S_N1 mechanism. Fast rotation of the benzylic moiety in the complex **103** of Plate 20 ($T > 50$ °C) explains the formation of the $\mathbf{92}^*_{R/S}$ racemate. If rotation is hampered by significant ion–nucleophile interactions (as in $\mathbf{104}_R$ or in $\mathbf{103}_R$ at $T < 50$ °C), predominant retention of configuration is observed. This may explain why some solvolytic reactions lead to a slight excess of the retained product in the liquid phase. However, the presence of the solvent cage may alter this picture and favor inversion of configuration even if a pure S_N1 solvolysis is taking place. This may happen when reorientation of the ion in the cage is slow and if the presence of the leaving group somewhat hampers the approach of the nucleophile from the frontside. However, inversion of configuration predominates even when the relative motionlessness of the ion in the solvent cage is due to a partial covalency of its interactions with the leaving group and the nucleophilic solvent (a S_N2 process). It is concluded that the solvolytic reactions are mostly governed by the lifetime and the dynamics of the species involved and if occurring in solution, by the nature of the solvent cage. Their rigid subdivision into the S_N1 and S_N2 mechanistic categories ap-

pears inadequate and the use of their stereochemistry as a mechanistic probe can he highly misleading.

4. Conclusions and outlook

The comprehension of enantioselective phenomena in chemical and biochemical processes requires the knowledge of the intrinsic interactions operating in related simplified models in the gas phase, in the absence of any solvation and ion pairing effects. The advantages connected with studying enantioselectivity in simple INC in the gas phase come from the possibility to make precise statements on their structure and stability as well as on the intrinsic factors governing their dynamics and reactivity in the lack of any perturbing environmental effects (solvation, ion pairing, cage viscosity, etc.). A survey of the most relevant studies along this line is reported in the present review. The resulting picture shows that MS techniques may provide detailed information on the relative stability of diastereomeric INC obtained by aggregation of chiral molecules around charged centers (proton or metal cations) or inside asymmetric molecular cages. Careful application of the complementary radiolytic method may give otherwise unaccessible information about the intrinsic factors governing the mechanism and the dynamics of classical stereoselective reactions normally occurring in solution.

Although we are still at an early stage in the study of chiral INC and of their enantioselective evolution in the gas phase, the future perspectives seem to be rather promising. The synergistic growth of novel devices for the vaporization and the ionization of biomolecules into MS may allow in the near future the structural characterization and the functionality of large chiral assemblies involved in complicated chemical and biochemical processes occurring in condensed phases. It could be only a matter of time before relatively simple reactions of biological significance, such as an enantioselective reaction in a receptor cavity, can be studied in the gas phase. Furthermore, tailor-made INC in dense gases at defined temperatures my serve as “microscopic test tubes” allowing some insight into the very first steps of chemistry under controlled solvation and hopefully into some of the riddles of solution chemistry as well.

Acknowledgements

The author acknowledges the contribution of his coworkers, as cited in the references. This work was supported by the Italian Ministero della Università della Ricerca Scientifica e Tecnologica (MIUR) e dal Consiglio Nazionale delle Ricerche (CNR).

References

[1] W. Kauzman, Rev. Mod. Phys. 31 (1959) 549.
[2] P.D. Schnier, J.S. Klassen, E.F. Strittmatter, E.R. Williams, J. Am. Chem. Soc. 120 (1998) 9605.
[3] F. Pichierri, M. Aida, M.M. Gromiha, A. Sarai, J. Am. Chem. Soc. 121 (1999) 6152.
[4] F. Hollfelder, A.J. Kirby, D.S. Tawfik, Nature 383 (1996) 60.
[5] M. Sawada, in: T. Matsuo, R.M. Caprioli, M.L. Gross, T. Seyama (Eds.), Biological Mass Spectrometry: Present and Future, Wiley, New York, 1994.
[6] M. Sawada, Mass Spectrom. Rev. 16 (1997) 733.
[7] C.A. Schalley, Int. J. Mass Spectrom. 194 (2000) 11.
[8] A. Filippi, A. Giardini, S. Piccirillo, M. Speranza, Int. J. Mass Spectrom. 198 (2000) 137.
[9] C.B. Lebrilla, Acc. Chem. Res. 34 (2001) 653.
[10] D. Dearden, Y. Liang, J.B. Nicoll, K.A. Kellersberger, J. Mass Spectrom. 36 (2001) 989.
[11] F.H. Fales, G.J. Wright, J. Am. Chem. Soc. 99 (1977) 2339.
[12] F.J. Winkler, D. Stahl, F. Maquin, Tetrahedron Lett. 27 (1986) 335.
[13] F.J. Winkler, J.S. Splitter, in: J.S. Splitter, F. Tureček (Eds.), Applications of Mass Spectrometry to Organic Stereochemistry, VCH Publishers, New York, 1994.
[14] M.A. Baldwin, S.A. Howell, K.J. Welham, F.J. Winkler, Biomed. Environ. Mass Spectrom. 16 (1988) 357.
[15] F.J. Winkler, R. Medina, J. Winkler, H. Krause, J. Chromatogr. A 666 (1994) 549.
[16] R. Sussmuth, G. Jung, F.J. Winkler, R. Medina, Eur. Mass Spectrom. 5 (1999) 298.
[17] E.N. Nikolaev, E.V. Denisov, M.I. Nikolaeva, J.H. Futrell, V.S. Rakov, F.J. Winkler, Adv. Mass Spectrom. 14 (1998) 279 (Chapter 12).
[18] F.J. Winkler, R. Medina, J. Winkler, H. Krause, J. Mass Spectrom. 32 (1997) 1072.
[19] E.V. Denisov, V. Shustryakov, E.N. Nikolaev, F.J. Winkler, R. Medina, Int. J. Mass Spectrom. Ion Process. 167/168 (1997) 259.
[20] E.N. Nikolaev, G.T. Goginashvili, V. Tal’rose, R.G. Kostyanovsky, Int. J. Mass Spectrom. Ion Process. 86 (1988) 249.
[21] E.N. Nikolaev, T.B. McMahon, Proceedings of the 43rd Annual Conference on Mass Spectrometry and Allied Topics, Atlanta, Georgia, 1995, p. 973.
[22] E.N. Nikolaev, E.V. Denisov, Proceedings of the 44th Annual Conference on Mass Spectrometry and Allied Topics, Portland, Oregon, 1996, p. 415.
[23] E.N. Nikolaev, E.V. Denisov, V.S. Rakov, J.H. Futrell, Int. J. Mass Spectrom. 182/183 (1999) 357.
[24] S. Hua, Y. Chen, L. Jiang, S. Xue, Org. Mass Spectrom. 21 (1986) 7.
[25] Y.Z. Chen, H. Li, H.J. Yang, S.M. Hua, H.Q. Li, F.Z. Zhao, N.Y. Chen, Org. Mass Spectrom. 23 (1988) 821.
[26] J. Martens, S. Lübben, W. Schwarting, Z. Naturforsch 46b (1991) 320.
[27] H.J. Yang, Y.Z. Chen, Org. Mass Spectrom. 27 (1992) 736.
[28] K. Hashimoto, Y. Sumida, S. Terada, I. Okamura, J. Mass Spectrom. Soc. Jpn. 41 (1993) 87.
[29] K. Hashimoto, Y. Sumida, S. Terada, K. Okamura, J. Mass Spectrom. Soc. Jpn. 41 (1993) 95.
[30] K. Okamura, Y. Sumida, Y. Fujiwara, S. Terada, H. Kim, K. Hashimoto, J. Mass Spectrom. Soc. Jpn. 43 (1995) 97.
[31] K. Hashimoto, K. Okamura, Y. Fujiwara, Y. Sumida, S. Terada, Adv. Mass Spectrom. 14 (1998) 1.
[32] R.G. Cooks, T.L. Kruger, J. Am. Chem. Soc. 99 (1977) 1279.
[33] S.A. McLuckey, D. Cameron, R.G. Cooks, J. Am. Chem. Soc. 103 (1981) 1313.
[34] L. Drahos, K. Vèkey, J. Mass Spectrom. 34 (1999) 79.
[35] J. Laskin, J.H. Futrell, J. Phys. Chem. A 104 (2000) 5484.
[36] X.H. Cheng, Z.C. Wu, C. Fenselau, J. Am. Chem. Soc. 115 (1993) 4844.

[37] Z.C. Wu, C. Fenselau, Rapid Commun. Mass Spectrom. 8 (1994) 777.
[38] B.A. Cerda, C. Wesdemiotis, J. Am. Chem. Soc. 118 (1996) 11884.
[39] B.A. Cerda, M.J. Nold, C. Wesdemiotis, in: R.M. Caprioli, A. Malorni, G. Sindona (Eds.), Selected Topics in Mass Spectrometry in the Biomolecular Sciences, Kluwer Academic, Dordrecht, 1997.
[40] B.A. Cerda, S. Hoyau, G. Ohanessian, C. Wesdemiotis, J. Am. Chem. Soc. 120 (1998) 2437.
[41] M.J. Nold, B.A. Cerda, C. Wesdemiotis, J. Am. Soc. Mass Spectrom. 10 (1999) 1.
[42] P.B. Armentrout, J. Am. Soc. Mass Spectrom. 11 (2000) 371.
[43] K. Vekey, G. Czira, Rapid Commun. Mass Spectrom. 9 (1995) 783.
[44] Z.P. Yao, T.S.M. Wan, K.P. Kwong, C.T. Che, Chem. Commun. 20 (1999) 2119.
[45] T. Vaisar, J. Urban, H. Nakanishi, J. Mass Spectrom. 31 (1996) 937.
[46] G. Fago, A. Filippi, A. Giardini, A. Laganà, A. Paladini, M. Speranza, Angew Chem. Int. Ed. Engl. 40 (2001) 4051.
[47] A. Paladini, D. Scuderi, A. Lagana, A. Giardini, A. Filippi, M. Speranza, Int. J. Mass Spectrom. 228 (2003) 349.
[48] R.G. Cooks, J.S. Patrick, T. Kotiaho, S.A. McLuckev, Mass Spectrom. Rev. 13 (1994) 287.
[49] W. Shen, P.S.H. Wong, R.G. Cooks, Rapid Commun. Mass Spectrom. 11 (1997) 71.
[50] G. Hofmeister, J.A. Leary, Org. Mass Spectrom. 26 (1991) 811; See, also V. Carlesso, C. Afonso, F. Fournier, J.C. Tabet, Comptes Rendues Chim. 6 (2003) 623.
[51] T.T. Dang, S.F. Pedersen, J.A. Leary, J. Am. Soc. Mass Spectrom. 5 (1994) 452.
[52] W.A. Tao, L. Wu, R.G. Cooks, Chem. Commun. 20 (2000) 2023.
[53] W.A. Tao, R.L. Clark, R.G. Cooks, Chem. Commun. 1 (2003) 136.
[54] W.A. Tao, R.G. Cooks, Anal. Chem. 75 (2003) 25A.
[55] W.A. Tao, D. Zhang, F. Wang, P.D. Thomas, R.G. Cooks, Anal. Chem. 71 (1999) 4427.
[56] W.A. Tao, D. Zhang, E.N. Nikolaev, R.G. Cooks, J. Am. Chem. Soc. 122 (2000) 10598.
[57] W.A. Tao, R.G. Cooks, Eur. J. Mass Spectrom. 8 (2002) 107.
[58] W.A. Tao, L. Wu, R.G. Cooks, F. Wang, J.A. Begley, B. Lampert, J. Med. Chem. 44 (2001) 3541.
[59] D. Zhang, W.A. Tao, R.G. Cooks, Int. J. Mass Spectrom. 204 (2001) 159.
[60] W.A. Tao, R.L. Clark, R.G. Cooks, Anal. Chem. 74 (2002) 3783.
[61] L. Wu, W.A. Tao, R.G. Cooks, J. Mass Spectrom. 38 (2003) 386.
[62] W.A. Tao, L. Wu, R.G. Cooks, J. Am. Soc. Mass Spectrom. 12 (2001) 490.
[63] W.A. Tao, R.G. Cooks, Angew Chem. Int. Ed. Engl. 40 (2001) 757.
[64] J. Chen, C.J. Zhu, Y. Chen, Y.F. Zhao, Rapid Commun. Mass Spectrom. 16 (2002) 1251.
[65] L. Wu, K. Lemr, T. Aggerholm, R.G. Cooks, J. Am. Soc. Mass Spectrom. 14 (2003) 152.
[66] W.A. Tao, F.G. Gozzo, R.G. Cooks, Anal. Chem. 73 (2001) 1692.
[67] D.V. Augusti, R. Augusti, F. Carazza, R.G. Cooks, Chem. Commun. 19 (2002) 2242.
[68] L. Wu, R.G. Cooks, Anal. Chem. 75 (2003) 678.
[69] M.J. Locke, R.L. Hunter, R.T. McIver, J. Am. Chem. Soc. 101 (1979) 272.
[70] M.J. Locke, R.T. McIver, J. Am. Chem. Soc. 105 (1983) 4226.
[71] C.H. Hu, M.Z. Shen, H.F. Schaefer, J. Am. Chem. Soc. 115 (1993) 2923.
[72] M.S. Gordon, J.H. Jensen, Acc. Chem. Res. 29 (1996) 536.
[73] J. Bertran, L. Rodriguez-Santiago, M. Sodupe, J. Phys. Chem. B 103 (1999) 2310.
[74] R.A. Jockusch, P.D. William, E.R. Williams, J. Am. Chem. Soc. 119 (1997) 11988.
[75] C.J. Chapo, J.B. Paul, R.A. Provencal, K. Roth, R.J. Saykally, J. Am. Chem. Soc. 120 (1993) 12956.
[76] Z.B. Maksic, B. Kovacevic, J. Chem. Soc. Perkin Trans. 2 (1999) 2623.
[77] P. Skurski, M. Gutowaki, R. Barrios, J. Simons, Chem. Phys. Lett. 337 (2001) 143.
[78] M. Gutowski, P. Skurski, J. Simons, J. Am. Chem. Soc. 122 (2000) 10159.
[79] P. Skurski, M. Rak, J. Simons, M. Gutowski, J. Am. Chem. Soc. 123 (2001) 11073.
[80] J. Rak, P. Skurski, J. Simons, M. Gutowski, J. Am. Chem. Soc. 123 (2001) 11695.
[81] R.R. Julian, J.L. Beauchamp, W.A. Goddard III, J. Phys. Chem. A 106 (2002) 32.
[82] R. Hodyss, R.R. Julian, J.L. Beauchamp, Chirality 13 (2001) 703.
[83] D. Zhang, L. Wu, K.J. Koch, R.G. Cooks, Eur. Mass Spectrom. 5 (1999) 353.
[84] (a) R.G. Cooks, D. Zhang, K.J. Koch, F.C. Gozzo, M.N. Eberlin, Anal. Chem. 73 (2001) 3646;
(b) Z. Takats, S.C. Nanita, R.G. Cooks, G. Schiosser, K. Vekey, Anal. Chem. 75 (2003) 1514.
[85] K.J. Koch, F.C. Gozzo, D. Zhang, M.N. Eberlin, R.G. Cooks, Chem. Commun. 18 (2001) 1854;
See also Z. Takats, S.C. Nanita, R.G. Cooks, Angew Chem. Int. Ed. Engl. 42 (2003) 3521.
[86] R.R. Julian, R. Hodyss, B. Kinnear, M.F. Jarrold, J.L. Beauchamp, J. Phys. Chem. B 106 (2002) 1219.
[87] K.J. Koch, F.C. Gozzo, S.C. Nanita, Z. Takats, M.N. Eberlin, R.G. Cooks, Angew Chem. Int. Ed. Engl. 41 (2002) 1721.
[88] (a) D. Schöder, Dissertation, TU Berlin, 1992, D3;
(b) D. Schröder, H. Schwarz, Top. Curr. Chem. 225 (2003) 133.
[89] J. Guo, J. Wu, G. Siuzdak, M.G. Finn, Angew Chem. Int. Ed. Engl. 38 (1999) 1755.
[90] M. Sawada, Y. Takai, H. Yamada, T. Kaneda, K. Kamada, T. Mizooku, K. Hirose, Y. Tobe, K. Naemura, Chem. Commun. 21 (1994) 2497.
[91] M. Sawada, Y. Takai, H. Yamada, S. Hirayama, T. Kneda, T. Tanaka, K. Kamada, T. Mizooku, S. Takeuchi, K. Ueno, K. Hirose, Y. Tobe, K. Naemura, J. Am. Chem. Soc. 117 (1995) 7726.
[92] M. Sawada, Y. Takai, T. Kaneda, R. Arakawa, M. Okamoto, H. Doe, T. Matsuo, K. Naemura, K. Hirose, Y. Tobe, Chem. Commun. 15 (1996) 1735.
[93] M. Sawada, Y. Takai, H. Yamada, J. Nishida, T. Kaneda, R. Arakawa, M. Okamoto, K. Hirose, T. Tanaka, K. Naemura, J. Chem. Soc. Perkin Trans. 2 (1995) 701.
[94] M. Sawada, H. Yamaoka, Y. Takal, Y. Kawai, H. Yamada, T. Azuma, T. Fujioka, T. Tanaka, Chem. Commun. 15 (1998) 1569.
[95] M. Sawada, H. Yamaoka, Y. Takai, Y. Kawai, H. Yamada, T. Azuma, T. Fujioka, T. Tanaka, Int. J. Mass Spectrom. 193 (1999) 123.
[96] C. Garcia, J. Guyot, G. Jeminet, E. Leize Wagner, H. Nierengarten, A. van Dorsselaer, Tetrahedron Lett. 40 (1999) 4997.
[97] G. Pócsfalvi, M. Lipták, P. Huszthy, J.S. Bradshaw, R.M. Izatt, K. Vékey, Anal. Chem. 68 (1996) 792.
[98] A. Dobó, M. Lipták, P. Huszthy, K. Vékey, Rapid Commun. Mass Spectrom. 11 (1997) 889.
[99] M. Sawada, M. Shizama, Y. Takai, H. Yamada, T. Kaneda, T. Hanafusa, J. Am. Chem. Soc. 114 (1992) 4405.
[100] M. Sawada, Y. Okamura, M. Shizuma, Y. Takai, Y. Hidaka, H. Yamada, T. Tanaka, T. Kaneda, K. Hirose, S. Misumi, S. Takahashi, J. Am. Chem. Soc. 115 (1993) 7381.
[101] M. Sawada, Y. Okami, H. Yamada, Y. Takai, S. Takahashi, T. Kaneda, K. Hirose, S. Misumi, Org. Mass Spectrom. 28 (1993) 1525.
[102] I.H. Chu, D.V. Dearden, J.S. Bradshaw, P. Huszthy, R.M. Izatt, J. Am. Chem. Soc. 115 (1993) 4318.
[103] D.V. Dearden, C. Dejsupa, Y. Liang, J.S. Bradshaw, R.M. Izatt, J. Am. Chem. Soc. 119 (1997) 353.

[104] R.B. Davidson, J.S. Bradshaw, B.A. Jones, N.K. Dalley, J.J. Christensen, R.M. Izatt, F.G. Morin, D.M. Grant, J. Org. Chem. 49 (1984) 353.
[105] Y. Liang, J.S. Bradshaw, R.M. Izatt, R.M. Pope, D.V. Dearden, Int. J. Mass Spectrom. 185–187 (1999) 977.
[106] Y. Liang, J.S. Bradshaw, D.V. Dearden, J. Phys. Chem. A 106 (2002) 9665.
[107] N.J. Haskins, M.R. Saunders, P. Camilieri, Rapid Commun. Mass Spectrom. 8 (1994) 423.
[108] M.P. So, T.S.M. Wan, T.W.D. Chan, Rapid Commun. Mass Spectrom. 14 (2000) 692.
[109] J. Ramirez, F. He, C.B. Lebrilla, J. Am. Chem. Soc. 120 (1998) 7387.
[110] J. Rarnirez, S. Ahn, G. Grigorean, C.B. Lebrilla, J. Am. Chem. Soc. 122 (2000) 6884.
[111] J.F. Gal, M. Stone, C.B. Lebrilla, Int. J. Mass Spectrom. 222 (2003) 259.
[112] S. Ahn, J. Ramirez, G. Grigorean, C.B. Lebrilla, J. Am. Soc. Mass Spectrom. 12 (2001) 278.
[113] G. Grigorean, C.B. Lebrilla, Anal. Chem. 73 (2001) 1684.
[114] M. Sawada, J. Mass Spectrom. Soc. Jpn. 45 (1997) 439.
[115] Y. Takai, Y. Okamura, T. Tanaka, M. Sawada, S. Takahashi, M. Shiro, M. Kawamura, T. Uchiyama, J. Org. Chem. 59 (1994) 2967.
[116] M. Sawada, M. Shizuma, Y. Takai, H. Adachi, T. Takeda, T. Uchiyama, Chem. Commun. 14 (1998) 1453.
[117] M. Shizuma, H. Adachi, M. Kawamura, Y. Takai, T. Takeda, M. Sawada, J. Chem. Soc. Perkin Trans. 2 (2001) 592.
[118] M. Shizuma, H. Adachi, A. Amemura, Y. Takai, T. Takeda, M. Sawada, Tetrahedron 57 (2001) 4567.
[119] M. Shizuma, H. Adachi, Y. Takai, M. Hayashi, J. Tanaka, T. Takeda, M. Sawada, Carbohydrate Res. 335 (2001) 275.
[120] Y. Takai, Y. Okamura, S. Takahashi, M. Sawada, M. Kawamura, T. Uchiyama, Chem. Commun. 1 (1993) 53.
[121] M. Shizuma, Y. Takai, M. Kawamura, T. Takeda, M. Sawada, J. Chem. Soc. Perkin Trans. 2 (2001) 1306.
[122] M. Shizuma, Y. Kadoya, Y. Takai, H. Imamura, H. Yamada, T. Takeda, R. Arakawa, S. Takahashi, M. Sawada, J. Org. Chem. 67 (2002) 4795, and references therein.
[123] M. Vincenti, A. Irico, Int. J. Mass Spectrom. 214 (2002) 23, and references therein.
[124] M.M. Stone, A.H. Franz, C.B. Lebrilla, J. Am. Soc. Mass Spectrom. 13 (2002) 964.
[125] T.M. Liang, K.K. Laali, M. Cordero, C. Wesdemiotis, J. Chem. Res. (S) 12 (1991) 354.
[126] B. Botta, M. Botta, A. Filippi, A. Tafi, G. Delle Monache, M. Speranza, J. Am. Chem. Soc. 124 (2002) 7658.
[127] A. Tafi, B. Botta, M. Botta, G. Delle Monache, A. Filippi, M. Speranza, Chem. Eur. J. (2004) in press.
[128] H. Tsukube, H. Sohmiya, J. Chem. Org. 56 (1991) 875.
[129] D.H. Williams, C. Bradley, G. Bojesen, S. Shantikarn, L.C.E. Taylor, J. Am. Chem. Soc. 103 (1981) 5700.
[130] T.J.D. Jørgensen, D. Delforge, J. Remacle, G. Bojesen, P. Roepstorff, Int. J. Mass Spectrom. 188 (1999) 63.
[131] E. Camara, M.K. Green, S.G. Penn, C.B. Lebrilla, J. Am. Chem. Soc. 118 (1996) 8751.
[132] S. Gong, E. Camara, H. Fei, M.K. Green, C.B. Lebrilla, Int. J. Mass Spectrom. 185–187 (1999) 401.
[133] D.E. Clemmer, R.R. Hudgins, M.F. Jarrold, J. Am. Chem. Soc. 117 (1995) 10141.
[134] P. Walden, Berlin 26 (1893) 210.
[135] J.K. Lardahl, E. Uggerud, Int. J. Mass Spectrom. 214 (2002) 277.
[136] C.A. Lieder, J.I. Brauman, J. Am. Chem. Soc. 96 (1974) 4028.
[137] J.C. Tabet, Tetrahedron 43 (1987) 3413.
[138] N.M. Sellier, C.T. Bouillet, D.L. Douay, J.C. Tabet, Rapid Commun. Mass Spectrom. 8 (1994) 891.
[139] J.C. Tabet, Spectrosc. Int. J. 5 (1987) 83.
[140] A. Filippi, M. Speranza, Int. J. Mass Spectrom. 199 (2000) 211.
[141] G. Angelini, M. Speranza, Chem. Commun. 5 (1978) 213.
[142] M. Speranza, G. Angelini, J. Am. Chem. Soc. 102 (1980) 3115.
[143] G. Angelini, M. Speranza, J. Am. Chem. Soc. 103 (1981) 3792.
[144] G. Angelini, M. Speranza, J. Am. Chem. Soc. 103 (1981) 3800.
[145] P. Crotti, M. Macchia, A. Pizzabiocca, G. Renzi, M. Speranza, Tetrahedron Lett. 28 (1987) 3383.
[146] P. Crotti, M. Macchia, A. Pizzabiocca, G. Renzi, M. Speranza, Gazz. Chim. Ital. 117 (1987) 739.
[147] S. Fornarini, C. Sparapani, M. Speranza, J. Am. Chem. Soc. 110 (1988) 34.
[148] S. Fornarini, C. Sparapani, M. Speranza, J. Am. Chem. Soc. 110 (1988) 42.
[149] P. Cecchi, A. Pizzabiocca, G. Renzi, M. Chini, P. Crotti, F. Macchia, M. Speranza, Tetrahedron 45 (1989) 4227.
[150] P. Cecchi, M. Chini, P. Crotti, A. Pizzabiocca, G. Renzi, M. Speranza, Tetrahedron 47 (1991) 4683.
[151] D.G. Hall, C. Gupta, T.H. Morton, J. Am. Chem. Soc. 103 (1981) 2416.
[152] T.H. Morton, Tetrahedron 38 (1982) 3195.
[153] R.D. Bowen, Acc. Chem. Res. 24 (1991) 364.
[154] T.H. Morton, Org. Mass Spectrom. 27 (1992) 353.
[155] D.J. McAdoo, T.H. Morton, Acc. Chem. Res. 26 (1993) 295.
[156] M. Aschi, F. Cacace, A. Troiani, Angew Chem. Int. Ed. Engl. 36 (1997) 83.
[157] A. Filippi, G. Roselli, G. Renzi, F. Grandinetti, M. Speranza, Chem. Eur. J. 9 (2003) 2072.
[158] A. Troiani, A. Filippi, M. Speranza, Chem. Eur. J. 3 (2003) 2063.
[159] A. Filippi, M. Speranza, Int. J. Mass Spectrom. 185–187 (1999) 425.
[160] M. Speranza, A. Filippi, Chem. Eur. J. 5 (1999) 834.
[161] M. Speranza, A. Filippi, Chem. Eur. J. 5 (1999) 845.
[162] A. Troiani, F. Gasparrini, F. Grandinetti, M. Speranza, J. Am. Chem. Soc. 119 (1997) 4525.
[163] A. Troiani, M. Speranza, J. Org. Chem. 63 (1998) 1012.
[164] M. Speranza, A. Troiani, J. Org. Chem. 63 (1998) 1020.
[165] A. Filippi, F. Gasparrini, M. Speranza, J. Am. Chem. Soc. 123 (2001) 2251.
[166] A. Filippi, M. Speranza, Chem. Eur. J. 9 (2003) 5274.
[167] A. Filippi, M. Speranza, J. Am. Chem. Soc. 123 (2001) 6077.
[168] L.A. Philips, D.H. Levy, J. Chem. Phys. 90 (1986) 4921.
[169] F. Cacace, G. Ciranni, P. Giacomello, J. Am. Chem. Soc. 103 (1981) 1513.
[170] E. Dezi, A. Lombardozzi, A. Pizzabiocca, G. Renzi, M. Speranza, Chem. Commun. 5 (1995) 547.
[171] G. Renzi, A. Lombardozzi, E. Dezi, A. Pizzabiocca, M. Speranza, Chem. Eur. J. 2 (1996) 316.
[172] E. Dezi, A. Lombardozzi, G. Renzi, A. Pizzabiocca, M. Speranza, Chem. Eur. J. 2 (1996) 323.
[173] F. Carrion, M.J.S. Dewar, J. Am. Chem. Soc. 106 (1984) 3531.
[174] R.D. Bach, G.J. Wolber, J. Am. Chem. Soc. 107 (1985) 1352.
[175] Y.S. Park, C.K. Kim, B.S. Lee, I. Lee, J. Phys. Chem. 99 (1995) 13103.
[176] For a review, see D. Samuel, B. Silver, Adv. Phys. Org. Chem. 3 (1965) 128.
[177] M.V. Merritt, S.J. Bell, H.J. Cheon, J.A. Darlington, T.L. Dugger, N.B. Elliott, G.L. Fairbrother, C.S. Melendez, E.V. Smith, P.L. Schwartz, J. Am. Chem. Soc. 112 (1990) 3560, and references therein.
[178] M.V. Merritt, D.B. Anderson, K.A. Basu, I.W. Chang, H.J. Cheon, N.E. Mukundan, C.A. Flannery, A.Y. Kim, A. Vaishampayan, D.A. Yens, J. Am. Chem. Soc. 116 (1994) 5551, and references therein.
[179] A. Thibblin, J. Phys. Org. Chem. 6 (1993) 287, and references therein.
[180] W. Linert, R.F. Jameson, Chem. Soc. Rev. 18 (1989) 477, and references therein.
[181] R. Larsson, Catal. Today 3 (1988) 387.
[182] J. March, Advanced Organic Chemistry, Wiley, New York, 1985.

[183] I. Dostrovsky, E.D. Hughes, C.K. Ingold, J. Chem. Soc. (1946) 173.
[184] T.W. Beniley, C.T. Bowen, W. Parker, C.I.F. Watt, J. Am. Chem. Soc. 101 (1979) 2486.
[185] W.P. Jencks, Chem. Soc. Rev. 10 (1982) 345.
[186] T.W. Bentley, C.T. Bowen, D.H. Morten, P.v.R. Schleyer, J. Am. Chem. Soc. 103 (1981) 5466.
[187] T.W. Bentley, C.T. Bowen, J. Chem. Soc. Perkin Trans. II (1978) 557.
[188] J. Dale, J. Chem. Educ. 75 (1998) 1482.